HEAT SINK CAPABILITY OF JET A FUEL: HEAT TRANSFER AND COKING STUDIES

L.E. Faith, G.H. Ackerman, H.T. Henderson

SHELL DEVELOPMENT COMPANY
A DIVISION OF SHELL OIL COMPANY

CASE FILE
COPY

prepared for

FINAL REPORT

HEAT SINK CAPABILITY OF JET A FUEL: HEAT TRANSFER AND COKING STUDIES

by

L. E. Faith, G. H. Ackerman, and H. T. Henderson

SHELL DEVELOPMENT COMPANY
A Division of Shell Oil Company
Emeryville, California 94608

prepared for

NATIONAL AERONAUTICS AND SPACE ADMINISTRATION

July 1971

(This page is blank)

FOREWORD

The work described herein was done at Emeryville Research Center, Shell Development Company, Emeryville, California, under the general supervision of K. D. Detling, Manager, Government Research Department. The work was authorized under NASA Contract NAS 3-12432 and was conducted under the technical direction of Mr. E. L. Warren, Project Manager, and Mr. Francis S. Stepka, Research Advisor, Air Breathing Engines Division, NASA Lewis Research Center.

Acknowledgement is made to A. C. Nixon for his valuable contributions as project supervisor before his retirement on 1 June 1970.

(This page is blank)

ABSTRACT

The operation of supersonic turbine aircraft can be extended by using more heat sink of the fuel for cooling. Experiments were run with Jet A fuel to determine the heat transfer characteristics and coking problems associated with this application. Selection of the fuel used was based on coker tests of fuels from several sources. Heat transfer to the fuel was studied and correlations were developed for both laminar and turbulent flow of the fuel. Considerable free convection in laminar flow enhanced the heat transfer and stabilized the flow at Reynolds numbers up to 15,000.

Coke deposits were measured for both deoxygenated and aerated fuel in tests up to 100 hours duration. A 100-hour test run with deoxygenated fuel at a heat flux of about 1 Btu/sec-in^2 (1.6 MW/m^2) was completed with coke deposits less than 1 mil thick. The maximum tube temperature at the end of the run was 1400°F (760°C), less than the 1450°F (788°C) maximum at the start of the test. Deposits were found to be more severe and more irregular with the aerated fuel, and carburization of the tube occurred at the higher temperatures reached in this case. Different tube materials were screened in coker tests, and selected ones were tested further in the heat transfer test rig. Results of these experiments did not indicate any obvious relationship between coking tendency and tube material. Tests showed that the tube temperature was the most important variable in determining deposition rate. Coke deposits were found to have two effects on heat transfer, a beneficial effect by acting as a turbulence promoter to increase the convective heat transfer coefficient and a detrimental effect by increasing the resistance to heat transfer.

Pressure oscillations in the test section were audible at certain turbulent flow conditions when the exit fuel was near its pseudocritical temperature. Amplitudes ranged up to 350 psi (2.4 MN/m^2) and primary frequencies varied from 1000 to 5000 Hz.

S-14115

(This page is blank)

CONTENTS

S-14115

CONTENTS (Contd)

ILLUSTRATIONS

ILLUSTRATIONS (Contd)

S-14115

ILLUSTRATIONS (Contd)

S-14115

TABLES

SUMMARY

The potential use of Jet A fuel as a heat sink for cooling turbine engines was investigated in order to determine the heat transfer and coking characteristics associated with this application. Experiments were run over a wide range of conditions to obtain data on heat transfer and coke deposition. Most of the work was done in a heat transfer test rig in which flowing fuel was heated in tubes of 1/16 and 1/8-inch (0.16 and 0.32 cm) inside diameter. Heat fluxes varied from 0.02 to 4.0 Btu/sec-in^2 (0.0327 to 6.54 MW/m^2). Fuel pressures and temperatures ranged up to 1000 psia (6.90 MN/m^2) and 1000°F (538°C). Residence times of the fuel in the test section varied from 0.024 to 9.5 seconds, and run times ranged up to 100 hours. Jet A fuel was used under both deoxygenated and aerated conditions.

Heat transfer in both laminar and turbulent flows was studied at Reynolds numbers from 40 to 600,000. Considerable free convection in laminar flow greatly enhanced the heat transfer and resulted in temperature differences between the top and bottom of the tubes up to 150°F (83°C). The free convection apparently stabilized the laminar flow at Reynolds numbers up to 15,000 for high Grashof numbers. Turbulent flow occurred at higher Reynolds numbers and in several cases at Reynolds numbers down to 2200. Correlations were developed for predicting heat transfer coefficients in the two flow regimes. The Nusselt number for heat transfer in laminar flow with free convection was dependent primarily on the Grashof number, and to a lesser extent on the Prandtl number and the ratio of the bulk fuel density to the fuel density at the wall conditions. The Reynolds number, Prandtl number, and ratio of bulk fuel temperature to wall temperature were used in heat transfer correlations for turbulent flow.

Different tube materials were screened in coker tests, and further experiments were run in the heat transfer test rig in order to determine the influence of selected tube materials on coke deposition. Deposit measurements on all materials in the coker tests were found to be small or moderate, and there was no obvious correlation between coking tendency and tube composition. The only variable found to have a significant effect on deposit formation with the deoxygenated fuel was the tube temperature. Test runs with this fuel in the heat transfer test rig showed that the rate of coke deposition in general was significantly greater at tube temperatures above 1340°F (727°C).

Coke deposits were found to have two major effects on heat transfer. One was the direct effect of creating additional resistance to heat transfer. This effect was appreciable for thick deposits at high heat fluxes. The second effect was indirect and did not depend on deposit thickness. A coke layer always exposed a rough surface to the fluid flow, which increased the turbulence of the fluid if the flow was not fully turbulent. This then resulted in a substantial improvement in the convective heat transfer coefficient.

S-14115

Oxygen was found to have a strong influence on coke deposition and heat transfer. Even after completion of a 100-hour test run at a heat flux of 1.0 Btu/hr-ft^2 (1.63 MW/m^2), deposits formed from deoxygenated fuel were relatively thin, less than 1 mil (25 μm). The use of aerated fuel resulted in heavier and more irregular deposits. In a 100-hour run with this fuel the deposit filled the tube completely at one point but was porous enough to allow flow. Heat transfer resistances of these heavier deposits were greater, and inside tube temperatures reached a maximum of 1610°F (877°C). Carburization of the tube occurred at this temperature. Thermal cracking of the fuel accompanied the coke deposition and yielded light hydrocarbons and hydrogen. Products of cracking and coke formation also caused discoloration of the fuel from white to yellow or amber. The extent of cracking was small, and the cracking hence was a negligible contribution to the heat sink of the fuel.

Pressure oscillations were audible at certain turbulent flow conditions, when the outlet temperature of the fuel was near its pseudocritical temperature. Amplitudes of pressure fluctuations ranged up to 350 psi (2.4 MN/m^2) at frequencies between 1000 and 5000 Hz. The pressure oscillations were more common and more severe at 500 psia (3.45 MN/m^2) than at 1000 psia (6.90 MN/m^2).

S-14115

INTRODUCTION

In order to extend the range and speed of supersonic turbine aircraft, additional cooling of the engine and airframe is required. In many turbine engines compressor bleed air is used for cooling engine components. However, as design speeds of aircraft are increased, the cooling capacity of this air becomes more limited due to the increase in its stagnation temperature. Hence, there are two factors which limit the use of air for cooling engines at higher speeds: (1) Cooling requirements are much greater, and (2) the available heat sink of the air is less.

A convenient source of additional cooling capacity is the fuel carried on board the aircraft. Kerosene fuels currently used for limited cooling on turbine aircraft have a temperature limit in this application of 350°F (177°C). It would be advantageous to raise this limit, but knowledge of the fuel characteristics and behavior above this temperature is needed. Previous work on hydrocarbon fuels[1] has shown that coking may not be excessive at higher temperatures, although these tests were generally short and limited to a few conditions. More information on the coking of hydrocarbon fuels is needed at different conditions and for longer times.

The heat sink of Jet A fuel, a kerosene type, is 135 Btu/lb (314 kJ/kg) in heating from 100 to 350°F (38 to 177°C). If the temperature limit of Jet A fuel were extended, this heat sink would increase to 485 Btu/lb (1127 kJ/kg) at 800°F (427°C) and 500 psia (3.45 MN/m²), and to 685 Btu/lb (1592 kJ/kg) at 1000°F (538°C). This additional heat sink would increase considerably the cooling that could be accomplished in a supersonic or hypersonic vehicle.

The use of Jet A fuel as a heat sink was investigated in order to determine the heat transfer characteristics and problems associated with this application. Experiments were designed to cover a wide range of conditions, in order to obtain data for developing heat transfer correlations which could be used in designing heat exchange systems using Jet A fuel as a coolant. In this investigation fuel deposits, their effect on heat transfer, and flow instabilities were observed and measured to determine the extent that these problems would limit this use of the fuel.

The primary portion of the work was done on a heat transfer test rig in which the fuel flowed through a resistance heated tube. Various heat fluxes were used from 0.02 to 4.0 Btu/sec-in² (0.0327 to 6.54 MW/m²). Fuel inlet pressure was either 500 or 1000 psia (3.45 or 6.90 MN/m²), and fuel temperatures varied from 100 to 1000°F (38 to 538°C). Tube temperatures ranged up to 1650°F (899°C). Flow rates were varied so that residence times of the fuel in the heated test section varied from 0.024 to 9.5 seconds. Run times ranged up to 100 hours, and oxygen content in the fuel was varied.

Throughout the experiments the fuel inlet and outlet pressure and temperature and the tube temperatures at various points were monitored. The fuel from the test rig was cooled, gas flow was measured, and liquid and gas products were analyzed periodically. After each experiment the used tube was

---

1) See References.

S-14115

cut into sections for observation of coke deposition, and those sections which were exposed to more severe conditions were analyzed by combustion analysis to determine the weight of deposit. Tube sections exposed to the most severe conditions were also metallurgically examined for carburization of the tube.

Various metals and alloys were investigated to determine the effect of different tube materials on coke formation. A large number of metals and alloys were screened in a modified Jet Fuel Thermal Oxidation Tester (JFTOT), after which a few materials were selected for further testing in the heat transfer test rig. Deposits formed on the tubes in the JFTOT tests were measured on the Beta-Ray Deposit Rater (BDR).

TEST EQUIPMENT

Heat Transfer Test Rig

Flow System

A flow diagram of the unit assembled for use in these tests is shown in Figure 1. After being deoxygenated by nitrogen sparging the fuel was charged to a 60-gallon (0.23 m³) nitrogen-blanketed feed tank. (Air-sparged fuel was used for the final 100-hour test, so the nitrogen blanket was deleted for this test.) This tank was arranged so that additional fuel, nitrogen or air sparged, could be added during a test if a high feed rate made this necessary.

The feed pump was a triplex diaphragm unit capable of delivering 50 gal/hr (0.19 m³/hr) at 1500 psig (10.4 MN/m²) discharge pressure. The pump rate was set at least 5 gal/hr (0.019 m³/hr) above the desired feed rate with the excess flow bypassing through a relief valve back to the feed tank, which provided a uniform flow past the oxygen analyzer probe. Pressure pulsations were minimized by a pulse dampener installed in the pump discharge line. An 8-μm membrane filter located immediately following the pump discharge prevented any foreign solid matter from entering the test section. Flow rate was maintained by a control system containing an orifice meter, a flow recorder-controller, and an air-operated control valve. Because of the required wide range of flow rates, 0.5 to 294 lb/hr (0.23 to 133 kg/hr), it was necessary to have a number of control valves and orifice plates of different sizes available for substitution into the system between tests. A 2-liter (0.002 m³) calibrated length of industrial glass pipe arranged in parallel with the feed tank was used to make spot checks on the flow rate prior to and at intervals during a test. The test section inlet pressure was maintained by a pressure recorder-controller which actuated a pressure control valve in the system discharge line.

Two variable transformers were used to provide the necessary power to the test unit. The first was connected across a preheater, which was a length of stainless steel tubing used to heat the fuel to the required 100°F (38°C) temperature at the test section inlet. The second transformer was

Figure 1 follows

S-14115
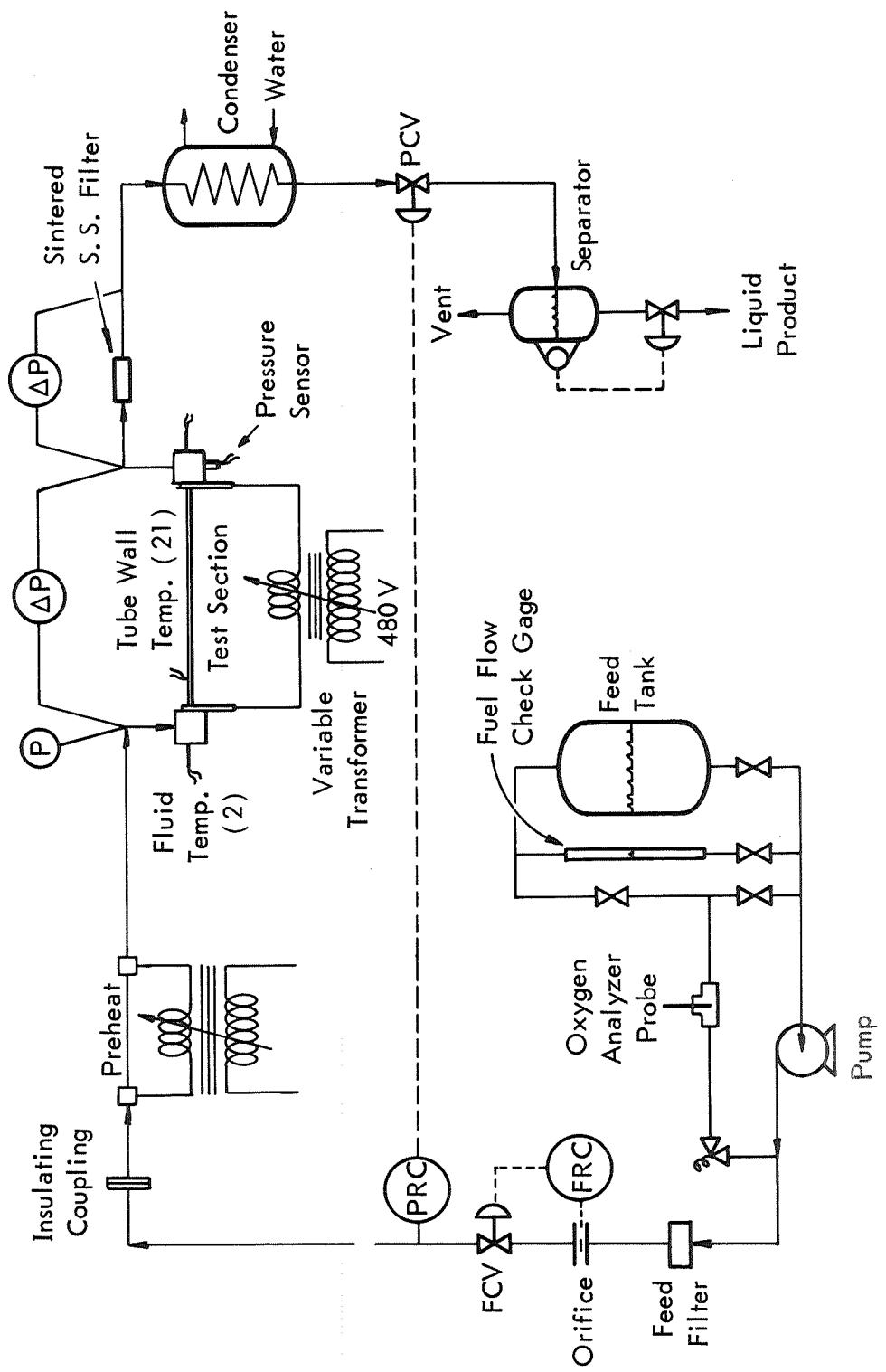
Figure 1. FLOW DIAGRAM OF HEAT TRANSFER TEST RIG

connected across the test section and was maintained at the power level required for the particular test in progress. Current through and voltage drop across the test section were constantly monitored and adjusted as necessary to compensate for line voltage changes, in order to maintain a constant heat flux during a test.

A sintered stainless steel filter with a nominal porosity of 5μm was positioned in the discharge line immediately following the test section to collect any coke particles present in the product stream. After the filter the product passed through a water cooled condenser, was reduced in pressure, and entered the separator vessel. Gaseous product was vented to a flare system, and liquid product was directed to storage for subsequent disposal.

Heat Exchange Test Sections

All test sections used in this study had 2-ft (0.61 m) heated lengths. Tube materials and diameters are given in Table I.

Table I. MATERIALS AND DIMENSIONS OF
HEAT EXCHANGE TEST SECTIONS

Tube Material	Nominal OD		True OD		True ID	
	inch	cm	inch	cm	inch	cm
Hastelloy C	1/8	0.32	0.1268	0.3221	0.0635	0.1613
Hastelloy C	3/16	0.48	0.1908	0.4846	0.1268	0.3221
Stainless Steel Type 316	1/8	0.32	0.1260	0.3200	0.0740	0.1880
L-605 (Haynes 25)	1/8	0.32	0.1278	0.3246	0.0651	0.1654

Electrical resistivity and thermal conductivity of the three tube materials are given in Figures 2 and 3. Note that Hastelloy C, which was the tube material used for most of the tests, has an essentially constant electrical resistivity over the temperatures encountered, and a constant heat flux (except for heat losses) could be assumed along the tube. However, this was not the case for the L-605 and stainless steel tubes. During the tests a variation in heat flux did exist along these tubes, and it was necessary to consider this when calculating inside tube temperatures as well as fluid temperatures.

A diagram showing a typical tube installed on the end-fitting blocks is shown in Figure 4. Before installation the tube sections were cut to the desired lengths, and nickel washers, 1/4-inch thickness x 1-inch OD (0.64 cm x 2.54 cm), were shrunk to fit onto the tube ends and welded in place. These washers were clamped to the end-fitting blocks by the copper bus bars as shown, and provided a seat for the sealing washer as well as a good electrical connection between the bus bars and the tube.

Figures 2, 3, and 4 follow

S-14115

Outside tube temperatures were measured by thermocouples whose junctions were spot-welded directly onto the tube. After spot-welding the junctions in place the tube was coated with a thin layer of ceramic cement. The thermocouple wires, electrically insulated from the tube by the cement layer, were wrapped in opposite directions one-half turn around the tube, and another layer of cement was applied over the tube and wires. The tube was insulated with about 1/2-inch (1.3 cm) of ceramic fiber mat and then with 3-inch (7.6 cm) OD magnesia pipe insulation. Some of the thermocouples were troublesome during the initial tests at high heat fluxes. This was minimized during later tests by more careful welding of the thermocouple wire pairs to a single point on the tube wall and by more complete electrical isolation of the recording instrument. Those thermocouples which gave unreliable data were readily identified during a test by a slow response of the recorder. These points were disregarded during data analysis and are not included in the data summaries.

Only 11 thermocouples were used initially. These were located alternately on the top and bottom of the horizontal tube. However, the difficulty mentioned above as well as the desire for better definition of the sometimes precipitous changes in the temperature profiles led finally to the installation of 10 additional thermocouples. These were spaced equally between the original locations. The final locations of the 21 thermocouples on the tube are shown in Figure 4.

Instrumentation

In addition to the control instruments and spot-welded thermocouples mentioned previously, the following instrumentation was also used in measuring and recording the test data.

Inlet pressure to the heat exchange section and pressure drops across this section and the product filter were measured by pressure transducers of the strain-gage type. A 0-1500 psia (0-10.4 MN/m^2) transducer was used for measuring the inlet pressure, and differential pressure transducers with ranges of 0-2.5, 0-25, and 0-500 psi (0-0.017, 0-0.17 and 0-3.45 MN/m^2) were used for measurements of pressure drop. The three measured pressures were continuously recorded on strip charts throughout each test run.

A crystal pressure sensor was mounted in one of the end-fitting blocks, initially in the inlet end and later the outlet end, to measure high frequency pressure pulsations. The signal from the sensor was amplified and displayed on an oscilliscope for visual observation. Photographs could be taken of interesting traces.

Fluid inlet and outlet temperatures, measured by sheathed thermocouples inserted into the end-fitting blocks (Figure 4), were recorded continuously on strip charts. The junctions of these couples were located only 1/16 inch (0.16 cm) from the ends of the tube to provide accurate measurements; however, at low flow rates there was sufficient heat loss from the fluid before it reached the exit thermocouple that measured outlet fluid temperatures were unreliable. In these cases exit fluid temperatures were calculated, using the measured power input, corrected for heat losses, and heat capacity data for the fuel.

-6-
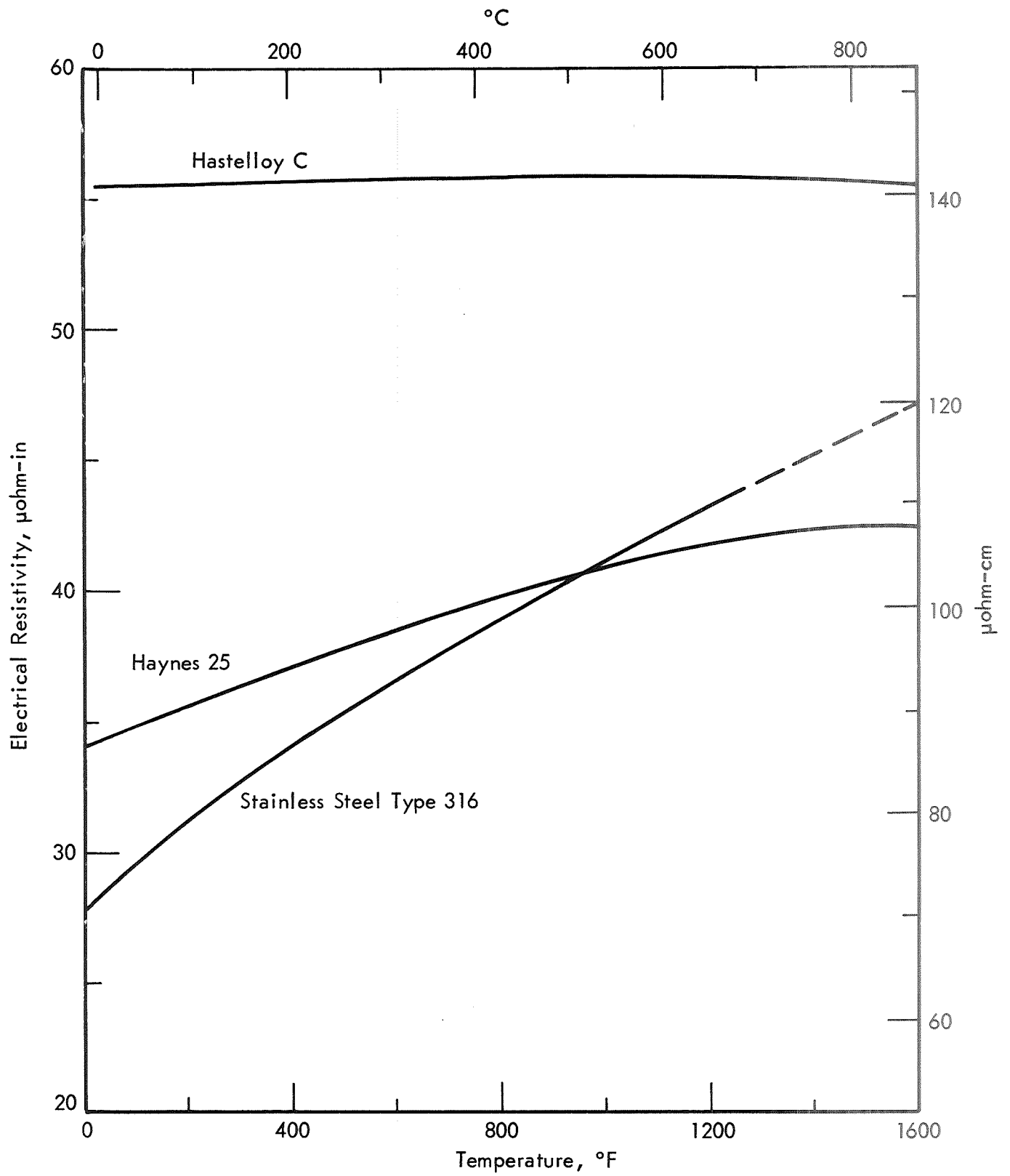
Figure 2. ELECTRICAL RESISTIVITY OF HEAT EXCHANGER TUBE MATERIALS
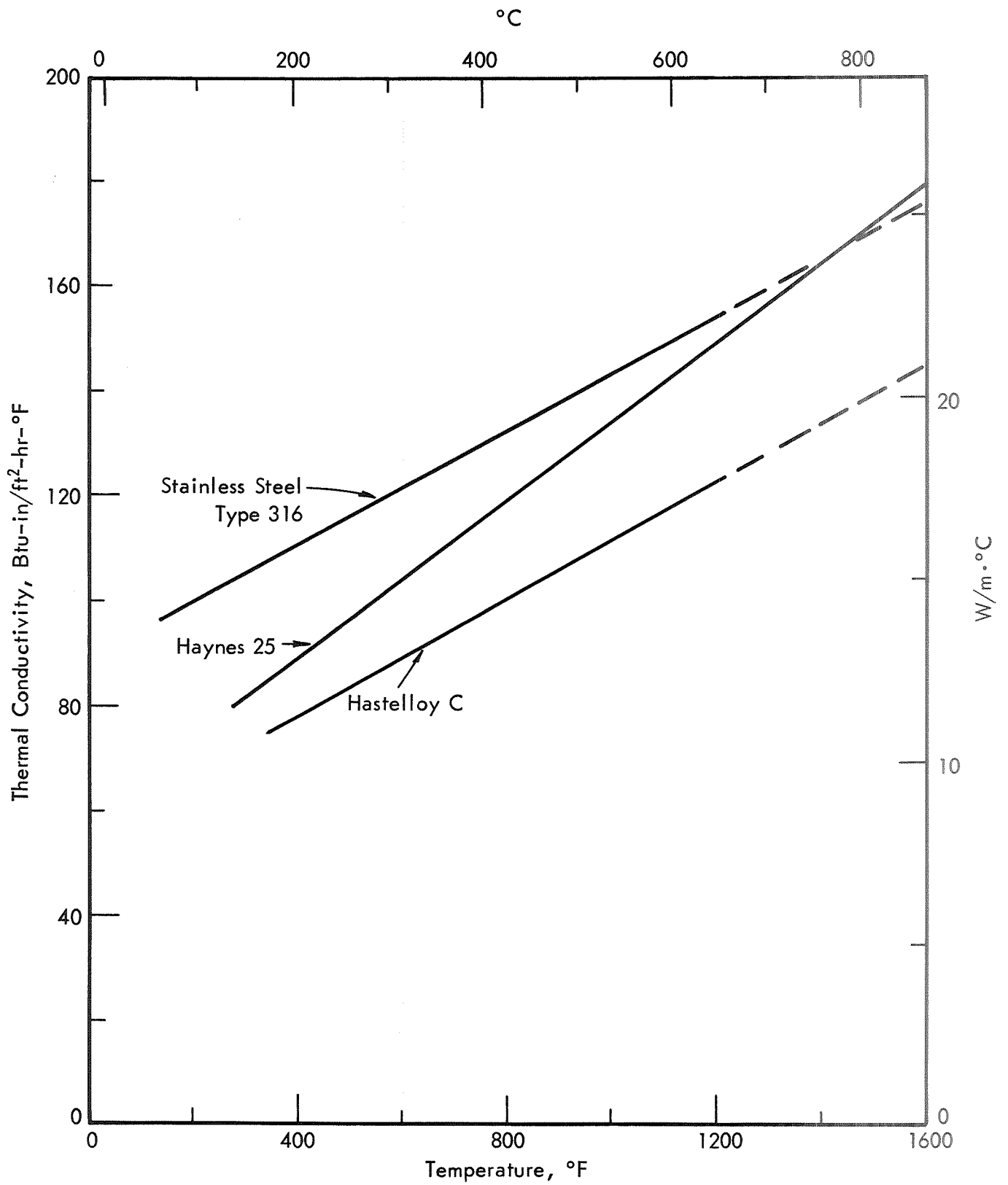
Figure 3.   THERMAL CONDUCTIVITY OF HEAT EXCHANGER TUBE MATERIALS
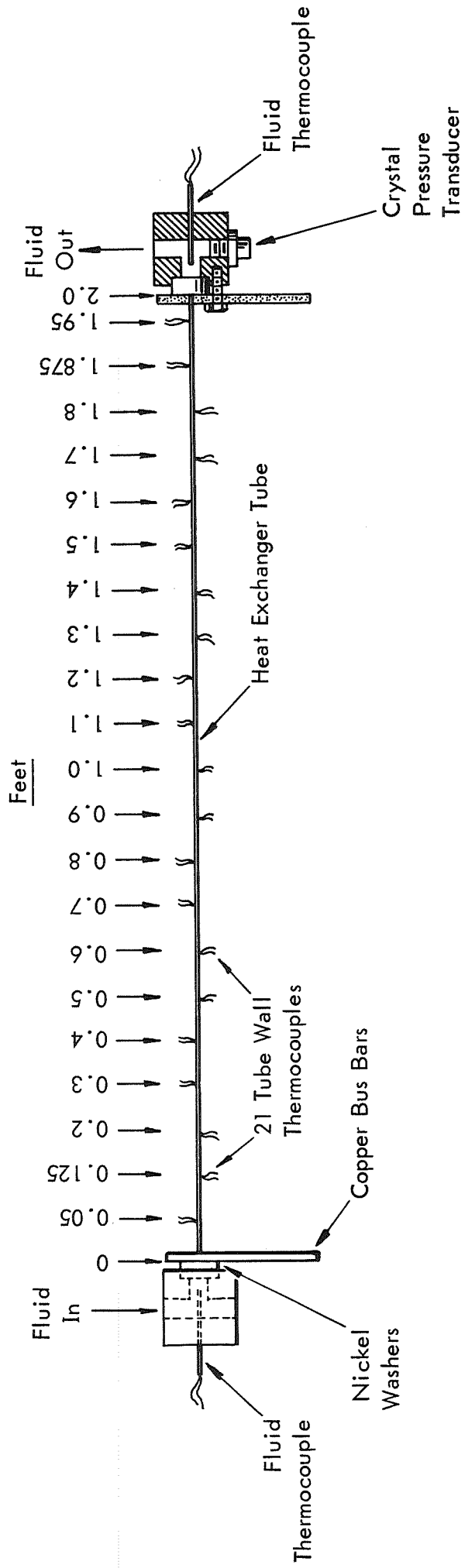
Figure 4. DIAGRAM OF HEAT EXCHANGE SECTION

S-14115
67374

Test Procedure

A test run was started by first setting the desired flow rate and inlet pressure. Then the inlet fuel was brought up to the desired 100°F (38°C) temperature. Finally the heat exchanger power was increased over a 5-10 minute period to give the required heat flux. Line voltage fluctuations required that frequent minor adjustments be made to the variable-transformer setting during a run. The feed rate controller required occasional small adjustment when spot checks showed some deviation from the desired flow rate. When shutting down, the reverse procedure was followed; first power was reduced and then the flow.

The 20-hour tests were run in 5-hour cycles, either one or two cycles per day. When only a single cycle was completed in a day, there was a normal shutdown-startup procedure between cycles. When two cycles were run per day, the break between cycles consisted of decreasing the temperature to 100°F (38°C) and then raising it to the test level again during a 15-minute period. The 100-hour tests were run in 10-hour cycles of one cycle per day. Thus, all breaks were complete shutdowns, but the down time was different, 14 hours overnight and 62 hours for a weekend.

Following each test the product filter was removed, rinsed with n-heptane, dried, and weighed to determine the amount of coke collected during the run. A new filter was weighed and installed preparatory to the next run. The exchanger tube was removed from the rig, cleaned of the ceramic cement layer, rinsed with n-heptane, and dried. It then was ready to be cut into sections for measurement of coke deposits.

Heat Loss

Heat loss from the tube wall was determined by the following procedure. A low power level was maintained across an empty insulated tube until the wall temperatures reached equilibrium. At this time power and temperature data were recorded. The resulting temperature profile was constant over most of the tube length with sharp changes only at the ends of the tube, so that end effects could be neglected. Hence, the heat loss was equal to the rate of heat generation, and the rate of heat generation was uniform and could be calculated from the power input. Measured heat loss per unit tube length as a function of outside tube temperature is given in Figure 5. For use in heat transfer calculations these data were reduced to a more convenient form by expressing them as heat fluxes for the two sizes of Hastelloy C tubes (Figure 6). Equations for the curves through the data are:

$$q = 0.090 \ T^{1.59} \text{ for } 1/8\text{-inch } (0.32 \text{ cm}) \text{ OD} \qquad (1)$$

$$q = 0.060 \ T^{1.57} \text{ for } 3/16\text{-inch } (0.48 \text{ cm}) \text{ OD} \qquad (2)$$

where q = heat flux based on inside tube surface area, Btu/hr-ft^2
           T = outside tube temperature, °F

Figures 5 and 6 follow

Equipment for Coker Testing

Jet Fuel Thermal Oxidation Tester

A modified Alcor Jet Fuel Thermal Oxidation Tester (JFTOT) was used to study the influence of tube metal composition on fuel thermal stability. This coker also was used to select the test fuel and to monitor its thermal stability during this program. The JFTOT is a miniature coker, the test section of which is an annular heater. A resistance heated inner tube is the test surface on which coke deposits form. A filter unit downstream of the test section is used to measure filter-plugging tendencies of the fuel during the test. The test section and the filter correspond to similar components in the ASTM fuel coker; however, the JFTOT has not yet been accepted by the ASTM for use in a standard test.

The JFTOT does offer significant advantages over the ASTM fuel coker in experimental work, chief among which are the rapidity of assembly, disassembly, and cleaning, and the need for only 1 liter ($0.001 \ m^3$) of fuel per test compared to 5 gallons ($0.02 \ m^3$) for the standard ASTM coker. Our JFTOT was specially designed and constructed by Alcor to withstand 1000 psig ($7.0 \ MN/m^2$) pressure and 1000°F (538°C) tube temperature. In our laboratory it has been modified further by installing a thermocouple in the discharge opening of the heater to measure liquid temperature in addition to the tube temperature profile usually measured. This arrangement allows the performances of the standard coker and the JFTOT to be compared directly on the basis of liquid temperature. Based on visual deposit ratings, such comparisons on Jet A fuel (F-187) showed agreement between the two methods within their reproducibility, which is within one code number. Further details of the design and operation of the JFTOT are given in the Appendix.

Beta-Ray Deposit Rater

The rating of deposits on the JFTOT tubes was done both visually and by the Beta-Ray Deposit Rater (BDR). Visual ratings are qualitative and are not always comparable, particularly among different metal substrates.

The BDR is an instrument that measures quantitatively the deposit on JFTOT tubes. In this rater a beam of low energy electrons impinges on the deposit and the tube surface, and the amount of backscatter of these electrons is measured to determine the deposit thickness. The backscatter of the electrons is a complex function of the average atomic number of the substrate surface, and the atomic number and surface density of the overlying deposit. The composition of the tube metal and calibration data for suitable organic films are used to interpret the instrument response and determine the thickness of the measured coke deposit. Calibration data for the instrument have been obtained for films on a wide range of substrate metals and alloys. These data fit a general correlation for backscatter count rate, in which the count rate is expressed as a function of the deposit thickness and the atomic numbers of the tube metal and deposit.
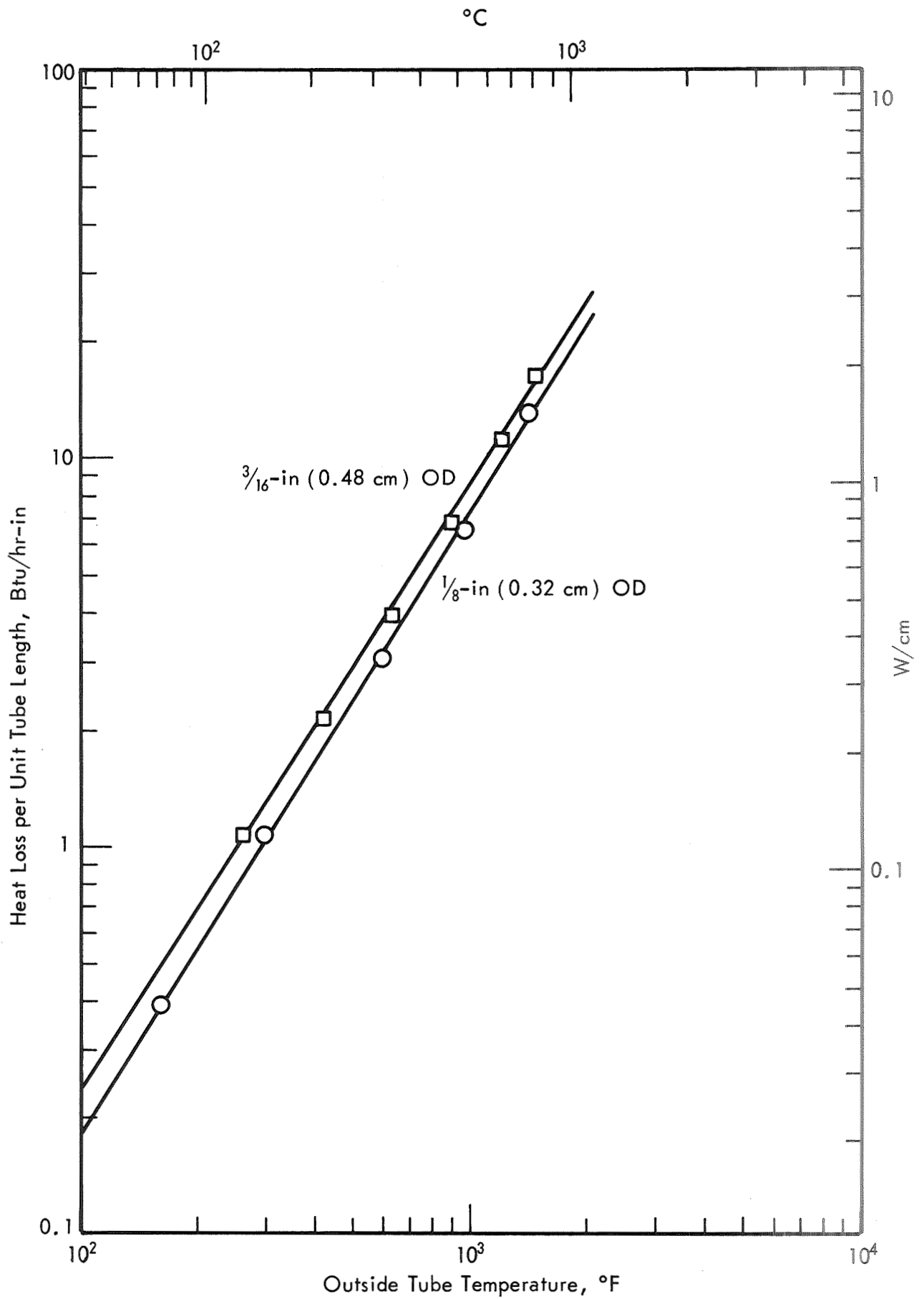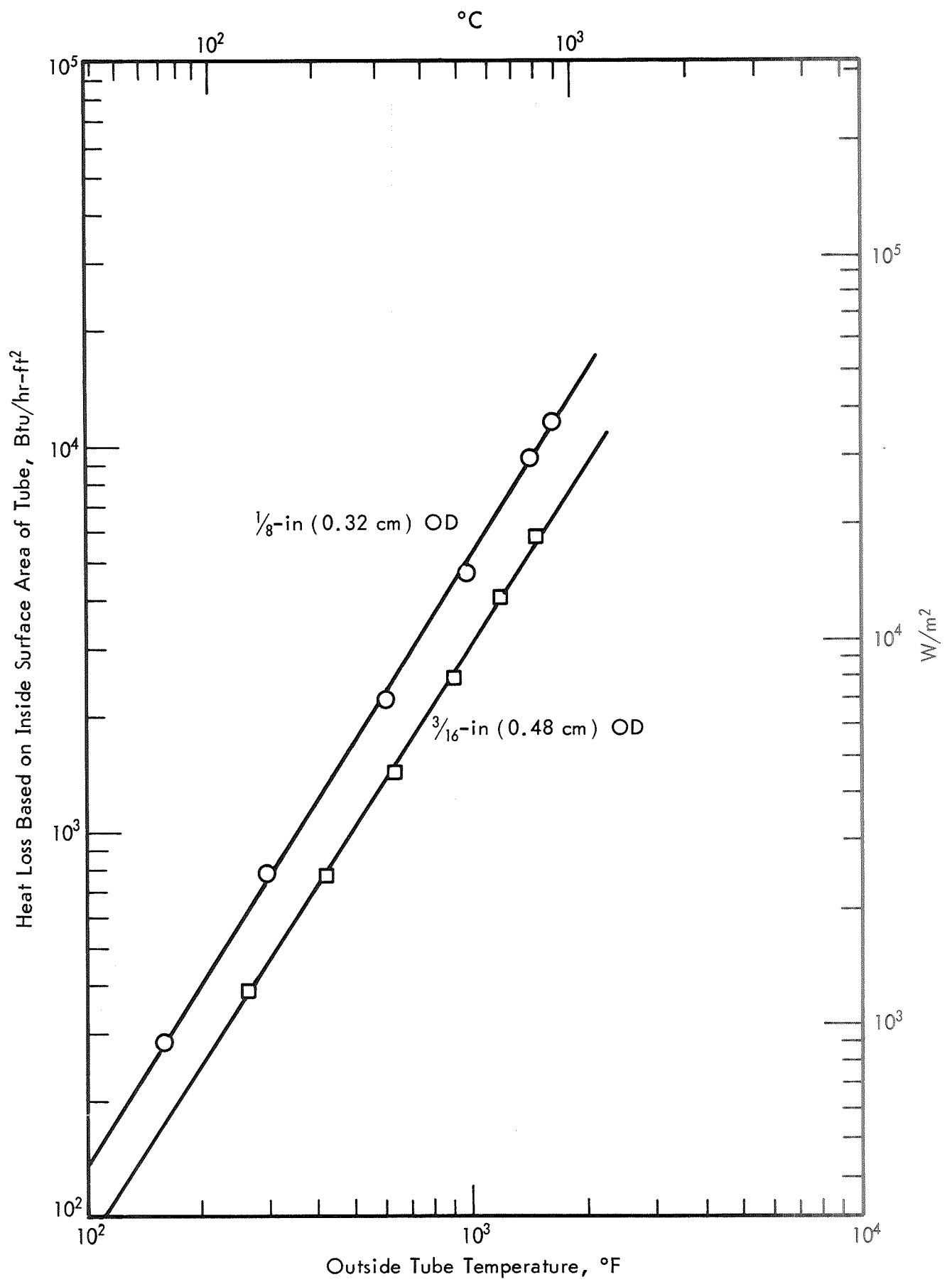
Figure 5.   HEAT LOSS FROM EXCHANGER TUBES

Figure 6.   HEAT LOSS FROM EXCHANGER TUBES

During the measurement of a deposit on a tube surface the tube is translated and rotated past an electron detector in the instrument. In this way the detector measures the backscatter of electrons from most of the tube surface. The signal from the detector is printed on a recorder chart, which is used to determine the maximum deposit thickness and the profile of the deposit. Further details of the design, construction, and use of the instrument appear in the Appendix.

FUEL SELECTION AND PROPERTIES

The fuels used in this work are specified by the ASTM Jet A turbine fuel designation, the specifications for which are listed in Table XIV in the Appendix. It was desired to use two fuels which differed in thermal stability breakpoint by 100°F (56°C) as measured by the standard CRC-ASTM coker. This was accomplished by using a fuel at two levels of oxygen content. In most of the heat transfer tests the fuel was used in a nitrogen-sparged or deoxygenated condition, at which the oxygen concentration was less than 0.5 ppm. For the final test the oxygen content of the fuel was raised to 66 ppm, the oxygen concentration of fuel in equilibrium with air at 1 atm (0.101 MN/m^2). This concentration was determined by gas-liquid chromatographic measurements.

Thermal Stability of Commercial Turbine Fuels

The thermal stability specification of Jet A turbine fuel requires that it pass the standard ASTM coker test at 300°F (149°C). A survey of the current commercial turbine fuel market showed that information generally was not available on actual coker ratings of fuels at different refineries, as control laboratory tests are normally run only to assure that fuels meet or exceed specifications. Because of this lack of information on thermal stability, it was impossible to select sources of two fuels with the desired difference in thermal stability. To determine the actual thermal stabilities of typical Jet A fuels, samples were obtained from seven refineries of Shell Oil Company and screened with our laboratory ASTM coker. This coker has been modified from the standard coker by substituting a gas drive for the pump. This modification results in more consistent ratings by eliminating the erratic and non-reproducible catalytic effects of debris produced from pump wear.

Sufficient coker runs were made with each fuel to determine its coker breakpoint temperature ($T_{2.5}$), i.e., the temperature at which the maximum code rating is between 2 and 3. Breakpoint temperatures for the fuels from the various refineries are shown in Table II. In some instances more than one sample was obtained from a refinery, and ranges of breakpoint temperatures are shown for these cases. Filter plugging generally was not limiting with these fuels and hence received little attention. All Shell Jet A fuels exceeded the minimum coker specification, generally by 100°F (56°C) or more. Moreover, the ratings for all but two fuels were bracketed between 400 and 450°F (204 and 232°C). Considerable effort was expended to obtain a fuel which rated above 450°F (232°C) to represent a fuel with high thermal stability. However, it was found that where such fuels occurred their compositions were not typical of normal refining. Therefore, a fuel with a breakpoint of 410°F

S-14115

(210°C) was selected, based upon it being representative of several samples with consistent ratings from the same refinery. Inspection data for this fuel, designated F-187 for laboratory use, are shown in Table XV of the Appendix.

Table II. ASTM COKER RATINGS OF SHELL
ATF-640 PRODUCTION TURBINE FUELS

Refinery Source of Fuel	Number of Samples	Range of Thermal Stability Breakpoint			
		Tube Rating[a]		Filter Rating[b]	
		°F	°C	°F	°C
A	6	405 - 450	207 - 232	> 415	> 213
B	9	400 - 420	204 - 216	> 415	> 213
C	1	420	216	> 425	> 218
D	1	435	224	> 440	> 227
E	1	415	213	410	210
F	2	420 - 485	216 - 252	> 450	> 232
G	1	390	199	> 425	> 218
Overall Range	21	390 - 485	199 - 252	> 410	> 210

a) Tube ratings are temperatures corresponding to code ratings of 2.5 max.
b) Filter ratings are temperatures at which the filter pressure drop reached the ASTM specification.

Physical Properties

Various analyses were made in order to determine the composition of the Jet A fuel used. These include analyses for hydrocarbon type, carbon number, ring number, degree of saturation, and impurities. Results of these analyses are shown in Table XVI of the Appendix. Fluorescent indicator analysis (FIA) showed that the aromatics content of the fuel was 15%, the balance being virtually all saturates. Using this value with the results of the mass spectrometer ring analysis, it can be deduced that the naphthene content of this fuel was about 47%.

Physical properties were estimated for the fuel, and several of these were used in later heat transfer calculations. These properties were based on experimental data or were calculated by well-known correlations or theoretical equations. Measurements of density, viscosity, thermal conductivity, and vapor pressure at various temperatures are listed in Table XVII of the Appendix. The enthalpy of the fuel was also obtained experimentally. Correlations for this property were developed based on

-10-

data obtained on the heat transfer test rig at temperatures up to 1000°F (538°C). Flow rates were sufficiently high that heat losses were relatively small and readily estimated. Measurements of power input corrected for heat losses, inlet and outlet fuel temperatures, and fuel flow rate were used to calculate fuel enthalpy. Results of the calculations and the derived correlating equations are shown in Figure 7.

Based on the experimental data, known correlations, and theoretical equations, physical properties were predicted for the fuel in the gas phase at different pressures and supercritical temperatures. Properties were also calculated for the liquid state at various saturation pressures and temperatures. Results of these calculations are listed in Tables XVIII and XIX of the Appendix.

Monitoring of Thermal Stability

When the fuel was obtained, it was stored in a railroad tank car and inhibited with 25 ppm IONOL® oxidation inhibitor to insure storage stability. The fuel was then nitrogen sparged until the dissolved oxygen content as measured by GLC analysis was reduced to less than 0.5 ppm. Afterwards a nitrogen blanket was kept over the fuel to maintain this low oxygen content.

ASTM coker and JFTOT tests were used to determine if the thermal stability specifications were met by the fuel and to detect any deterioration in fuel stability during the tests on the heat transfer test rig. When the fuel was acquired it was rated by the ASTM coker and then was tested monthly by the JFTOT to assure a constant thermal stability. No deterioration was detected over a period of one year. JFTOT ratings and ASTM coker ratings at similar conditions agreed within one code number. Later ratings were made from 2.5-hour runs on the JFTOT and correlated with ratings determined from 5-hour runs. Thereafter the shorter run times were used for monitoring the fuel.

All the coker tests were run under air-saturated conditions, whereas all except the last one in the heat transfer test rig were made with the dissolved oxygen content below 0.5 ppm. The fuel was saturated with air for the thermal stability tests in order to meet the requirements of the standard ASTM method in the Jet A specifications. This also allowed for easier and simpler control of the coker tests so as to obtain reproducible results. Deposit ratings for these tests were obtained visually by the conventional Tuberator method. Later the BDR was available for use and provided more accurate ratings.

HEAT TRANSFER STUDY

Test Conditions

All test runs which provided data for the heat transfer correlations were made with deoxygenated Jet A fuel (oxygen content less than 0.5 ppm) and Hastelloy C heat exchange tubes. The initial series of tests consisted of twenty-four 5-hour runs using 1/8-inch (0.32-cm) OD Hastelloy C tubes. Nominal operating conditions for these runs were combinations of the conditions given

-11-

in Table III. Other 5-hour tests were made later at the five conditions given in Table IV using 3/16-inch (0.48 cm) OD Hastelloy C tubes. One of these was started at 0.2 Btu/sec-in^2 (0.33 MW/m^2), 500°F (260°C), and 1000 psia (6.90 MN/m^2). After 0.5 hour the pressure was changed to 500 psia (3.45 MN/m^2) for the rest of the 5-hour period. In this way heat transfer data were obtained at two conditions while using one tube during a single test run. Coke formation was negligible at this fuel outlet temperature.

Table III. CONDITIONS FOR 5-HOUR HEAT
TRANSFER TESTS (SMALL TUBES)

1/8-inch OD x 24-inch L (0.32 cm x
61 cm) Hastelloy C Test Sections

Heat Flux		Fuel Outlet Temperature		Inlet Pressure	
Btu/sec-in^2	MW/m^2	°F	°C	psia	MN/m^2
4	6.54	500	260	500	3.45
1	1.63	800	427	1000	6.90
0.2	0.327	1000	538		
0.02	0.0327				

Table IV. CONDITIONS FOR 5-HOUR HEAT
TRANSFER TESTS (LARGE TUBES)

3/16-inch OD x 24-inch L (0.48 cm x
61 cm) Hastelloy C Test Sections

Heat Flux		Fuel Outlet Temperature		Inlet Pressure	
Btu/sec-in^2	MW/m^2	°F	°C	psia	MN/m^2
0.02	0.0327	1000	538	1000	6.90
0.2	0.327	1000	538	500	3.45
0.2	0.327	500	260	1000	6.90
0.2	0.327	500	260	500	3.45
1.0	1.63	800	427	500	3.45

-12-

Figure 7. ENTHALPY OF JET A FUEL

$$h = 0.453 + 0.462\,(T-100) + 3.33 \times 10^{-4}\,(T-100)^2$$

$$h = 0.473(T-100) + 2.75 \times 10^{-4}\,(T-100)^2$$

Experimental Data

▽ 200–400 psia
☐ 400–500 psia
△ 600–700 psia
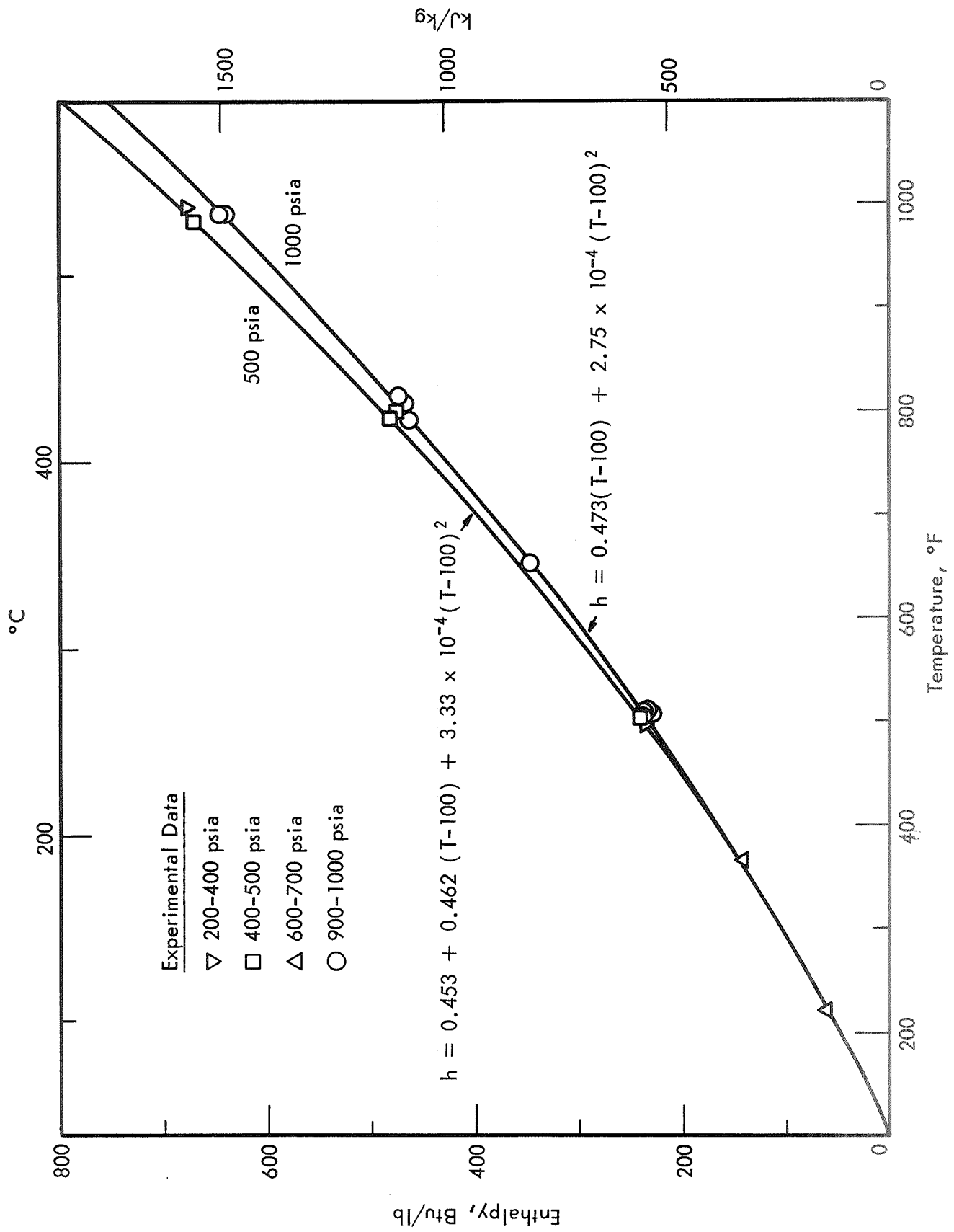◯ 900–1000 psia

1000 psia

500 psia

kJ/kg

°C

Temperature, °F

Enthalpy, Btu/lb

Experimental Results and Discussion

Data obtained during the 5-hour test runs are summarized in Table XX in the Appendix. Conditions and results listed included nominal test conditions and measured temperatures, pressure drops, flow rates, and weights of coke deposits. In many tests the product gas rate was insignificant and could not be measured. In other runs sufficient cracking of the fuel occurred, so that a measurable gas flow was produced. Tube temperatures were recorded throughout each test run, and representative temperature profiles are shown in Figures 8 to 17. In several runs there was little change in the tube temperatures, and the plotted curve is an average for the entire run. Where a change in temperature occurred during a test, profiles obtained at the start and end of the run are shown. Bulk fluid temperatures calculated from data on power input, flow rate, and enthalpy are also plotted.

At the higher heat fluxes of 1 and 4 Btu/sec-in^2 (1.63 and 6.54 MW/m^2) the flow rate was high and the flow was turbulent. In many runs the heat transfer coefficient was lower and the tube temperature highest where the fuel was near its pseudocritical temperature (Runs 30, 32, and 34; Figures 8 and 9). This relatively low value of the heat transfer coefficient near the critical temperature of the fluid has been observed in other work.[2,3] Reynolds numbers varied from 8000 to 600,000 in Runs 24 to 34 and from 2000 to 150,000 in Runs 36 to 46. In this latter series the flow was not completely turbulent near the inlet of each tube, and the heat transfer coefficient was low. Coke formation at this point during the test (Runs 40 and 46) caused more turbulence, which improved the heat transfer coefficient and decreased the tube temperature.

At heat fluxes of 0.2 and 0.02 Btu/sec-in^2 (0.327 and 0.0327 MW/m^2) the flow was generally laminar, but there was considerable free convection at the higher heat flux. The temperatures along the top and bottom of the tubes differed significantly in many of the runs, in some cases as much as 150°F (83°C) for the large tubes (Runs 75 and 77; Figure 16). At the lower heat flux the temperature differences between the fuel and the tube were smaller, and naturally the temperature differences between the top and bottom of the tube were also smaller. Reynolds numbers at various thermocouple locations during these runs varied from 40 to 28,000.

The temperature differences between the top and bottom of the tubes were due to free convection imposed on the laminar flow. As the fuel at the wall was heated, its density became less and it rose in the boundary layer from the bottom to the top of the tube, thus causing the top of the tube to become hotter than the bottom. The fuel then circulated down into the core of the fluid flowing through the tube, while colder fuel from this core moved toward the bottom of the tube. Variations in wall thickness around the tube circumference could account for only a small fraction of the observed temperature differences, and insulation was packed so tightly around the tube that these differences were not caused by free convection outside the tube.

Correlation of Data

Correlations were determined for heat transfer at the two flow regimes observed during the test runs. The flow was laminar at low flow rates, and heat transfer was enhanced considerably by the presence of free convection. Turbulent flow occurred at high flow rates with no indication of free convection.

Figures 8 through 17 follow

A representative portion of the data is plotted in <u>Figure 18</u>. In this figure experimental tube temperatures were used with calculated fuel temperatures to determine heat transfer coefficients, which are plotted as Nusselt numbers versus Reynolds numbers. Nusselt numbers in these test runs varied from 6 to 1100 and Reynolds numbers from 40 to 600,000. At low values of the Reynolds and Nusselt numbers the flow was laminar with considerable free convection. The transition to turbulent flow was indicated by the tube temperature profiles at Nusselt numbers of 25 to 30, even though Reynolds numbers varied up to values over 10,000 before transition occurred. Turbulent flow occurred at Nusselt numbers above 30, and in some cases Reynolds numbers were almost as low as 2200.

Data obtained during test runs at the two lowest heat fluxes were analyzed together to determine a correlation for heat transfer enhanced by free convection. The correlation was determined by linear regression using equations in logarithmic form. Different parameters were used in order to determine the variables which were most significant. The variables considered included Reynolds number, Prandtl number, Raleigh number, Grashof number, ratio of wall temperature to bulk fluid temperature, ratios of density and viscosity at these two temperatures, and dimensionless tube length. Experimental data were expressed as heat transfer coefficients in the form of a Nusselt number. Different forms of each dimensionless group were considered by using fluid properties based on the bulk fluid, mean film, and tube temperatures.

The Grashof number was the most significant variable for laminar flow heat transfer enhanced by free convection. The Raleigh number was equally significant, but this group was split into the more elementary Grashof number and Prandtl number. These latter two variables taken independently yielded a slightly better fit of the data than the Raleigh number alone.

The Grashof number is basically defined in terms of a temperature difference and a coefficient of thermal expansion, which should be based on a mean film or wall temperature. An alternate form of the Grashof number can be based on the difference in densities at the bulk fluid and wall temperatures. The density difference was considered more appropriate for defining the Grashof number in our tests, since temperature differences between the wall and the bulk fluid were large, and different phases frequently existed in these two regions. Fluid properties at the bulk fluid conditions were used as much as possible to define the correlating variables, since the equation then would be simpler to use in predicting heat transfer coefficients.

The data for laminar flow heat transfer enhanced by free convection are plotted in <u>Figure 19</u> as a function of the Grashof number, which is defined as follows:

$$Gr_B^! = \frac{gd^3 \rho_B (\rho_B - \rho_W)}{\mu_B^2} \qquad (3)$$

-14-   Figures 18 and 19 follow

Figure 8. TUBE AND FLUID TEMPERATURES FOR 5-HOUR RUNS 26, 28/84 AND 32

Figure 9. TUBE AND FLUID TEMPERATURES FOR 5-HOUR RUNS 24, 30 AND 34

Figure 10. TUBE AND FLUID TEMPERATURES FOR 5-HOUR RUNS 38, 40 AND 46

Tubes: ⅛ inch (0.32 cm) OD Hastelloy C
Heat Flux: 1 Btu/sec-in² (1.63 MW/m²)
Inlet Pressure: 1000 psia (6.90 MN/m²)

Run 38
Exit Fluid: 500°F (260°C)

Run 40
Exit Fluid: 800°F (427°C)

Run 46
Exit Fluid: 1000°F (538°C)

Tube
0 hr
5 hr

Bulk Fluid
0-5 hr

0-5 hr

Figure 11. TUBE AND FLUID TEMPERATURES FOR 5-HOUR RUNS 36, 42 AND 44

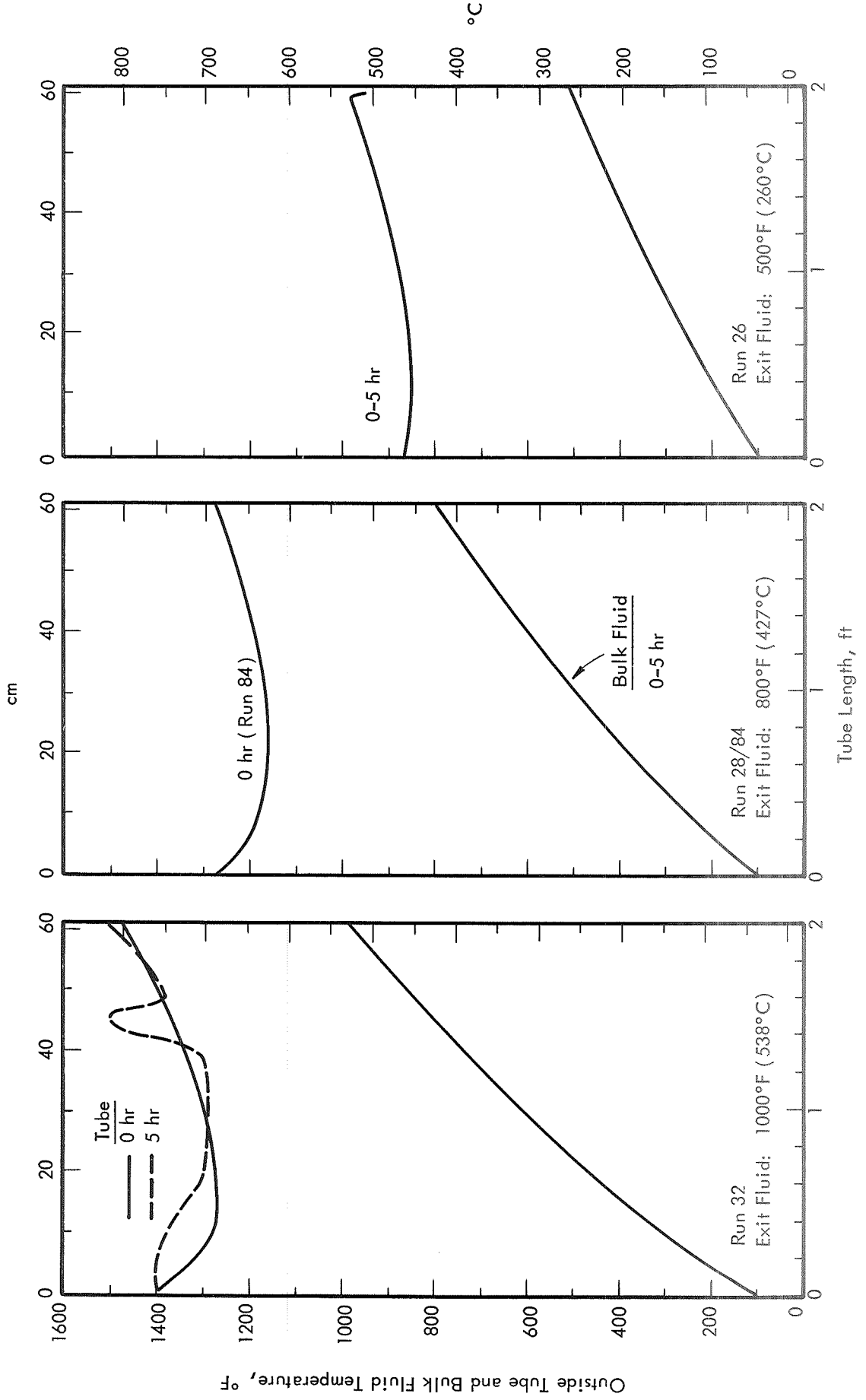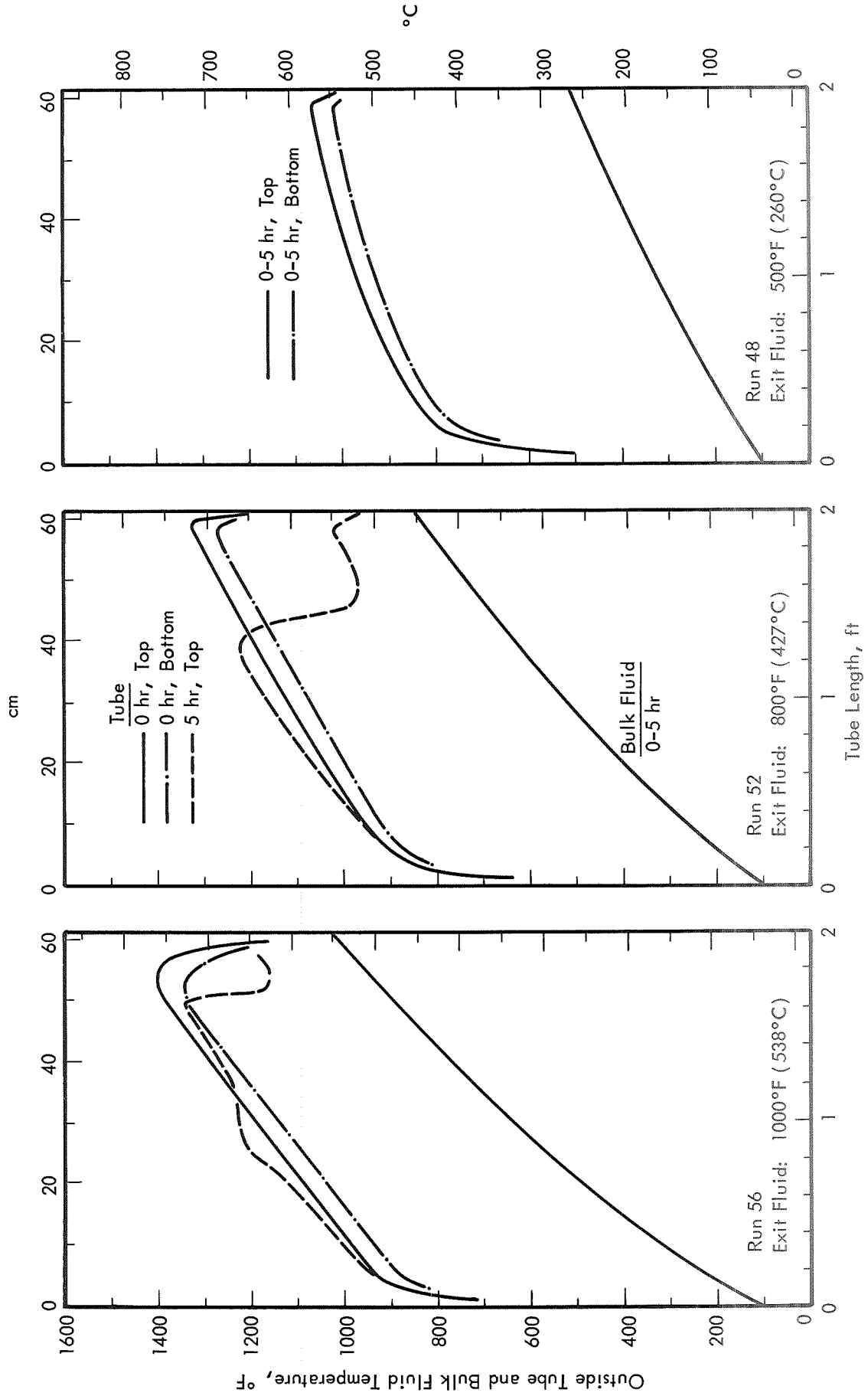Figure 12. TUBE AND FLUID TEMPERATURES FOR 5-HOUR RUNS 48, 52 AND 56

S-14115
67374

Figure 13. TUBE AND FLUID TEMPERATURES FOR 5-HOUR RUNS 50, 54 AND 58

Tubes: ⅛-in (0.32 cm) OD Hastelloy C
Heat Flux: 0.2 Btu/sec-in² (0.327 MW/m²)
Inlet Pressure: 500 psia (3.45 MN/m²)

Tube
0-5 hr, Top
0-5 hr, Bottom

Bulk Fluid
0-5 hr

Run 50
Exit Fluid: 500°F (260°C)

Run 54
Exit Fluid: 800°F (427°C)

Run 58
Exit Fluid: 1000°F (538°C)

Tube Length, ft

cm

°C

Outside Tube and Bulk Fluid Temperature, °F

S-14115
67374
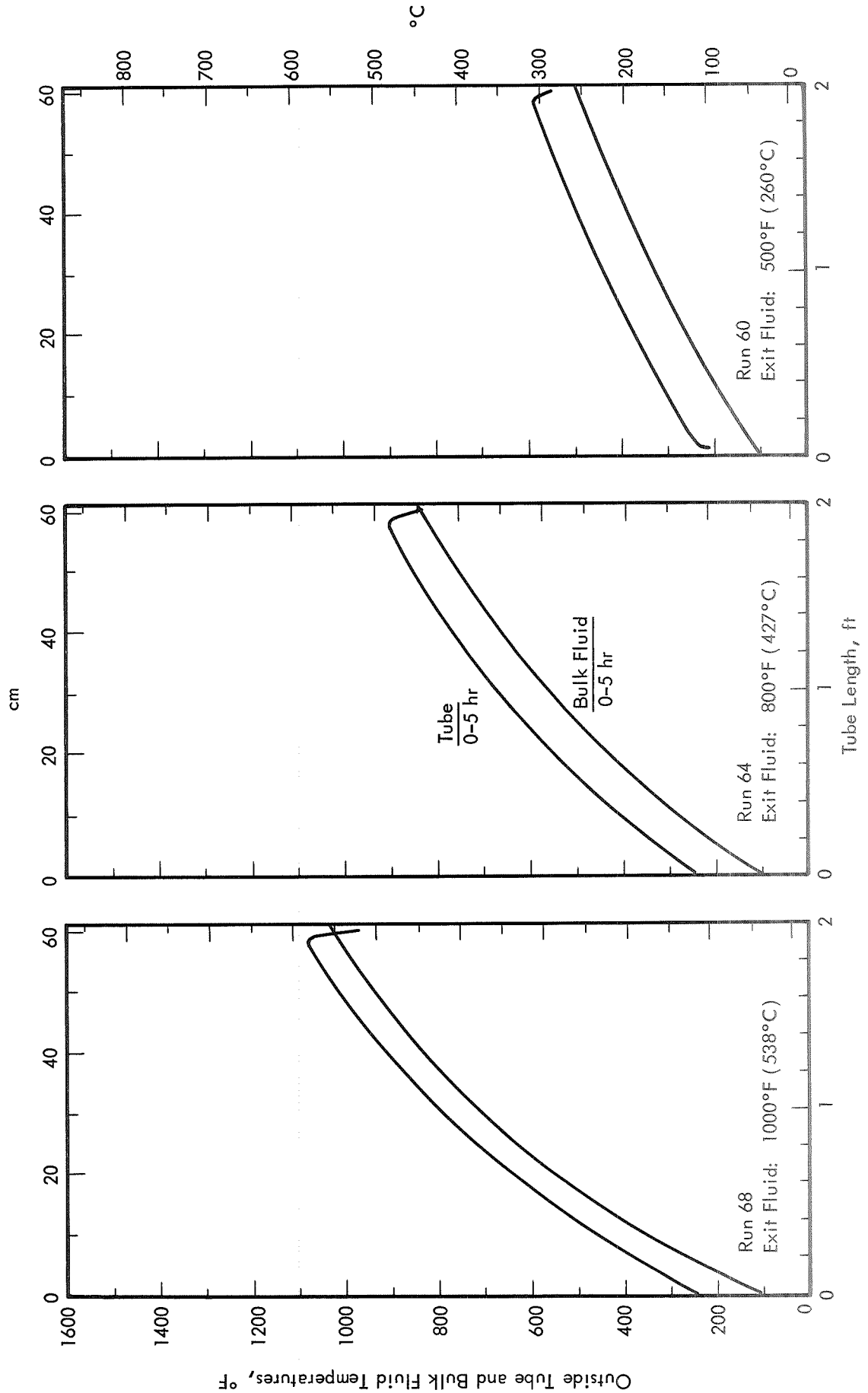
Figure 14. TUBE AND FLUID TEMPERATURES FOR 5-HOUR RUNS 60, 64 AND 68

S-14115
67374
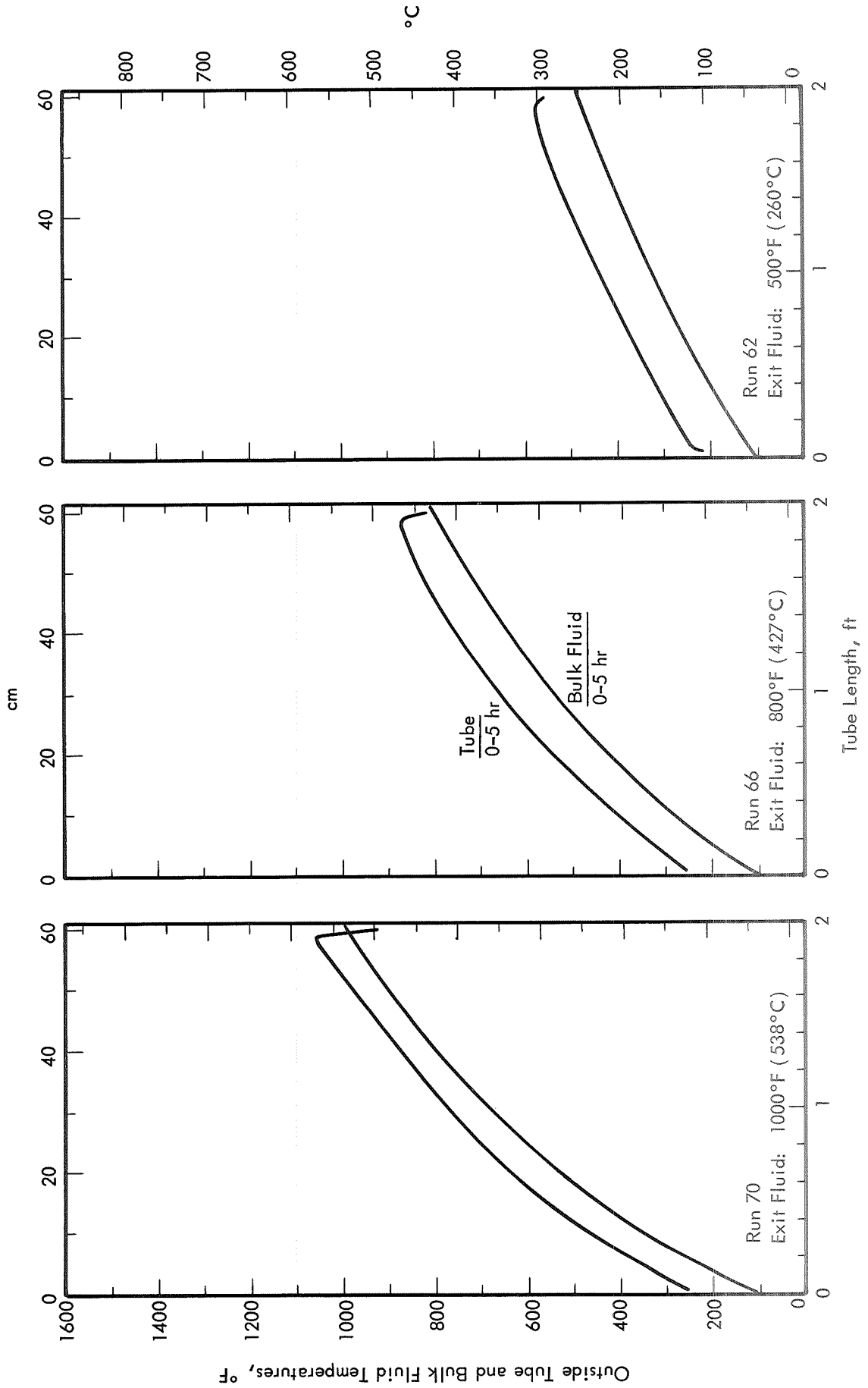
Figure 15. TUBE AND FLUID TEMPERATURES FOR 5-HOUR RUNS 62, 66 AND 70
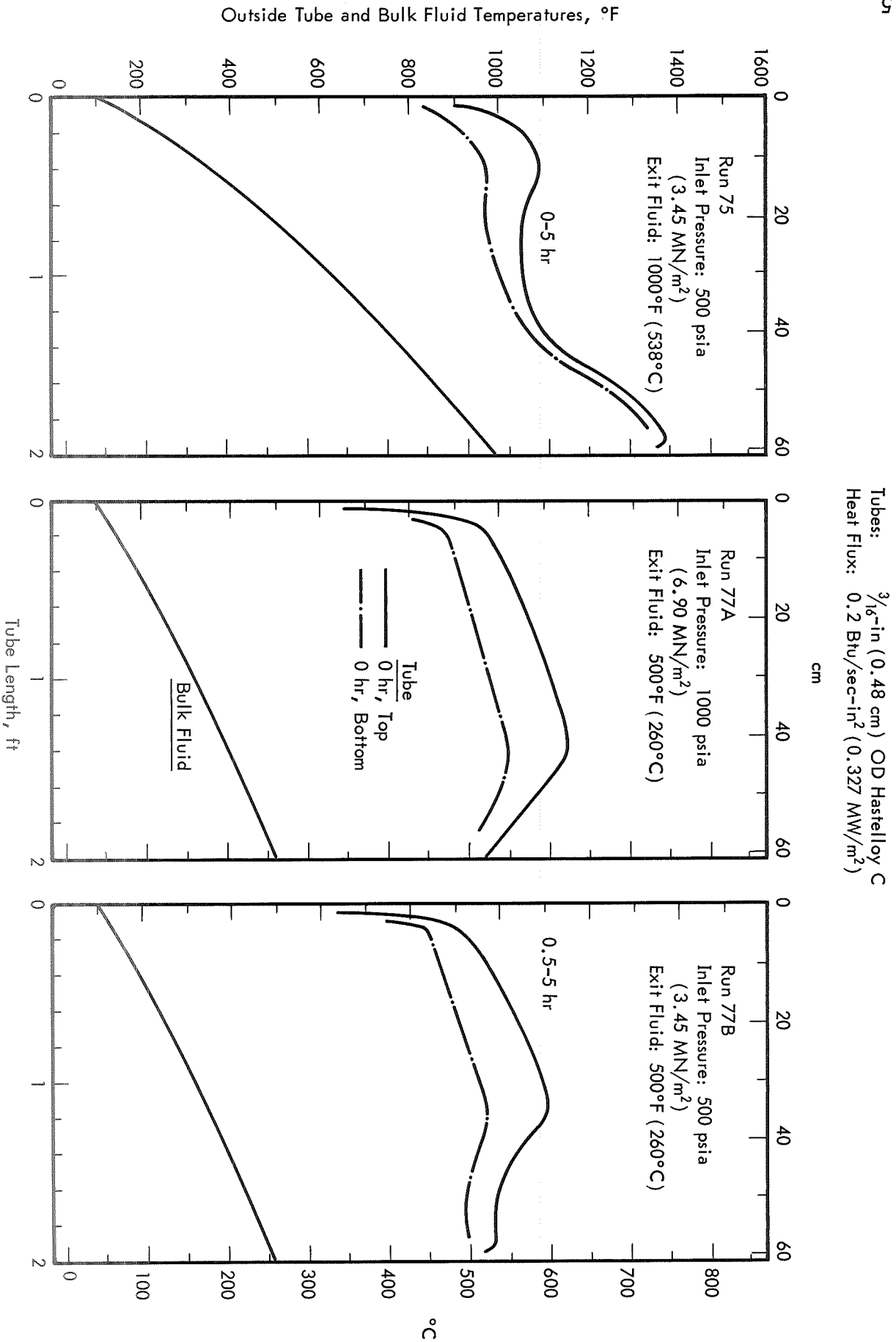
Figure 16. TUBE AND FLUID TEMPERATURES FOR 5-HOUR RUNS 75, 77A AND 77B
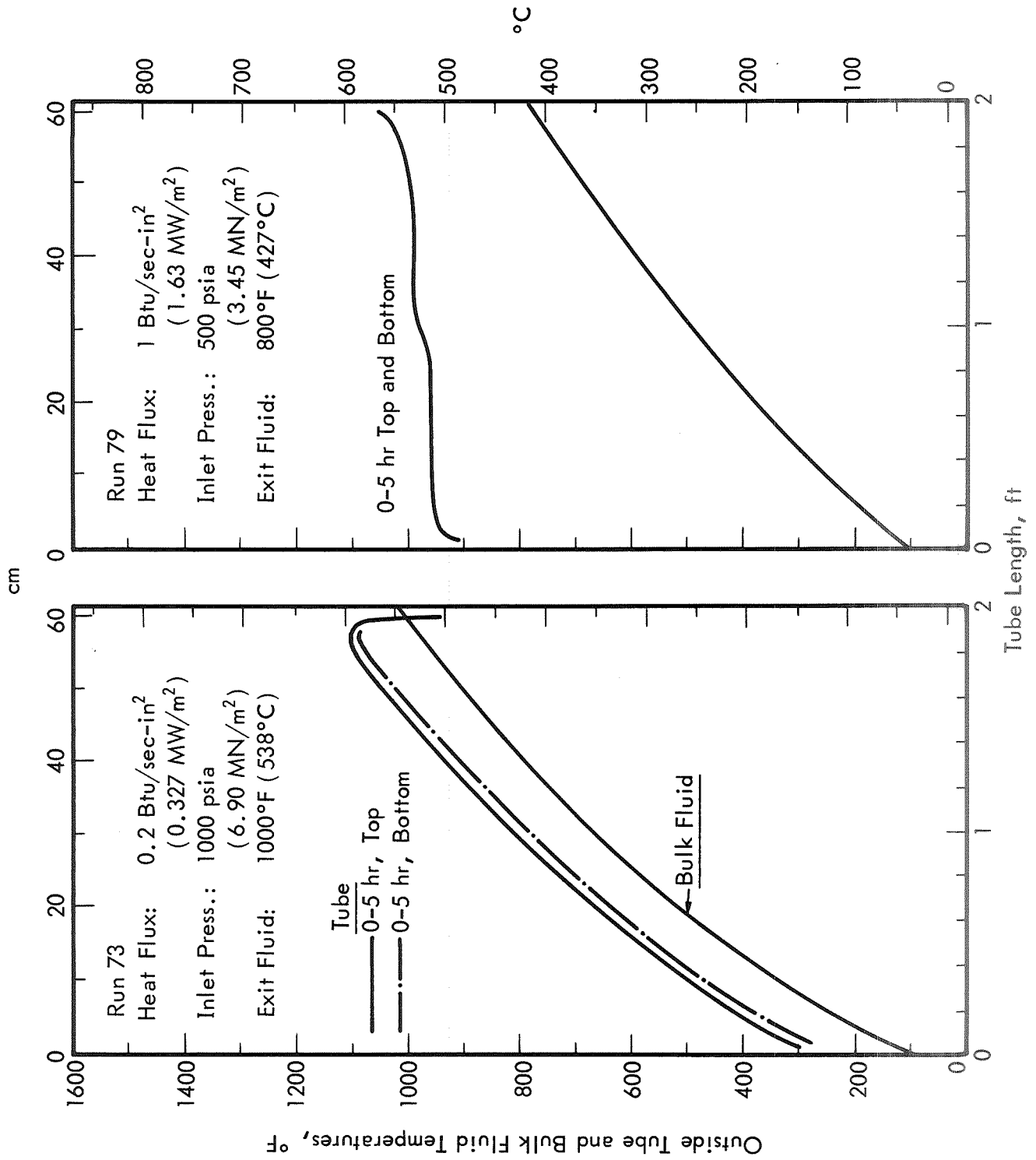
Figure 17. TUBE AND FLUID TEMPERATURES FOR 5-HOUR RUNS 73 AND 79

Tubes: $^3/_{16}$-in (0.48 cm) OD Hastelloy C
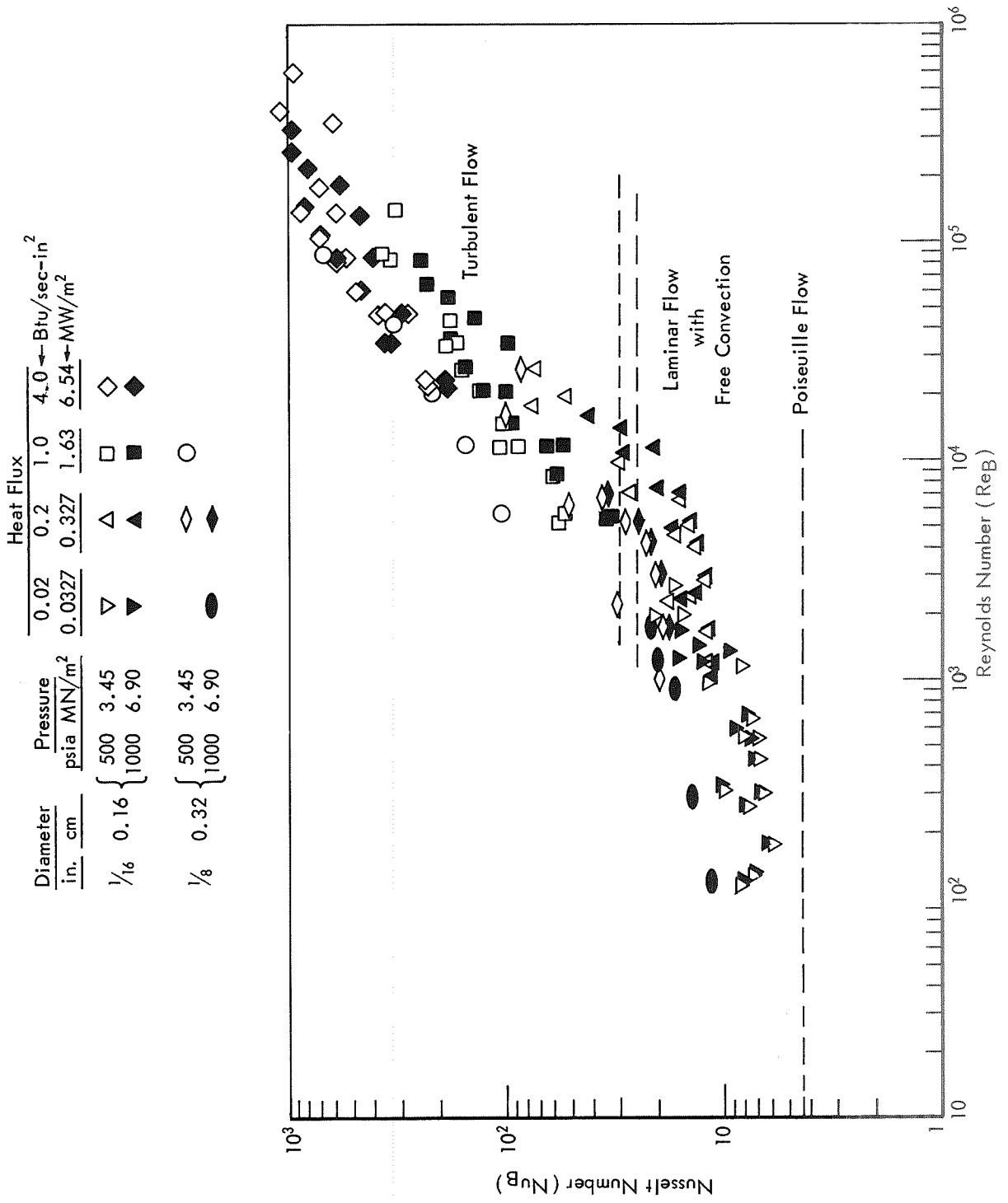
Figure 18. EXPERIMENTAL HEAT TRANSFER DATA

S-14115
67374
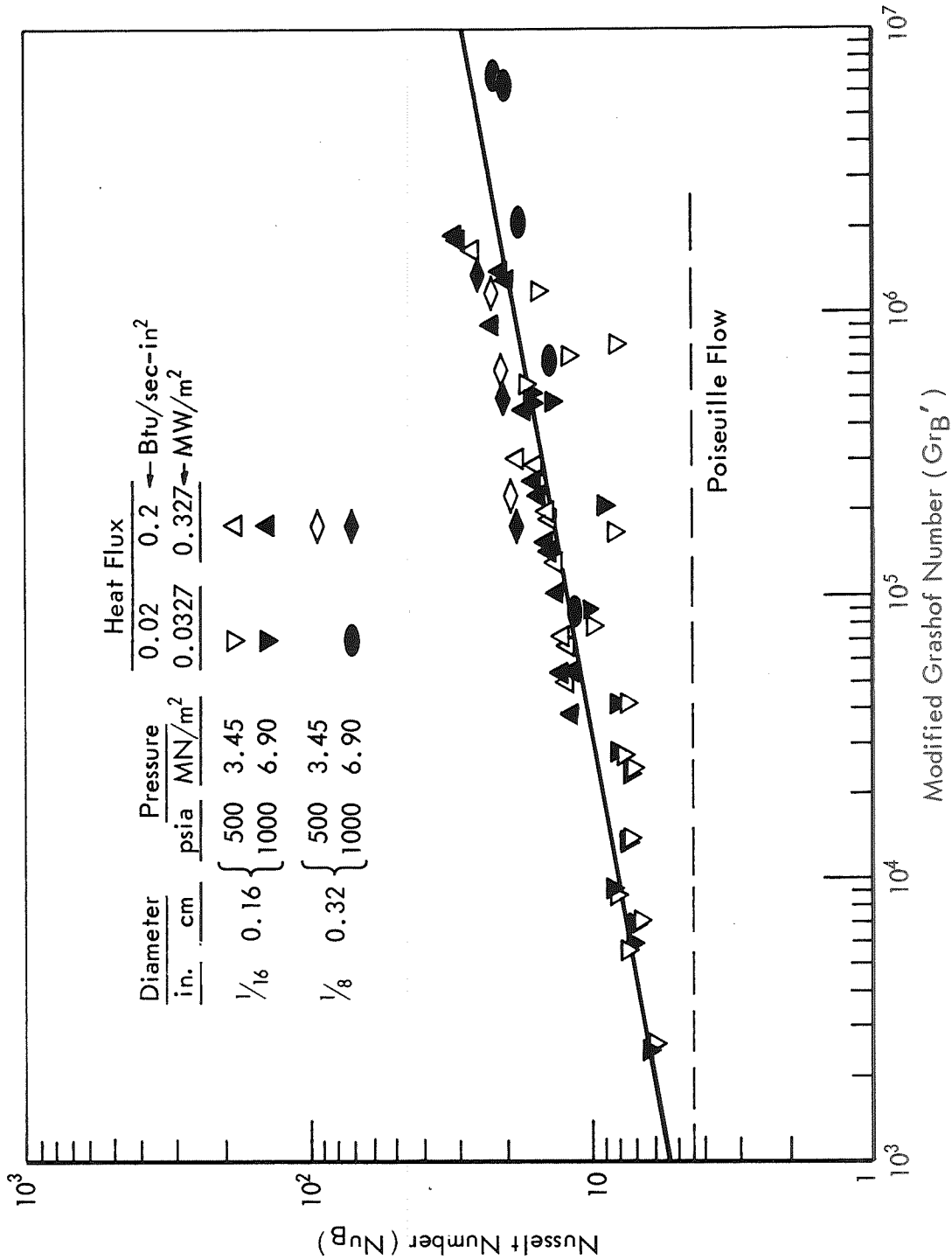
Figure 19. DATA FOR HEAT TRANSFER IN LAMINAR FLOW WITH FREE CONVECTION

```
Gr' = Modified Grashof number
  g = gravitational acceleration
  d = tube diameter
  ρ = fluid density
  μ = fluid viscosity
```
subscript B = bulk fluid conditions
subscript W = local mean wall conditions

The data at the higher heat flux lie along the curve with very little scatter. The data for the lower heat flux extend over a wider range of Grashof number and have more scatter. This deviation is due to less accuracy in the data, which was caused by more significant heat losses at the lower heat flux.

Analysis of the experimental data resulted in the following equation for heat transfer in laminar flow with free convection:

$$Nu_B = Nu_P \left[1 + a(Gr_B')^b \; Pr_B^{\;c} \left(\frac{\rho_B}{\rho_W} \right)^d \right] \tag{4}$$

where
$$a = 0.0255 \quad \text{(coefficient for the local mean Nusselt number)}$$
$$b = 0.316 \pm 0.019$$
$$c = 0.149 \pm 0.056$$
$$d = 0.353 \pm 0.046$$
$$Nu = \text{Nusselt number}$$
$$Nu_P = \text{Nusselt number for Poiseuille flow} = 4.364$$
$$Pr = \text{Prandtl number}$$

The standard deviation for this equation was 25%. A plot of experimental and predicted values is shown in Figure 20. This figure also shows the greater deviation of the data at the lower heat flux.

Different values were determined for the coefficient in the above correlation in order to predict the different temperatures along the top and bottom of the tube:

$$a = \begin{cases} 0.0237 & \text{(top of tube)} \\ 0.0273 & \text{(bottom of tube)} \end{cases}$$

These coefficients are used in Equation (4) to calculate Nusselt numbers which will predict the local maximum or minimum wall temperature. In this use the symbol ρ_W refers to the fluid density at the local mean wall temperature as defined for Equation (3).

-15-   Figure 20 follows

The above equation was found to give the best fit of the data without being too cumbersome. Other parameters were considered in the correlation, but the fit improved only marginally. The form of Equation (4) was selected so that it would reduce to the prediction for laminar flow in the absence of free convection.

During tests in which flow transition occurred, the change from laminar flow was sharp, but the approach to fully turbulent flow was gradual. Because of this, data on which the turbulent flow correlation was based ranged in Reynolds numbers from 40,000 upwards to 400,000. The following equation resulted from correlation of the data:

$$Nu_B = a \, Re_B{}^b Pr_B{}^c \tag{5}$$

where

$a = 0.00466$
$b = 0.927 \pm 0.048$
$c = 0.628 \pm 0.058$
$Re = $ Reynolds number

The standard error for this correlation was 10.6%. <u>Figure 21</u> shows the deviation of the experimental data from the Nusselt numbers predicted by equation (5).

Some improvement in the fit of the turbulent flow correlation was obtained by using a temperature ratio, which resulted in the following equation with a standard deviation of 7.7%:

$$Nu_B = a \, Re_B{}^b Pr_B{}^c \left(\frac{T_B}{T_W} \right)^d \tag{6}$$

where

$a = 0.525$
$b = 0.582 \pm 0.059$
$c = 0.554 \pm 0.043$
$d = 1.084 \pm 0.148$
$T = $ absolute temperature

<u>Figure 22</u> compares the experimental data with Nusselt numbers predicted by this equation. This figure shows that a slightly better fit of the data is obtained by the addition of the temperature ratio to those parameters used in Equation (5).

Equation (5) has an exponent on the Reynolds number which is in the expected range for turbulent flow. The exponent on the Reynolds number in Equation (6) is appreciably lower than this. Hence, Equation (6) should not be extrapolated outside the range of the data. Equation (5) is more straightforward to use in predicting heat transfer coefficients than Equation (6), and the standard deviations for these two equations are not too different. For these reasons Equation (5) generally should be the preferred heat transfer equation for turbulent flow.

Figures 21 and 22 follow

S-14115

Diameter		Pressure		Heat Flux	
in.	cm	psia	MN/m²	0.02	0.2 ← Btu/sec-in²
				0.0327	0.327 ← MW/m²
$\frac{1}{16}$	0.16 $\left\{\vphantom{\begin{matrix}a\\b\end{matrix}}\right.$	500	3.45	▽	△
		1000	6.90	▼	▲
$\frac{1}{8}$	0.32 $\left\{\vphantom{\begin{matrix}a\\b\end{matrix}}\right.$	500	3.45		◇
		1000	6.90	⬬	◆

$$Nu_B = Nu_P \left[1 + a(Gr_B')^b Pr_B^c \left(\frac{\rho_B}{\rho_W}\right)^d \right]$$
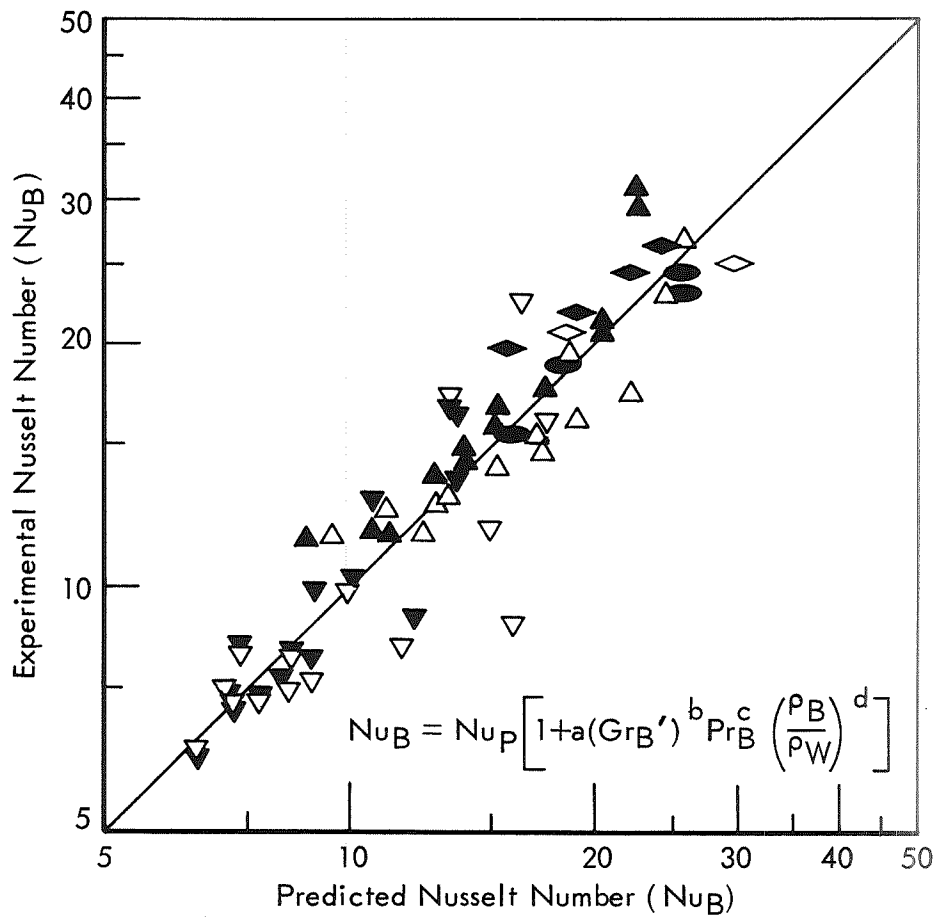
Figure 20. CORRELATION OF DATA FOR HEAT TRANSFER IN LAMINAR FLOW WITH FREE CONVECTION
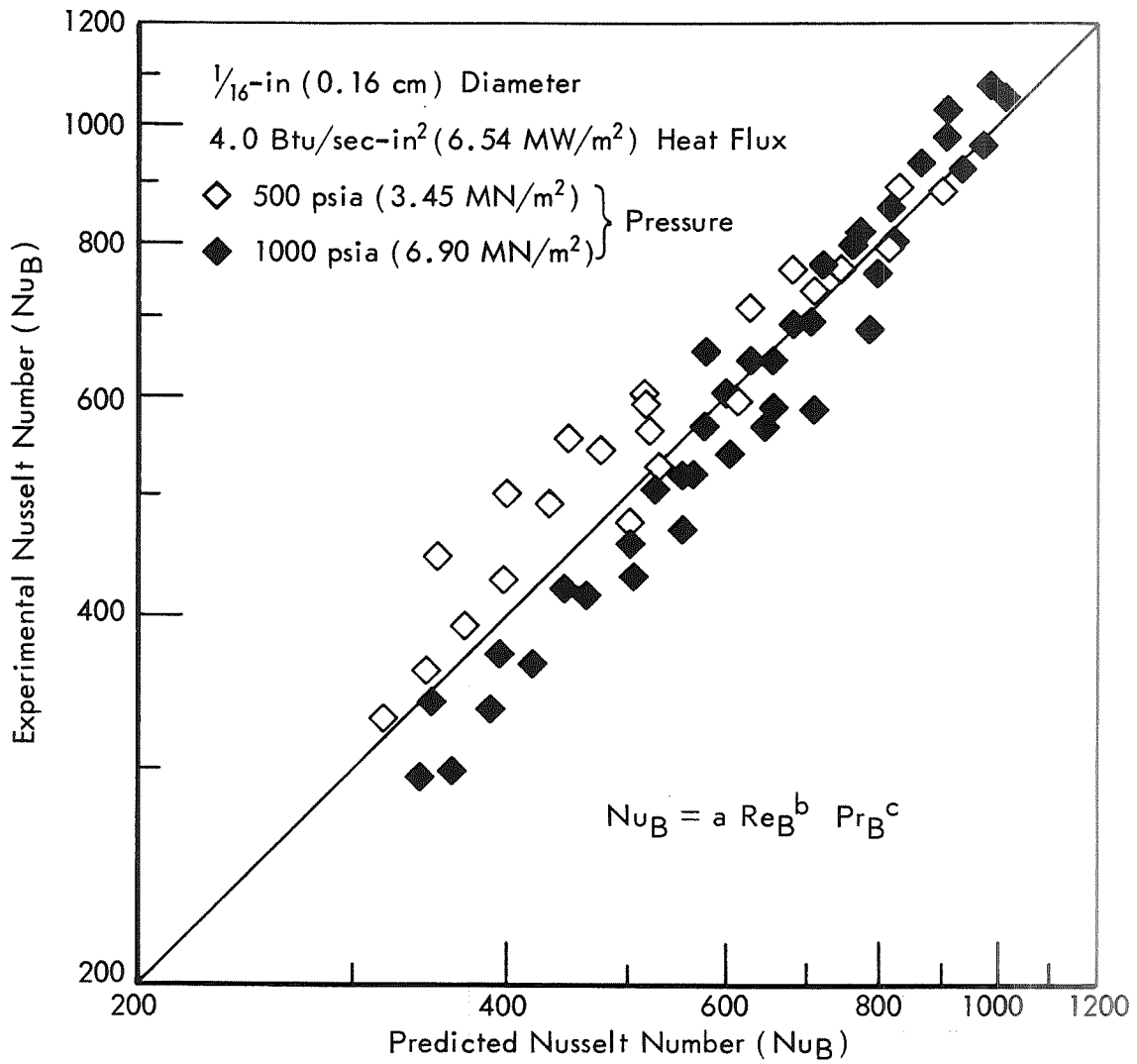
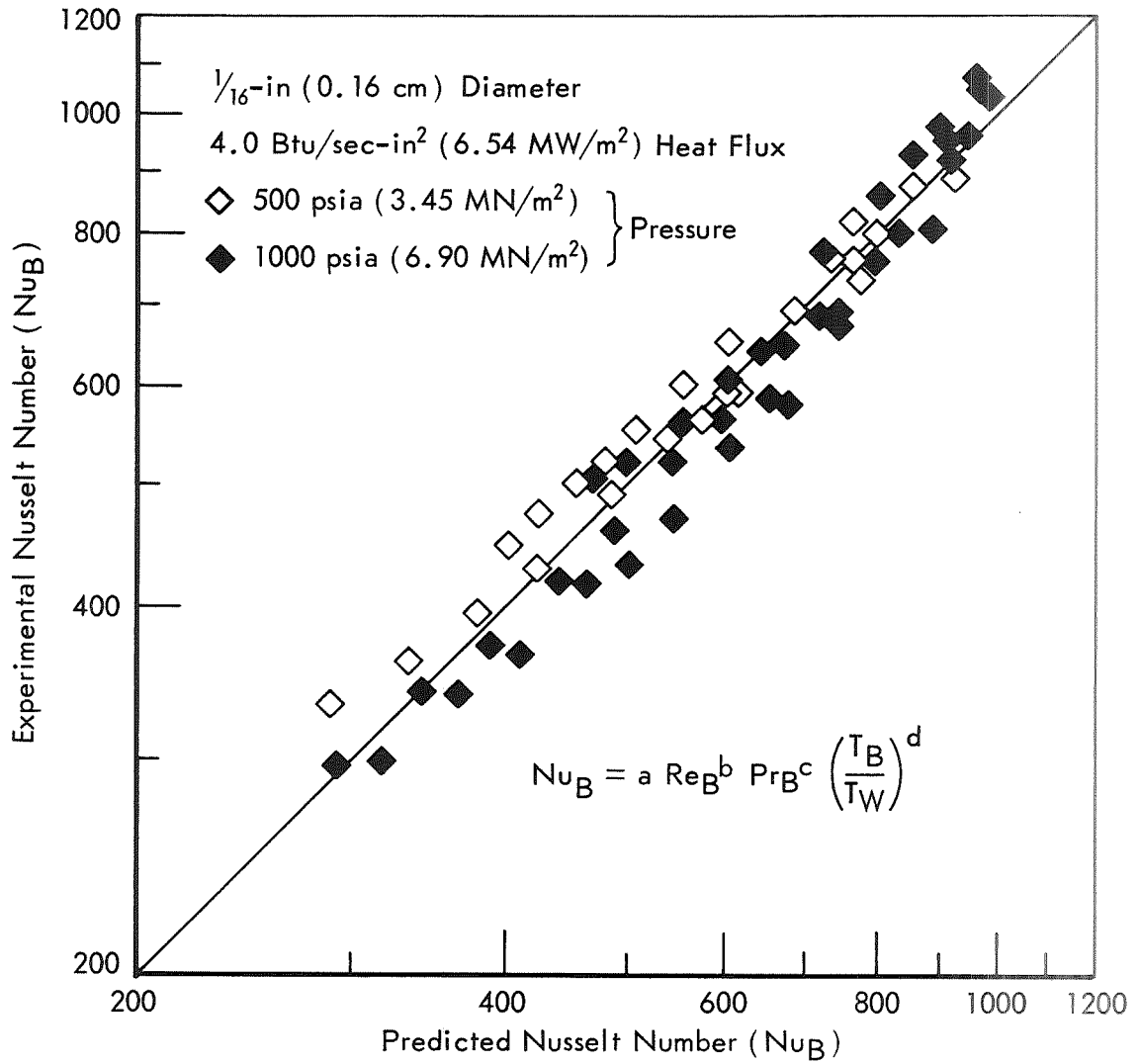Figure 21. CORRELATION OF DATA FOR TURBULENT FLOW HEAT TRANSFER

Figure 22. CORRELATION OF DATA FOR TURBULENT FLOW
HEAT TRANSFER

It is desirable to have criteria for predicting the type of flow regime for given conditions. These should depend primarily on the Reynolds number and secondarily on the Grashof number, since the Reynolds number is characteristic of the flow, and the Grashof number is an indication of the extent of free convection.

Figure 23 is a plot of the data, Grashof number versus Reynolds number, with the type of flow indicated for different regions on the graph. Laminar flow with free convection occurred at low Reynolds numbers. This type of flow apparently was stabilized by free convection, which is indicated by the increased limit on the Reynolds number for laminar flow at high Grashof numbers. At this condition laminar flow occurred at all Reynolds numbers below 5000. Between Reynolds numbers of 5000 and 15,000 there were conditions at which laminar flow occurred and other conditions at which turbulent flow occurred. The flow was turbulent at all Reynolds numbers above 15,000.

COKE DEPOSITION STUDY

Coker Tests

Tube Materials and Test Conditions

In addition to time, temperature, and pressure, catalytic effects of the heat transfer surface can influence the thermal stability of a fuel. For example, in tests using a standard ASTM-CRC fuel coker, Smith[4] found that copper had a significant harmful effect on jet fuel thermal stability, beryllium had a moderate effect, and lead and tungsten were slightly harmful. Seventeen other metals, including aluminum, chromium, cobalt, iron, and nickel, had no significant effect at test temperatures up to 400°F (204°C). The total fuel-metal contact time was about 10 seconds, of which only 4 seconds was the exposure time of the bulk liquid at the control temperature. Other researchers[5,6] also have reported the harmful effects of copper on thermal stability, but little appears to have been reported of the effects of different metals on deposition at higher temperatures and shorter residence times.

In this investigation fourteen different tube materials were tested with air-saturated Jet A fuel (F-187) in the JFTOT. Twelve of these are listed with their compositions in Table V. The other two materials were TD nickel and stainless steel type 304, both with aluminized surfaces. Efforts were made to obtain additional metals, such as Rene 41, Hastelloy X, Incoloy 800, and other stainless steels containing high percentages of nickel, cobalt, chromium, and molybdenum. These were particularly difficult to obtain in the proper size to fabricate JFTOT tubes. Mill runs were not justified since compositions of these alloys were intermediate to those in Table V. L-605 alloy was obtained by a special mill run since it was uniquely high in cobalt and tungsten.

Testing of Jet A fuel on the JFTOT has shown a consistent visual rating of code 2 with an aluminum tube. Conditions for this result were 410°F (210°C) liquid temperature, 300 psig (2.1 MN/m²) fuel pressure, and 5-hour run times. Since most other metals have less favorable effects on thermal stability than aluminum, 410°F (210°C) and 300 psig (2.1 MN/m²) were chosen as the standard conditions for JFTOT screening tests with different tube materials.

-17-

Figure 23 follows

Table V. COMPOSITIONS OF MATERIALS FOR ALCOR JFTOT TUBES

Tube Material	Average Atomic Number	Typical Composition, %											
		Ni	Co	Cr	Mo	Fe	C	Al	Cu	Mn	W	Si	Other
Hastelloy C	31.16	54.6	2.5	15.5	16	5	0.08	--	--	1.0	4	1.0	0.35 V
Monel 400[a]	27.89	(65.17)[b]	--	--	--	1.2	0.13	--	32.33	1.05	--	0.09	0.008 S
Inconel 600	27.21	(72.0)[b]	--	15.5	--	10	0.15	--	0.5	1.0	--	0.5	0.015 S
Stainless Steel Type 316[a]	26.2	13.28	--	16.75	2.50	65.14	0.05	--	--	1.73	--	0.51	0.035 P+S
Stainless Steel Type 304	25.5	9	--	19	--	72	0.08	--	--	--	--	--	--
Stainless Steel Type 446	24.6	--	--	25	--	75	0.35	--	--	--	--	--	--
TD Nickel	29.15	2.0%w	(2.2%w)[b]	Thorium Dioxide dispersed in Nickel (a Cermet)									
Nickel 200[a]	27.47	(99.56)[b]	--	--	--	0.04	0.06	--	0.01	0.26	--	0.04	0.005 S
Cartridge Brass	28.7	30	--	--	--	--	--	--	70	--	--	--	--
1015 Steel	25.96	--	--	--	--	99.85	0.15	--	--	--	--	--	--
L-605 (Haynes 25)	33.49	9.90	51.75	19.85	--	1.60	0.12	--	--	16.5	15	0.60	0.15 P+S
6061-T6 Aluminum	13.3	--	--	0.2	--	0.7	--	97.52	0.28	0.15	--	0.6	{ 0.25 Zn / 0.15 Ti / 1.0 Mg }

a) Compositions of these materials are given as certified by the supplier.
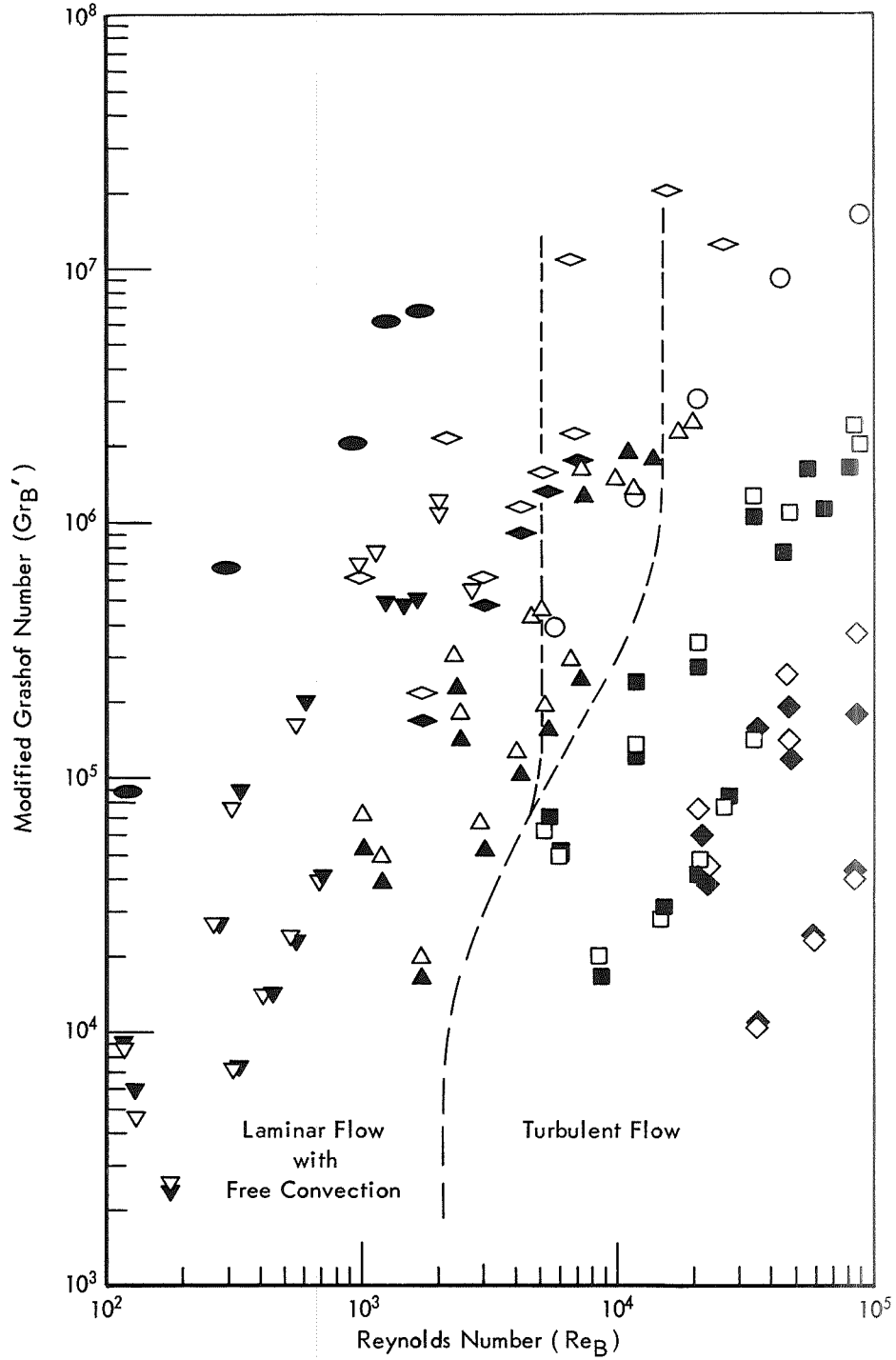b) Predominantly nickel; cobalt normally less than 0.25%.

Figure 23. FLOW REGIMES DURING HEAT TRANSFER TO JET A FUEL

JFTOT tests can be run by maintaining a constant liquid temperature or a constant tube temperature. The catalytic activities of metals should be compared by rating the materials at identical temperatures. However, because of differences in tube dimensions and thermal properties, temperature profiles for the various metals would be different. Also, the point of maximum temperature would occur at different locations along the tube length. Hence, it is difficult to maintain similar temperatures for the different metals. On the other hand, the fuel flow rate, liquid effluent temperature, and heat flux can be duplicated easily in each test, and these were chosen as the basis for the conditions in the screening tests.

It is possible that the results for the relative coking tendencies of the metals are valid only for temperatures in the neighborhood of 410°F (210°C) and perhaps only for the particular fuel tested. This temperature is low compared to temperatures encountered in the heat transfer tests, which is a reason for screening tube materials at a higher temperature. Certainly, reaction mechanisms change and become more or less prominent as temperature changes. Also, the type of coke likely to form at the higher temperatures in the heat transfer tests could be a different type than that formed in the coker. However, coker deposits are thermal oxidation products and as such probably are subject to catalytic effects of metals more so than coke derived from high temperature exposure, such as during thermal cracking. Thin coker-type deposits, because they occur at lower temperatures, may be the type that forms at the inception of heavy coke formation, and hence may be more dependent on metal types than the heavier deposits from cracking reactions.

The selection of 410°F (210°C) as the screening temperature was also dictated by the equipment characteristics. First, accurate measurement of deposit thicknesses by the BDR with the present low energy electron source and calibration data is limited to 3000 Å (0.3 μm). This limit can be extended by using a more energetic radiation source if calibration data are available, but such a change would be accompanied by a sensitivity loss in measuring low deposit thicknesses. It was anticipated that the selected temperature level for the screening tests would produce deposits within the current range of the BDR. Second, selection of the mild 410°F (210°C) temperature would avoid possible bending of the JFTOT tubes during coker tests. At higher temperatures thermal expansion causes these tubes to bend, which can result in more difficult measurement on the BDR.

Results and Discussion

After each tube was run in the JFTOT, the deposit thickness was measured by the BDR. Before measuring the deposit, the tube was rinsed with pure grade n-heptane and dried with nitrogen. After being measured, the deposit was carefully removed, and the clean tube was rated once again for calibration.

The radiation count rate from the deposit is produced by the BDR as a continuous recording versus tube length. Calibration curves are used for different metals to convert from count rate to deposit surface density (deposit weight per unit surface area of the tube). The profiles resulting from these conversions are integrated to determine the total deposit mass and the maximum deposit thickness. In the calculations an average atomic

-19-

number of 6 was assumed for all deposits, based on published deposit composi-
tions by Nixon.[7] Results of the deposit measurements for the fourteen tube
metals are shown in Table VI.

The manner in which deposits formed varied among the tubes. In
certain tubes the deposits occurred in narrow bands. In these instances the
maximum deposit depth could be considerable, but the total mass of deposits
would be small, as illustrated by Hastelloy C. In contrast to this the deposit
in some cases was dispersed over the major portion of the tube surface but
was nowhere very thick, such as the deposit measured on brass. Hence, both
the maximum and total deposition was recorded to describe the coke deposit.
If the coking tendency of a fuel-metal combination were not great, the total
deposits on a coker tube might be small. However, deposition might occur at
a certain temperature at which all of the deposit would form in a restricted
area causing a possible hot spot. This would be reflected by a high value
for the maximum deposit thickness.

Of the tube materials tested stainless steel type 446 (a high
chromium steel) and aluminum had the smallest deposits. The detectable deposit
thickness for the stainless steel is less than for aluminum, because of the
greater efficiency of electron scatter associated with the higher atomic
number of iron. However, both stainless steel type 446 and aluminum must be
considered equivalent within the precision of these tests.

A problem which caused difficulty in measuring deposits on aluminum
was the presence of small amounts of iron deposits which masked the organic
deposits. This interference was discovered recently when it was found that
part of the code 2 visual rating of Jet A fuel on aluminum tubes was not due
to organic matter but to iron, perhaps in the form of oxides. The presence
of metals of high atomic numbers such as iron in deposits reduces the detec-
tion level of organic deposits on aluminum, but this has little effect in
rating deposits on other metals.

Nickel apparently has no independent effect on the rate of deposit
formation, as shown by the following facts. Nickel 200 and Inconel 600
(72% Ni) had only slight deposits, and so did stainless steels type 446
(0% Ni) and type 316 (13% Ni). Yet deposition on stainless steel type 304
(9% Ni) was markedly worse than on all the other metals. Hence, there was
no apparent correlation of deposit tendency with nickel concentration.

The two aluminized metals were of special interest. It was assumed
at first that the surfaces of these tubes were essentially pure aluminum.
However, scanning of the clean tubes with the BDR revealed that the aluminum
was only a surface diluent. The count rate from the aluminized surface of
stainless steel type 304 corresponded to a metal of atomic number 18.7, or a
surface of 54.4% aluminum. Similarly, the count rate on aluminized TD-nickel
indicated an atomic number of 26.8 for the bare metal, or a surface of only
14.6% aluminum. These results explain why the aluminized tubes, although an
improvement over the base alloy, were more prone to form deposits than aluminum.

Table VI. BETA-RAY DEPOSIT RATINGS FOR JFTOT TUBES OF DIFFERENT METALS

Jet A Fuel (Lab. Record No. F-187)
410°F (210°C) Liquid Temperature
300 psig (2.1 MN/m²) Pressure

Tube Metal	Beta-Ray Deposit Rating		
	Maximum Depth[a]		Total Mass,[b]
	Å	μm	μg
Stainless Steel Type 446	< 20	<0.002	<0.5
Aluminum	<160	<0.016	<0.5
Nickel 200	360	0.036	0.5
Stainless Steel Type 316	300	0.030	1.5
Inconel 600	440	0.044	1.2
Aluminized TD Nickel	240	0.024	2.4
Monel 400	550	0.055	3.0
TD Nickel	440	0.044	7.2
Aluminized Stainless Steel Type 304	560	0.056	4.3
Cartridge Brass	540	0.054	16.8
Hastelloy C	1840	0.184	3.6
L-605 (Haynes 25)	2220	0.222	19.1
1015 Steel	1460	0.146	28.3
Stainless Steel Type 304	2400	0.240	35

a) Calculated from measured surface density by assuming a deposit density of 1.2 g/cm³ (1200 kg/m³).
b) Determined by integration of the deposit surface density versus length.

S-14115

Nevertheless, the presence of aluminum gave a synergistic benefit in each metal, since the aluminized surfaces had less deposit than would have been predicted by a linear interpolation of the deposit measurements between pure aluminum and either stainless steel type 304 or TD nickel. Actually, aluminized TD nickel yielded much better results than TD nickel and had less deposit than most of the other tube materials.

A unique alloy among those tested was L-605, because of its high cobalt and tungsten content. Heavy deposits were measured on this tube, which may have been due to either or both of these elements.

Hastelloy C alloy produced only moderate overall deposits, but in a narrow band the maximum deposit density was one of the heaviest encountered. Nickel 200 had the same type of deposit distribution although at a lower level. This result could be attributed to a catalytic effect which occurs when a certain temperature is reached.

Because of its high copper content, brass (70% copper) was expected to be among those metals with the heaviest deposits, as was Monel 400 (32% copper). However, the tests showed that the brass had a widespread deposition, which was never very thick. Perhaps this correlates with the fact that copper causes deposit formation in fuels at low temperatures, i.e., a particular high temperature may not induce as great an increase in deposition in the presence of copper as with other metals. The deposit profile for Monel was somewhat intermediate between that of brass and nickel, its two principal components. The other tube with a heavy deposit was 1015 steel, essentially pure iron containing 0.15% carbon. This might suggest an adverse effect of iron, which is in agreement with the results for stainless steel type 304 (72% iron). However, stainless steel type 446 (75% iron) had one of the lightest deposits. Hence, there appears to be no simple correlation of coking tendency with either iron, nickel, or chromium, taken separately. Rather, the observed effects appeared to be the net results of not only the individual metals, but of synergistic and antagonistic interactions of the elements. Perhaps even more important than the effect of a given element is the crystal or grain structure of the metal and the surface energies and electron availabilities associated with them.

Selection of Tube Materials for 20-Hour Coking Tests

There were several considerations in the selection of the tubes to be used in the 20-hour coking tests. First, it was desirable to select tube materials which would have potential use in high temperature environments. These materials should have desirable high temperature properties with an important property being high tensile strength. Second, the metals chosen for these tests should have a tendency to remain free of coke deposits. The results of the screening tests on the JFTOT coker showed that deposits were small on most of the prospective materials and moderate on others. Other factors which influenced the choice of tube materials were availability in the proper dimensions and the cost of obtaining tubing.

Three materials were selected from those listed in Table V for the 20-hour coking test runs: Hastelloy C, stainless steel type 316, and L-605. Hastelloy C was chosen since it was the standard material used in the other

-22-

tests of this project. This material also has been used in other heat transfer and coking studies with different fuels. It also has good tensile strength at high temperature and was available for use. The deposit formed on Hastelloy C in the JFTOT tests was light to moderate, indicating no serious problems with deposition on this material.

One of the stainless steels was desired for the 20-hour coking tests, for which type 316 was selected, since it has desirable physical properties and deposits formed on this material during JFTOT tests were very light. It was also readily available.

L-605 was chosen since its composition differs appreciably from the other two materials selected. The coke deposits formed on L-605 during the JFTOT tests were moderate, but this was not considered to be a serious problem. This material also has good strength at high temperature and it is resistant to oxidation. L-605 was not readily available, but some tubing was eventually obtained for the coking tests.

The three materials chosen for the 20-hour coking tests all have desirable physical properties at high temperatures and have potential use in future applications. Among these materials there is a large variation in composition, which, as the JFTOT coking tests showed, resulted in some difference in the coking tendencies.

Extended Coking Tests

Experimental Conditions and Results

The 5-hour test runs described earlier were made primarily to obtain data for heat transfer correlations. Those tubes which were subjected to the more severe conditions were submitted to combustion analysis to determine the extent of coke deposition. The results of these measurements are included along with the heat transfer data in Table XX.

The results from the 5-hour runs were used to select two conditions for the 20-hour coking tests. The 20-hour tests were run to determine the effect of tube material on coke deposition in the deoxygenated fuel. These tests were run in 5-hour cycles as described in the test procedure (p. 7). Each tube material was used in two runs at the conditions listed in Table VII. A total of six test runs was made using 1/8-inch (0.32 cm) tubes of Hastelloy C, stainless steel type 316, and L-605 (Haynes 25) alloy.

Table VII. CONDITIONS FOR 20-HOUR COKING TESTS

Heat Flux		Fuel Outlet Temperature		Inlet Pressure	
Btu/sec-in^2	MW/m^2	°F	°C	psia	MN/m^2
4	6.54	1000	538	1000	6.90
0.2	0.327	1000	538	1000	6.90

-23-

Table XXI presents the data summary for these tests, and Figures 24 and 25 show the profiles of the tube temperature at run times of 0, 5, and 20 hours for each test. Deposit profiles are also shown on the same figures to illustrate the correlation between tube temperature and coke deposit. The change in tube temperature with time is illustrated in Figures 26 and 27 for two points in each of the 20-hour tests with Hastelloy C tubes. Changes in the tube pressure drop for all six tests as functions of time are shown in Figures 28 and 29. Figure 30 shows the effect of time on the filter pressure drop during the three tests at the higher heat flux. During the three tests at the lower heat flux the filter pressure drop was less than 0.001 psi (7 N/m^2).

The final tests were two 100-hour runs to study the effect of coking on heat transfer over extended times. Conditions for both tests were similar; only the oxygen concentration in the feed was varied, in order to determine the effect of oxygen on coke deposition. The feed for the first test (Run 101) was deoxygenated Jet A fuel as used in all the previous tests. Aerated (air-saturated) Jet A fuel was used as feed during the second test (Run 113). The nominal operating conditions for these tests are listed in Table VIII. These tests were run in 10-hour cycles as described in the test procedure (p. 7).

Table VIII. CONDITIONS FOR 100-HOUR COKING TESTS

	Nominal		Actual	
Heat Flux, Btu/sec-in^2 (MW/m^2)	1.0	(1.63)	0.94	(1.54)
Inlet Pressure, psia (MN/m^2)	1000	(6.90)	1000	(6.90)
Outlet Fuel Temperature, °F (°C)	1000	(538)	960	(516)

At the start of the first 100-hour run operation was erratic due to continual pressure surging, and it was necessary to reduce the power input to stabilize the system. The actual conditions of the test run are given in Table VIII. These conditions were maintained for the rest of the run and were also used during the second 100-hour test with the aerated fuel. Data recorded at different times throughout each of the tests are presented in Table XXII.

The following illustrations show the data in various forms for these tests. Figure 31 shows the profiles of tube temperature taken at twelve different times during Run 101. These show the effect of coke deposition on heat transfer. Several profiles are shown to indicate at what times changes in the heat transfer coefficient and tube temperature occurred. Figure 32 shows tube temperatures at two thermocouple locations as recorded at 20-minute intervals. Temperatures at these two points usually were local maxima during most of the test run. The pressure drops across the heat exchanger tube and the product filter as functions of time are shown in Figure 33. The rate of light gas formation, which is indicative of cracking severity, is shown in Figure 34.

Figures 24 through 34 follow

S-14115

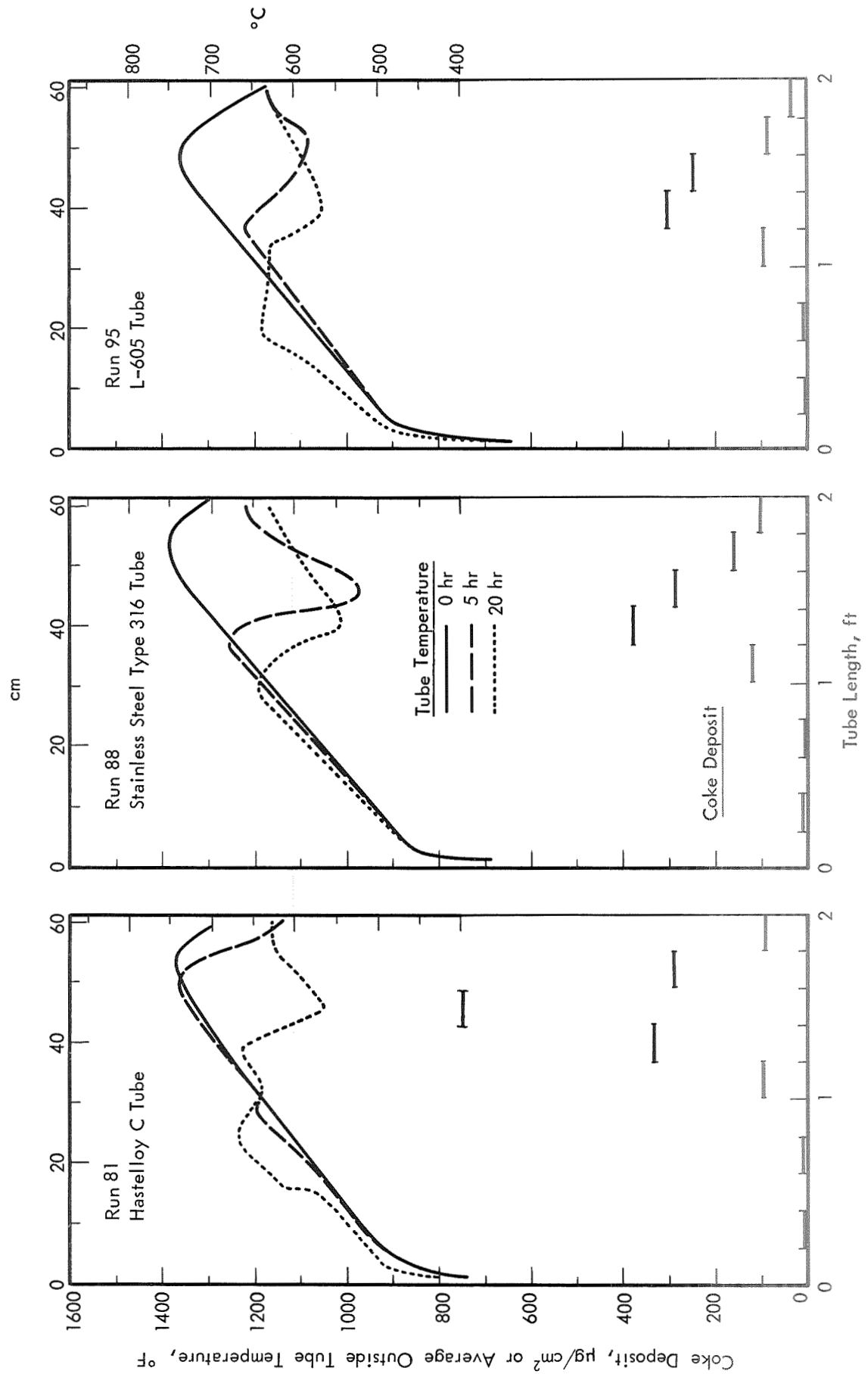Figure 24. TUBE TEMPERATURES AND COKE DEPOSITS FOR 20-HOUR RUNS 81, 88 AND 95

Figure 25. TUBE TEMPERATURES AND COKE DEPOSITS FOR 20-HOUR RUNS 85, 91 AND 98

Heat Flux: 4 Btu/sec-in² (6.54 MW/m²)
Inlet Pressure: 1000 psia (6.90 MN/m²)
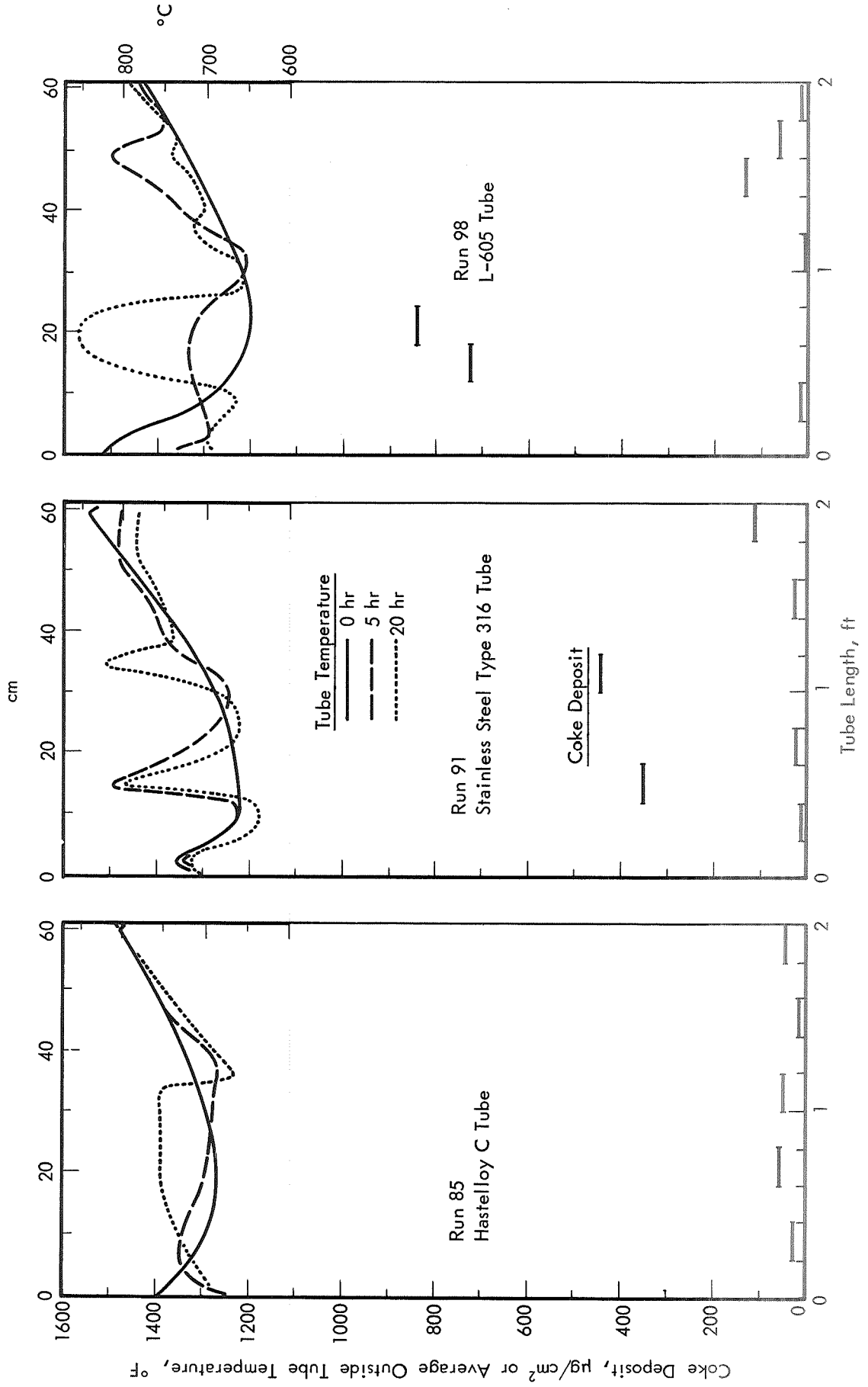Exit Fluid: 1000°F (538°C)

Run 85
Hastelloy C Tube

Run 91
Stainless Steel Type 316 Tube

Tube Temperature
0 hr
5 hr
20 hr

Coke Deposit

Run 98
L-605 Tube

S-14115
67374

Tube: ⅛-in (0.32 cm) OD Hastelloy C
Heat Flux: 0.2 Btu/sec-in² (0.327 MW/m²)
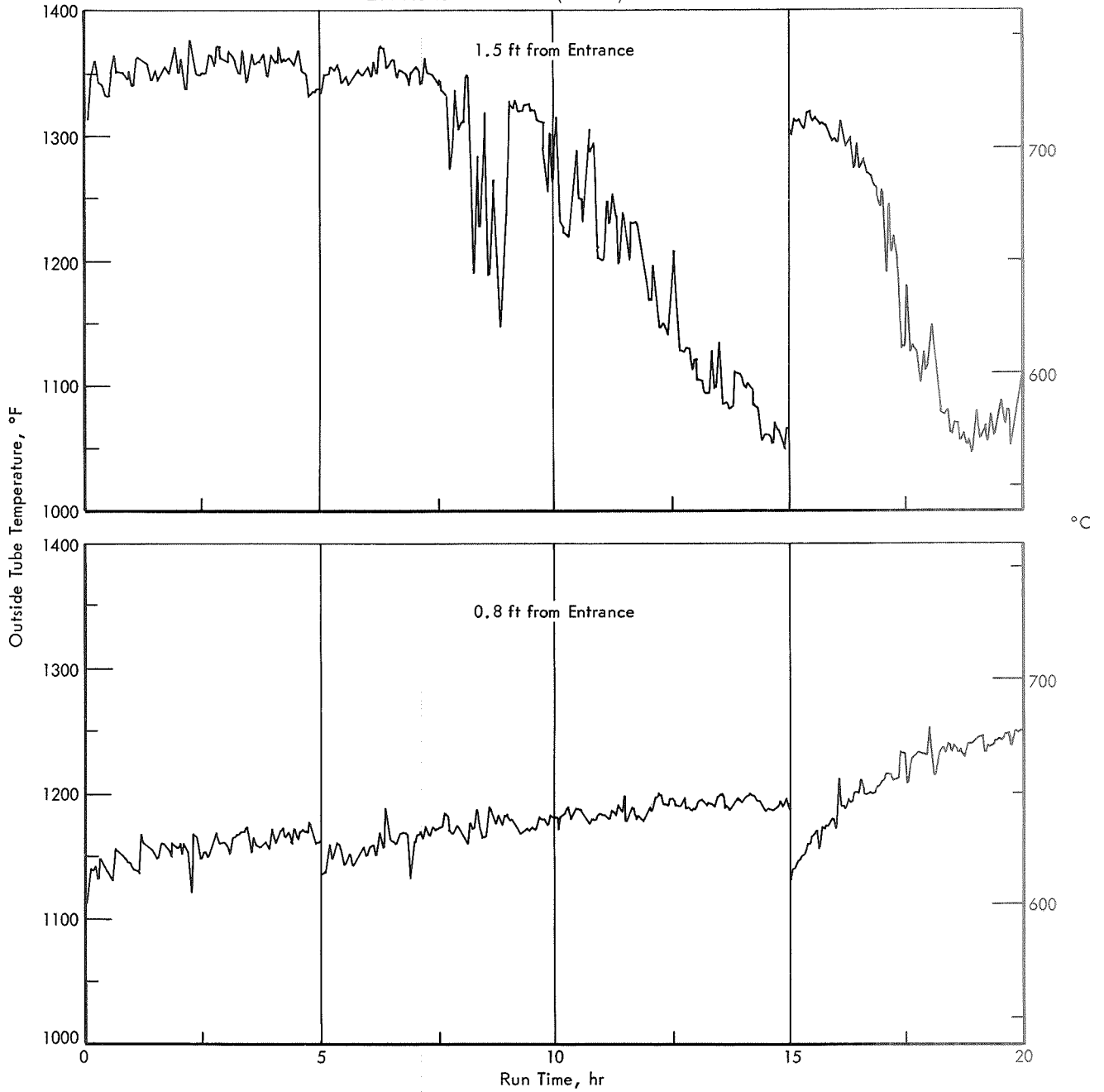Inlet Pressure: 1000 psia (6.90 MN/m²)
Exit Fluid: 1000°F (538°C)

1.5 ft from Entrance

0.8 ft from Entrance

Run Time, hr

Figure 26.   TUBE TEMPERATURES DURING 20-HOUR RUN 81
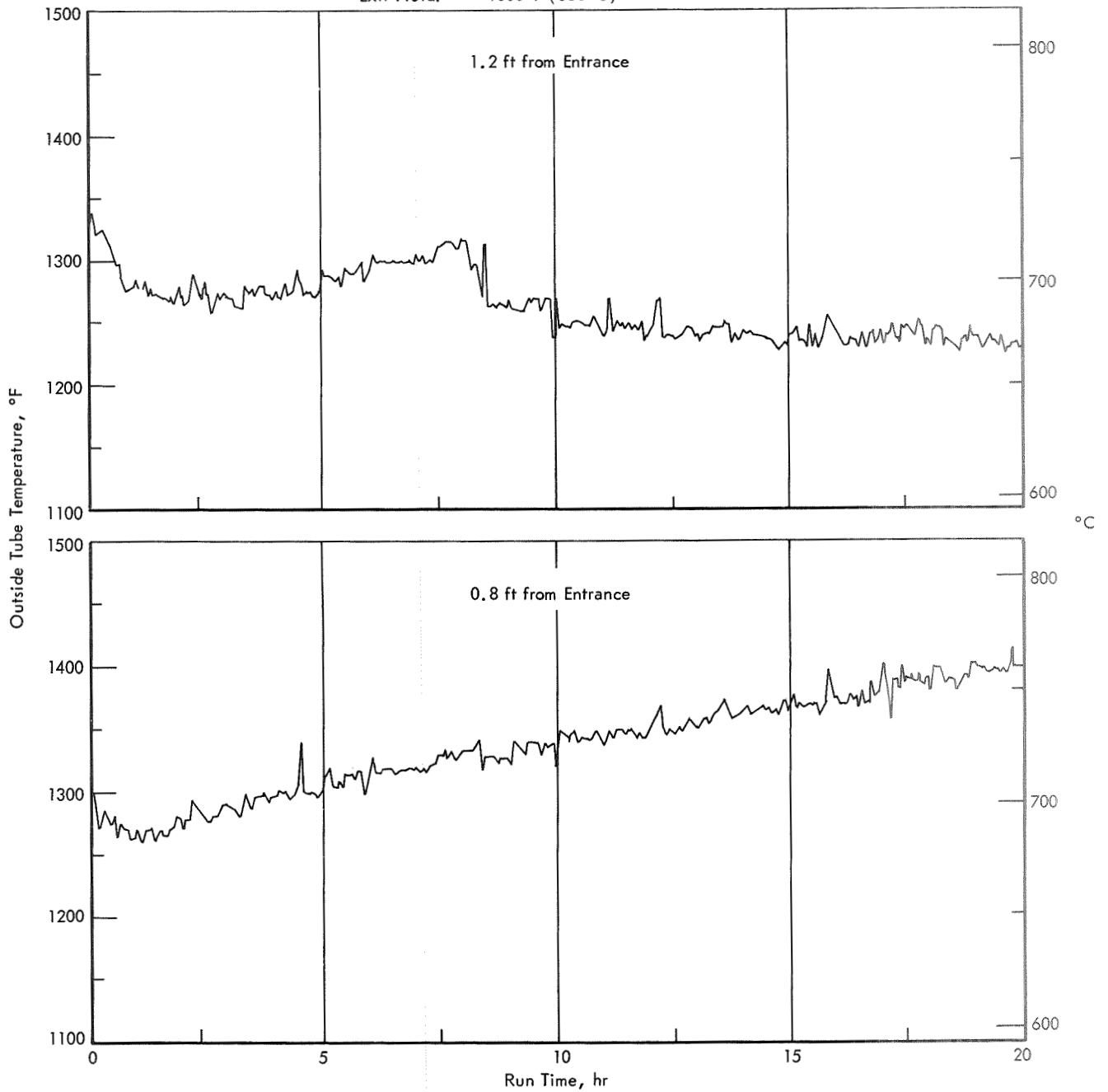
Figure 27.   TUBE TEMPERATURES DURING 20-HOUR RUN 85
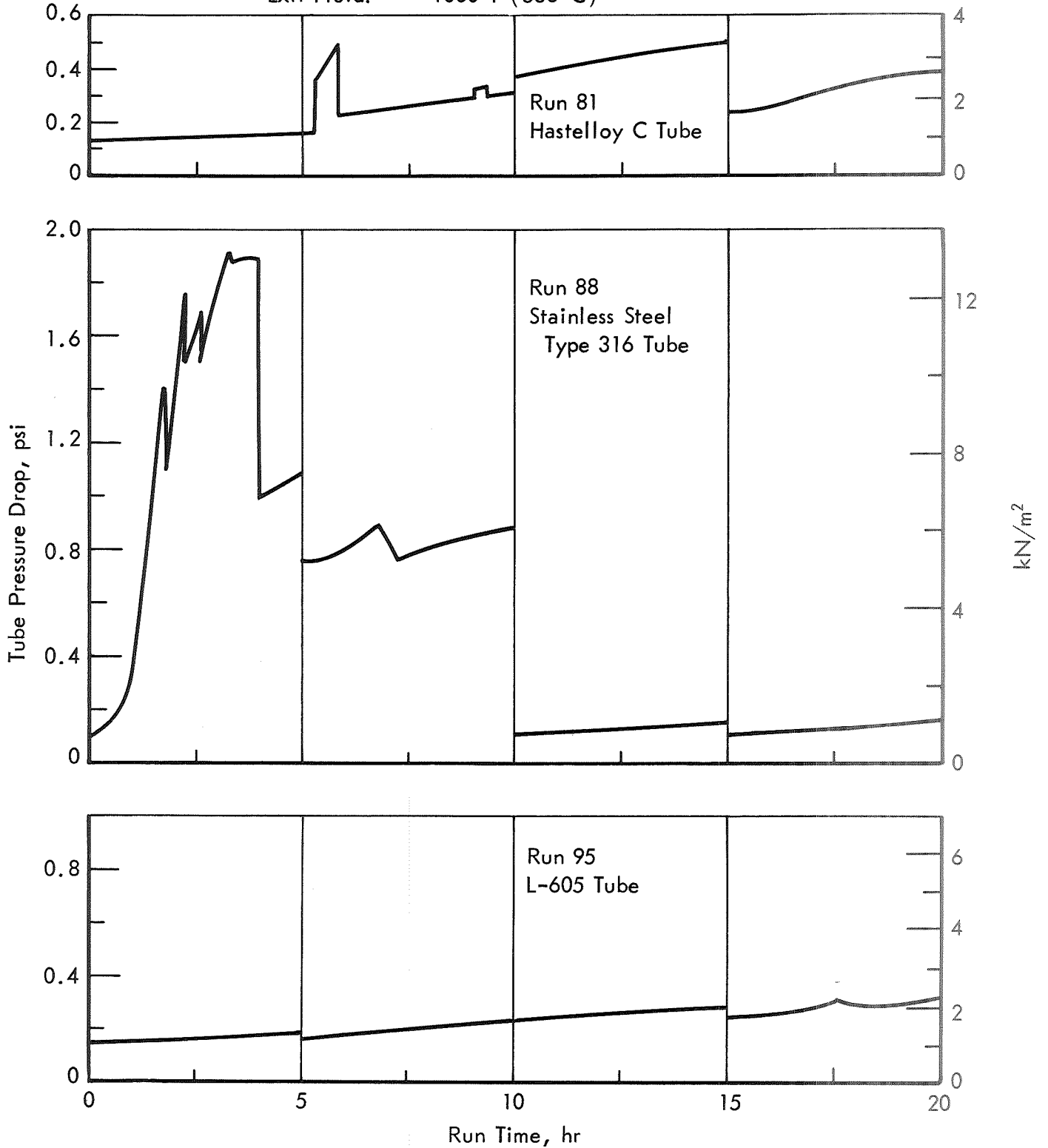
Figure 28. TUBE PRESSURE DROP DURING 20-HOUR RUNS 81, 88 AND 95
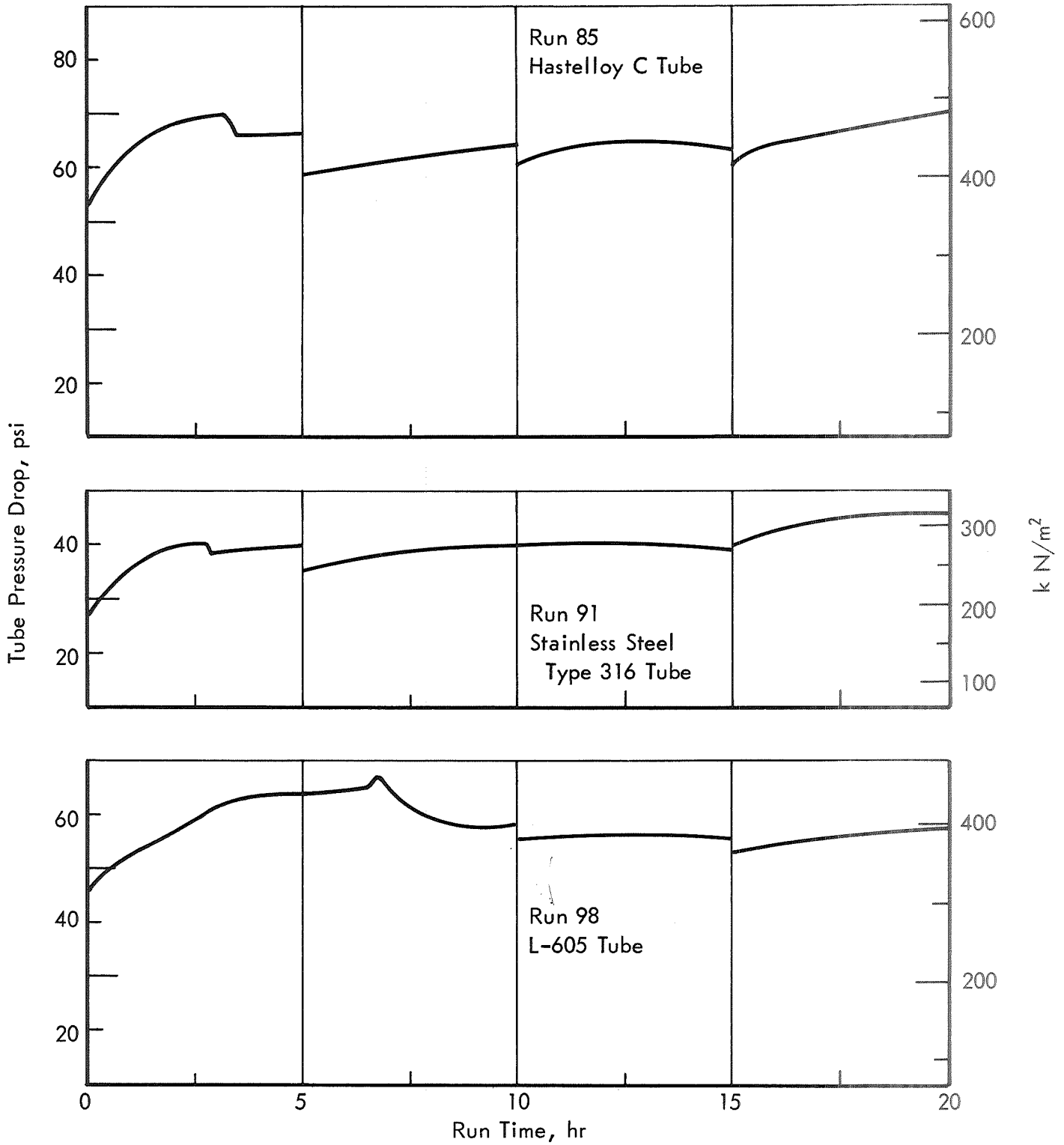
Figure 29. TUBE PRESSURE DROP DURING 20-HOUR RUNS 85, 91 AND 98

Heat Flux: 4 Btu/sec-in^2 (6.54 MW/m^2)
Inlet Pressure: 1000 psia (6.90 MN/m^2)
Exit Pressure: 1000°F (538°C)

Figure 30.   FILTER PRESSURE DROP DURING 20-HOUR RUNS 85, 91 AND 98

Figure 31. TUBE TEMPERATURE PROFILES DURING 100-HOUR RUN 101 WITH DEOXYGENATED FUEL

S-14115
67374

Figure 32.   TUBE TEMPERATURES DURING 100-HOUR RUN 101
WITH DEOXYGENATED FUEL

Figure 33. TUBE AND FILTER PRESSURE DROPS DURING 100-HOUR RUN 101 WITH DEOXYGENATED FUEL

Figure 34. PRODUCT GAS RATE DURING 100-HOUR RUN 101 WITH DEOXYGENATED FUEL

Figures similar to the above illustrations are presented for Run 113 with aerated fuel. Profiles of the tube temperature at various times are shown in Figure 35, 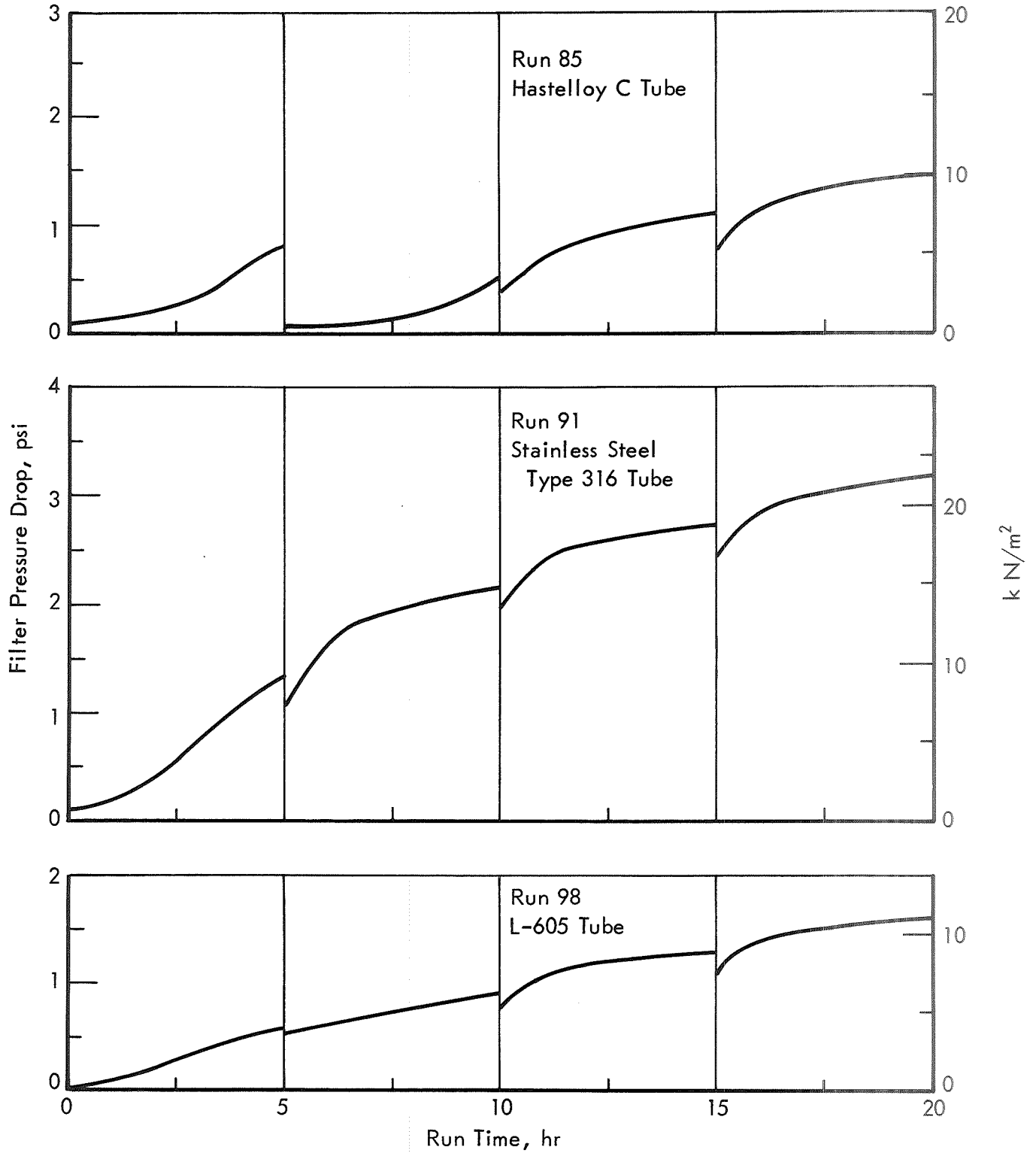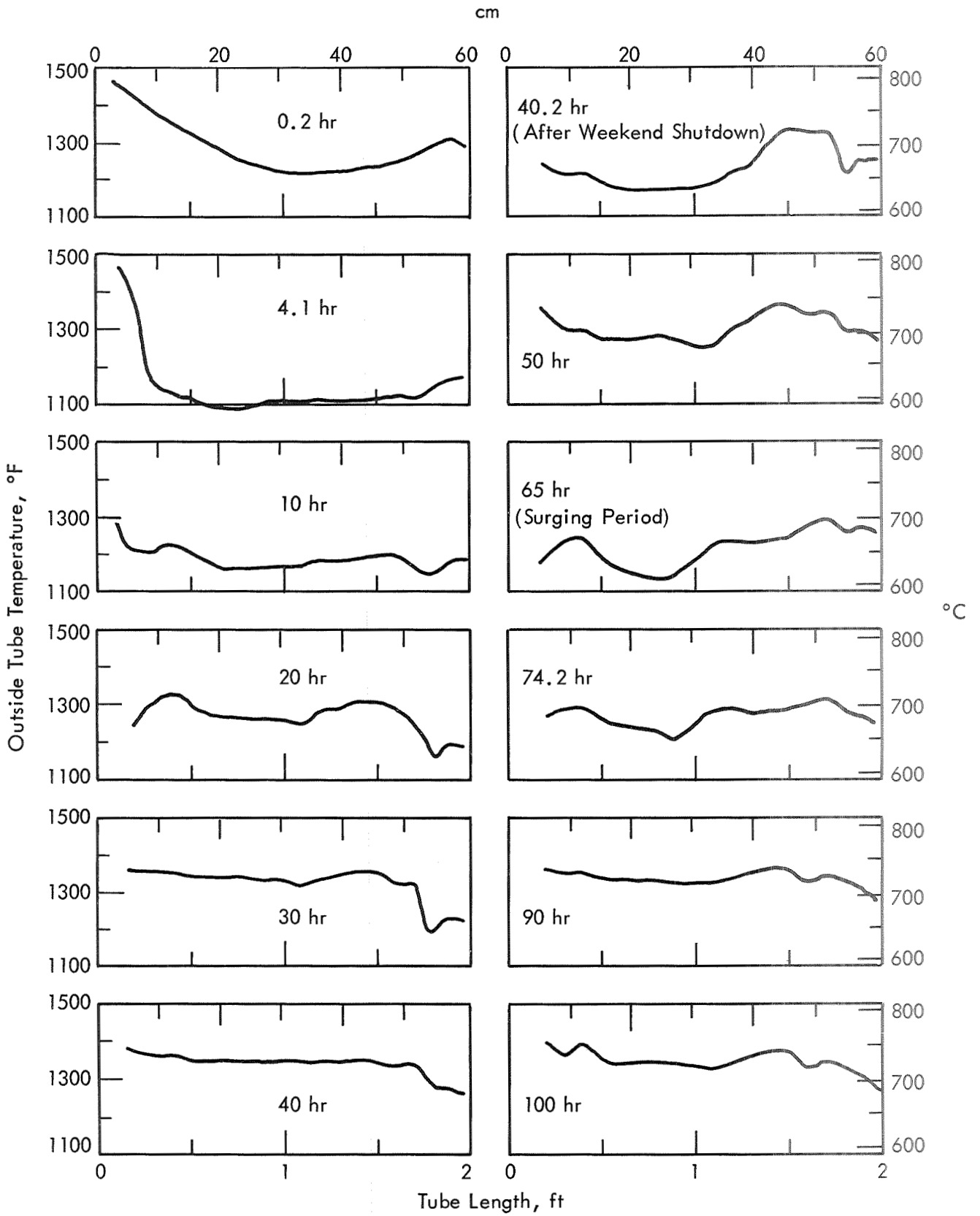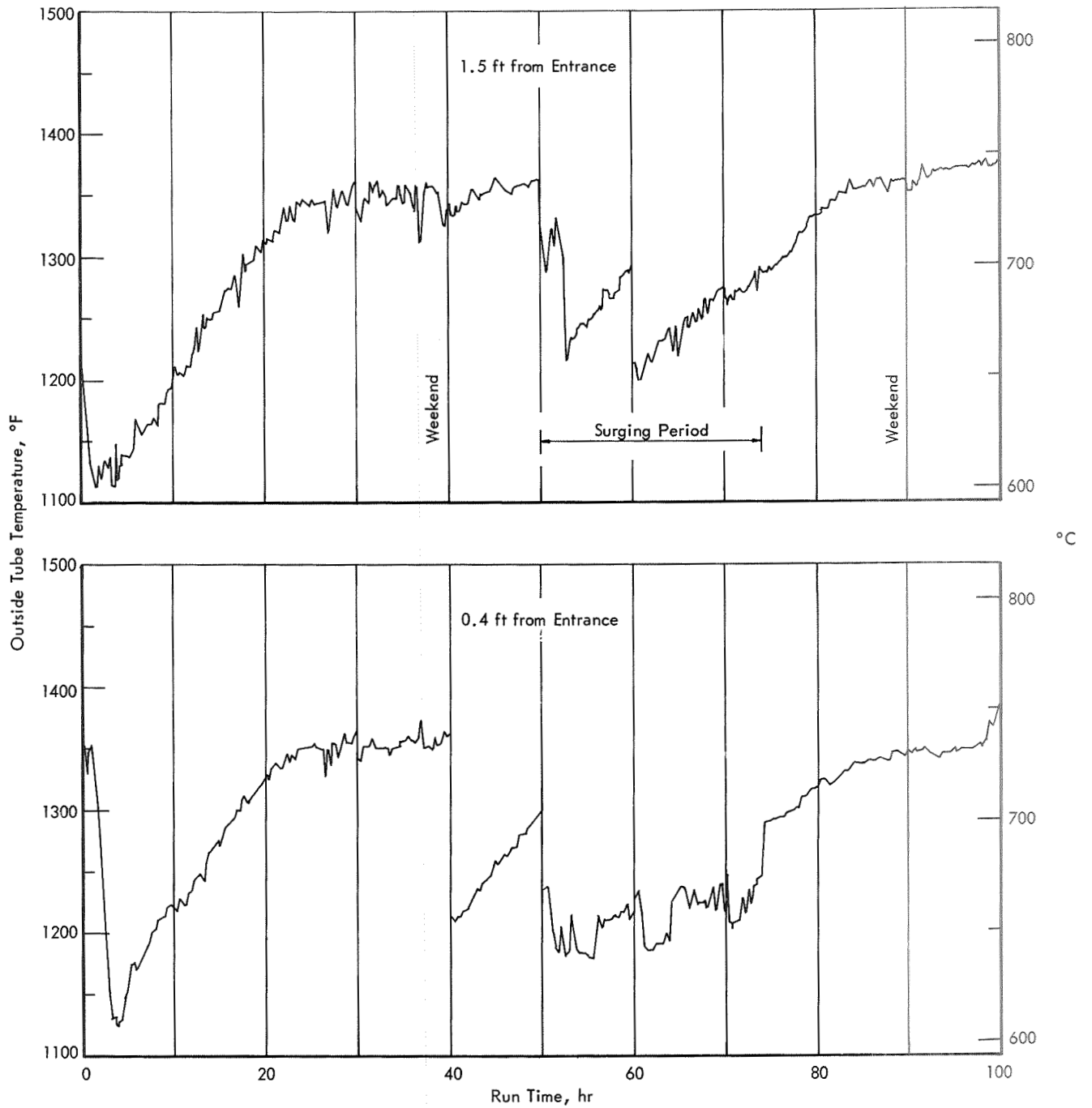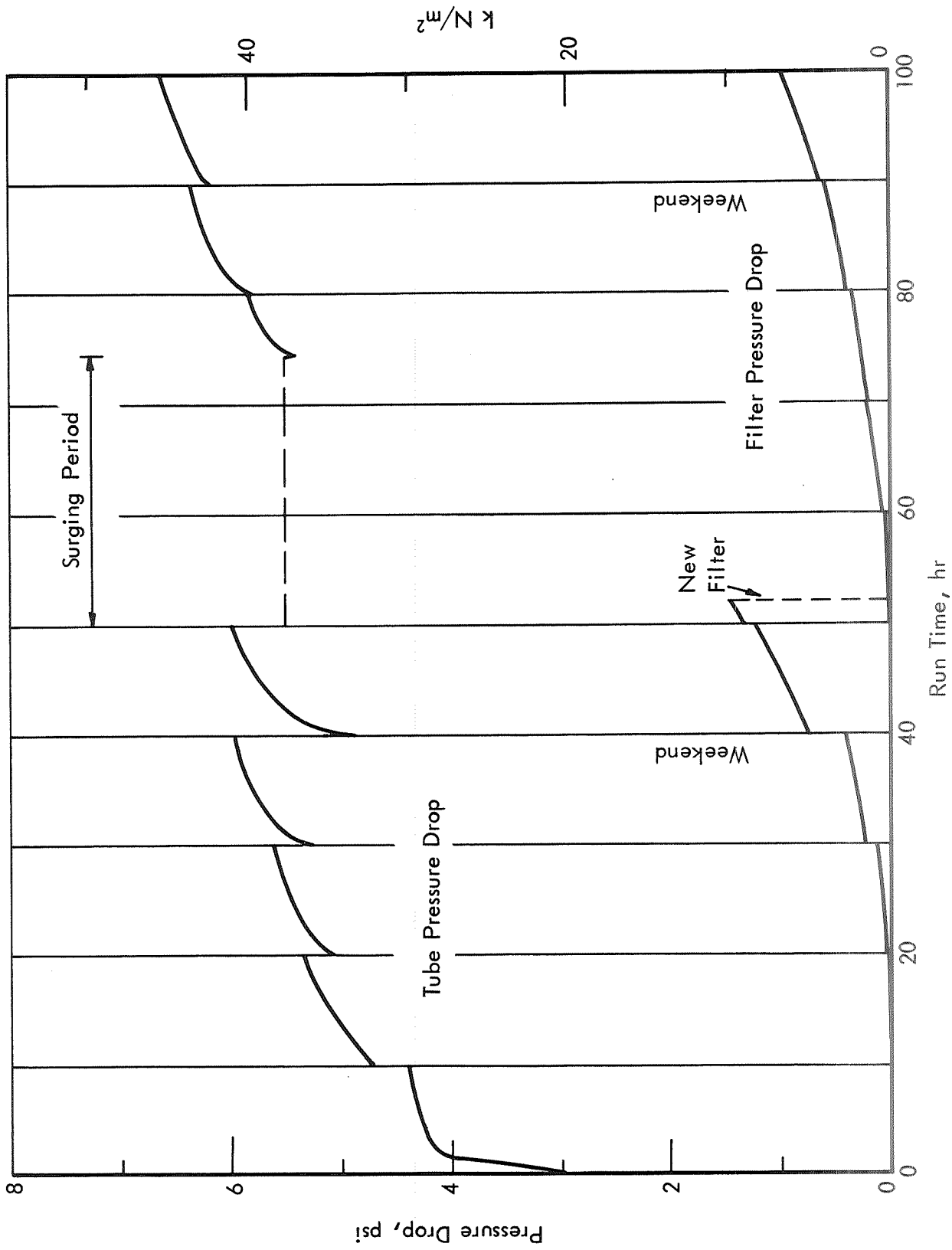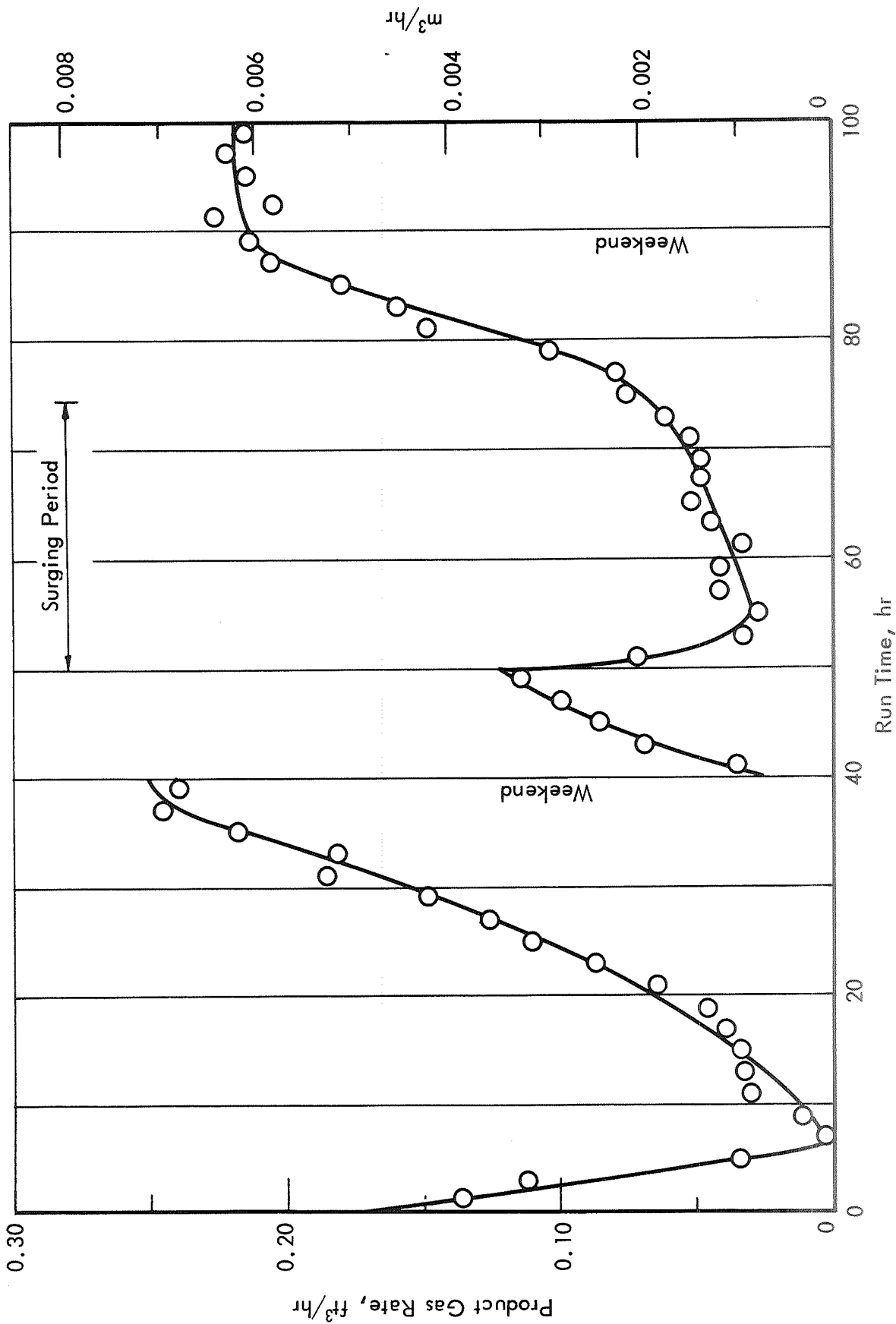curves of thermocouple temperatures as functions of time in Figure 36, the tube pressure drop in Figure 37, the pressure drop across the product filter in Figure 38, and the product gas rate in Figure 39.

The tube temperatures declined immediately following the start of each of the 100-hour tests. This was caused by initial coke deposits creating a rougher surface, which increased fluid turbulence and improved heat transfer. This improvement in heat transfer continued for different times up to 10 hours, depending on the location along the tube, until a minimum tube temperature was reached. Afterwards tube temperatures began rising slowly, and these temperatures generally continued to rise throughout the remainder of the test as additional coke deposits accumulated. These changes are shown for a few points along the heat exchanger tubes in Figures 32 and 36.

In Figures 40 and 41 the profiles of tube temperature are shown for the beginning and end of each test run along with a profile for the lowest temperature at each point. Profiles of the coke deposit are included to show the correspondence between the amount of coke deposition and the increase in the tube temperature. Heavy local deposits during Run 113 resulted in very high temperature peaks at two locations along the tube, which almost forced early termination of the test.

In Run 101 it appeared that the coke deposit did not adhere firmly to the tube. During a weekend shutdown at the 40-hour point a substantial portion of the coke deposit apparently left the tube surface. This resulted in lower temperatures along much of the tube length when the test was resumed. This phenomenon was not observed at the 90-hour weekend shutdown.

Unstable operation was encountered during the period of 50 to 74 hours in Run 101. The instability was evident as an oscillation of pressure and flow rate. These surges in pressure commenced with the startup at 50 hours and continued despite efforts to prevent them by minor changes in the power, flow rate, and pressure. Also, a new filter was installed in this attempt to eliminate the pressure surges. The instability terminated abruptly and operation was smooth once again at 74 hours.

Oscilloscope traces (Figure 42) photographed during Run 101 showed the difference between the stable and unstable operation experienced in this test. Photograph A shows a trace taken at 2 hours of operation, while operation was smooth. This trace shows that the pressure was oscillating at a frequency about 600 Hz and an amplitude of 3 psi (21 kN/m^2). Photograph B was taken at 60 hours and shows the pressure oscillation that was characteristic of the unstable operation. The instability was characterized by a low frequency pressure surging of 2.5 Hz and 35 psi (240 kN/m^2) amplitude. There was a burst of high frequency oscillation at the peak of each surge, and its form is shown in Photograph C. In this instance the frequency was about 800 Hz and the amplitude 30 psi (210 kN/m^2). The frequency spectrum at the peak of a surge is shown in Photograph D. Photograph A is typical of the quiescent period during the unstable operation shown in Photograph B.

Figures 35 through 42 follow

Gas product flow rate, liquid product color, and analyses of the liquid and gas products (Table XXIII) all gave indication of the relative amount of thermal reaction of the fuel during test runs. Jet A fuel consists of hydrocarbons mostly in the range of C_9 to C_{16}. When cracking occurs, the concentration of light hydrocarbons increases, as illustrated by the appearance of C_3 to C_8 hydrocarbons in several analyses. Since some of these hydrocarbons remain in the gas phase upon cooling, the cracked fuel yields a greater flow rate of gas product. Discoloration of the liquid fuel from water-white to yellow or amber also accompanies cracking.

The most severe cracking occurred in Run 56 and at the start of Runs 81, 88, and 95, all at the same conditions. These runs had the highest flow rate of gas product, the greatest hydrocarbon concentration in the gas product, the greatest concentration of C_3 to C_8 hydrocarbons in the liquid product, and the most pronounced discoloration (amber). The gas product flow rate and the concentration of C_3 to C_8 hydrocarbons in the liquid showed that at least 4% of the feed reacted. In Runs 81, 88, and 95 a decrease in the maximum tube temperature caused the rate of cracking to decline as the run proceeded, as shown by decreases in the gas product flow rate, hydrocarbon concentration in the gas product, and C_3 to C_8 hydrocarbon concentration in the liquid product. Also, the initial liquid product was amber and gradually changed to a very light yellow.

A severe cracking condition was encountered in Run 73, during which at least 2% of the fuel reacted. A tube of 1/8-inch (0.32 cm) ID was used in this run, and the extent of cracking was greater than with a tube of 1/16-inch (0.16 cm) ID at the same heat flux, inlet fuel pressure and temperature, and outlet fuel temperature (Run 68). These conditions required a flow rate twice as great through a volume four times as great in Run 73 as in Run 68. Hence, the residence time of the fuel was about twice as long and the cracking more severe in Run 73 than in Run 68.

Analyses for the final stages of the two 100-hour test runs are included in Table XXIII. The liquid product from Run 101 remained water-white throughout the test, while the product from Run 113 was very light yellow. Hence, cracking was almost nonexistent in these runs.

Specimens from tubes used in the 20 and 100-hour test runs were examined by metallographic analyses. These specimens had the heaviest deposits and had been exposed to the highest temperatures in each run. Results of these analyses are presented in Table IX.

Table IX. CARBURIZATION OF HEAT EXCHANGE TUBES

Run	Tube Material	Run Time, hr	Maximum Surface Temperature		Depth of Carburization	
			°F	°C	mil	μm
85	Hastelloy C	20	1275	691	0	0
91	Stainless Steel Type 316	20	1375	746	0	0
98	L-605	20	1385	752	0	0
101	Hastelloy C	100	1330	721	0	0
113	Hastelloy C	100	1610	877	2.4	60

S-14115
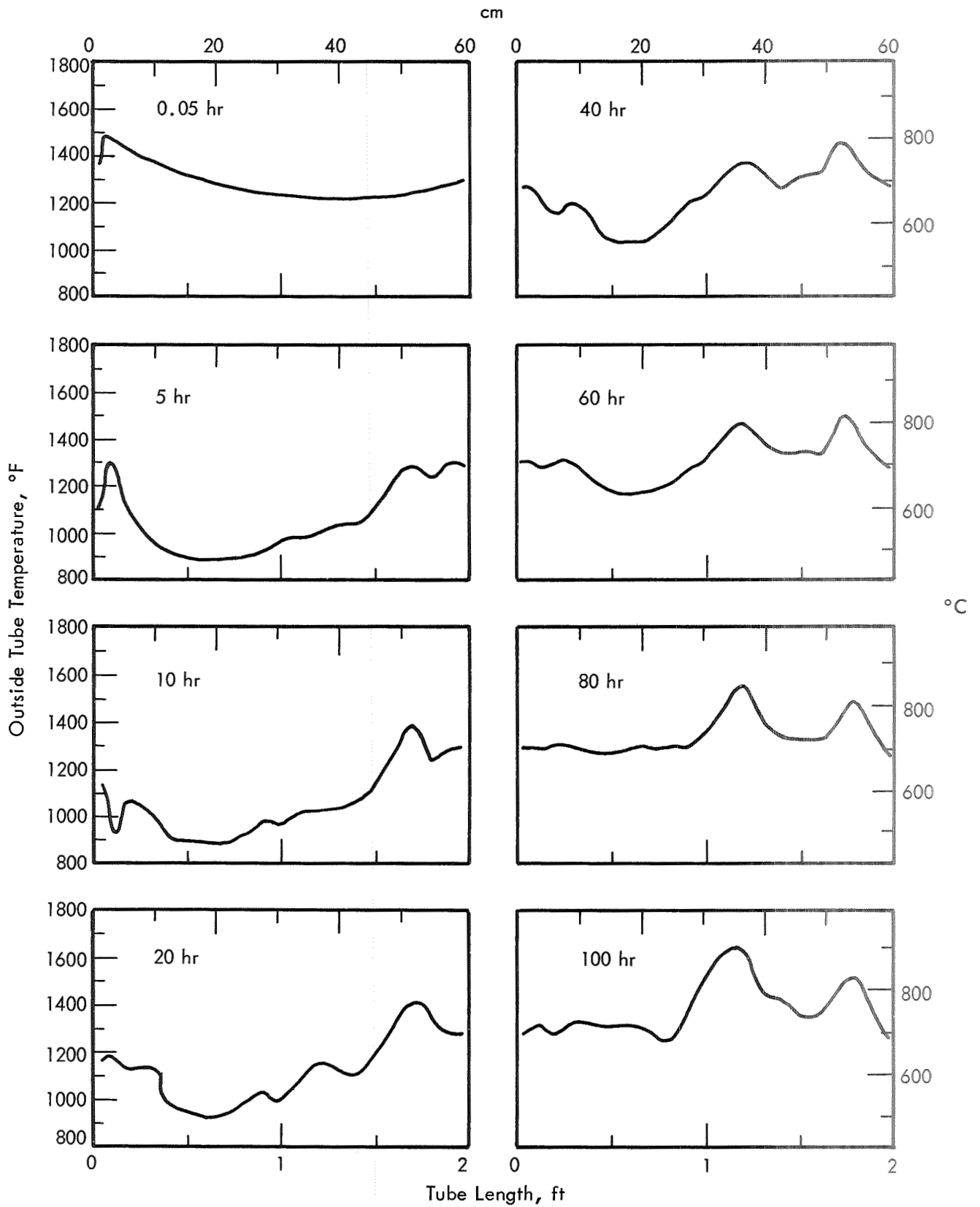
Figure 35.   TUBE TEMPERATURE PROFILES DURING 100-HOUR RUN 113
WITH AIR-SATURATED FUEL
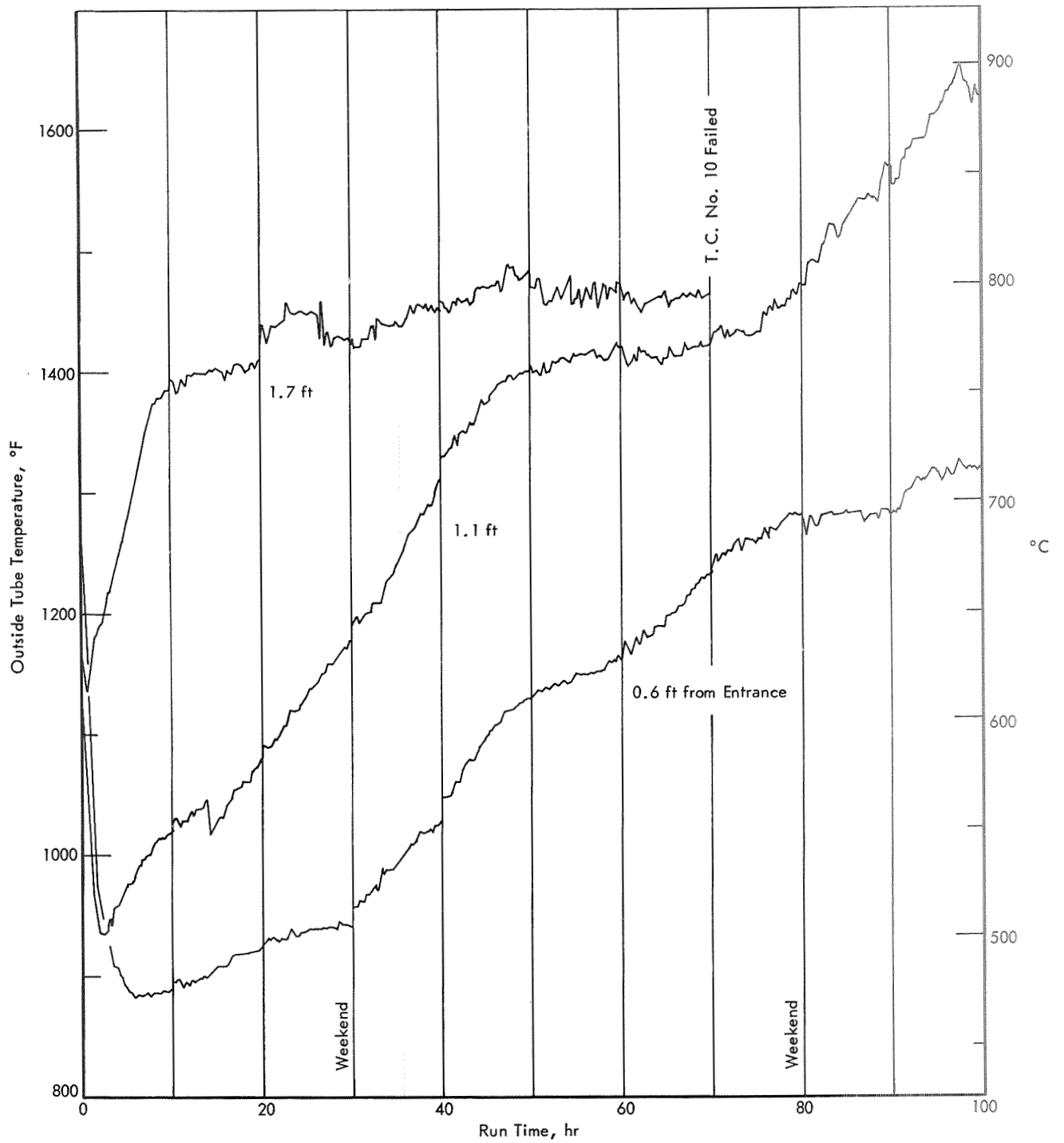
Figure 36.   TUBE TEMPERATURES DURING 100-HOUR RUN 113 WITH AIR-SATURATED FUEL
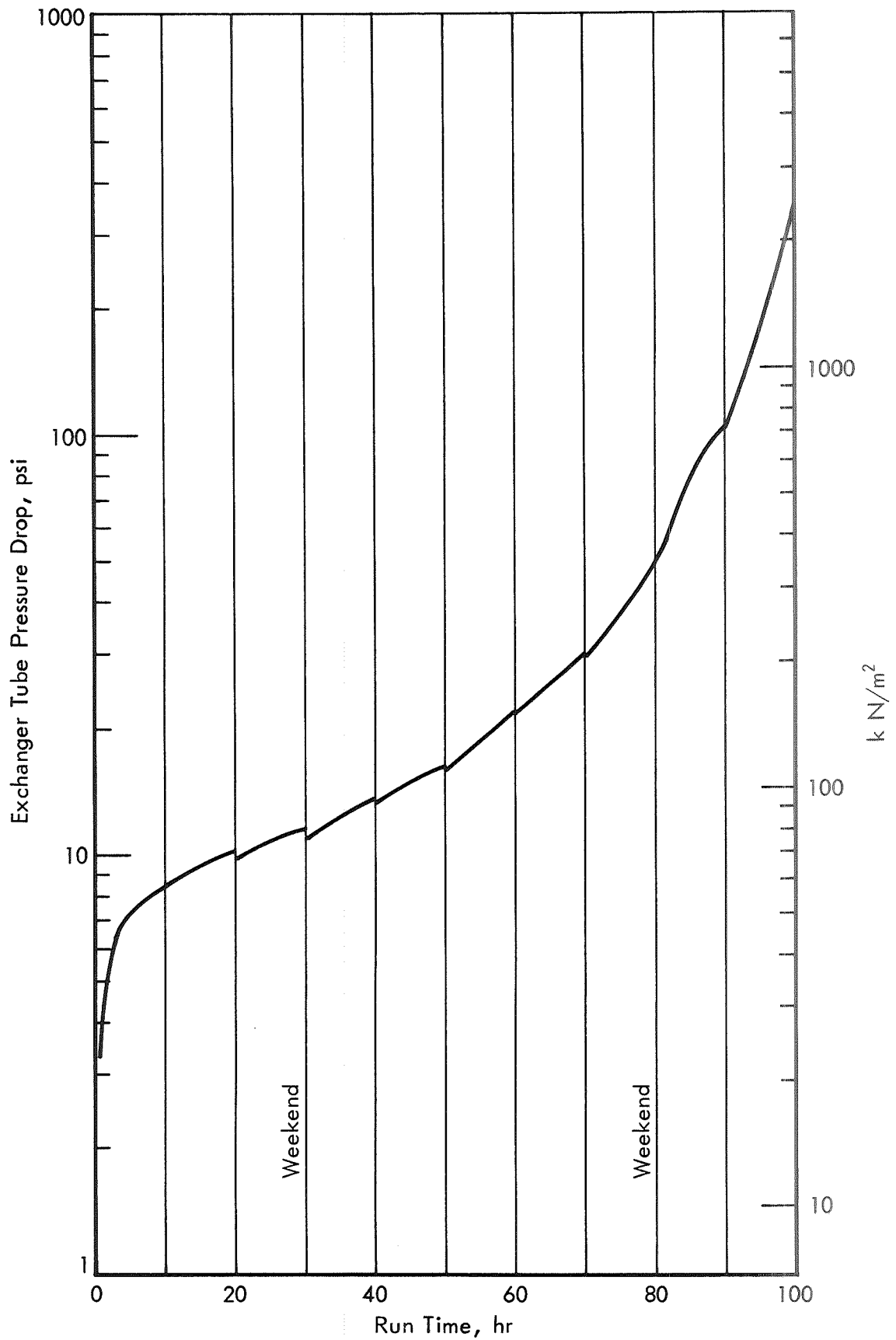
Figure 37. TUBE PRESSURE DROP DURING 100-HOUR RUN 113
WITH AIR-SATURATED FUEL

S-14115
67374
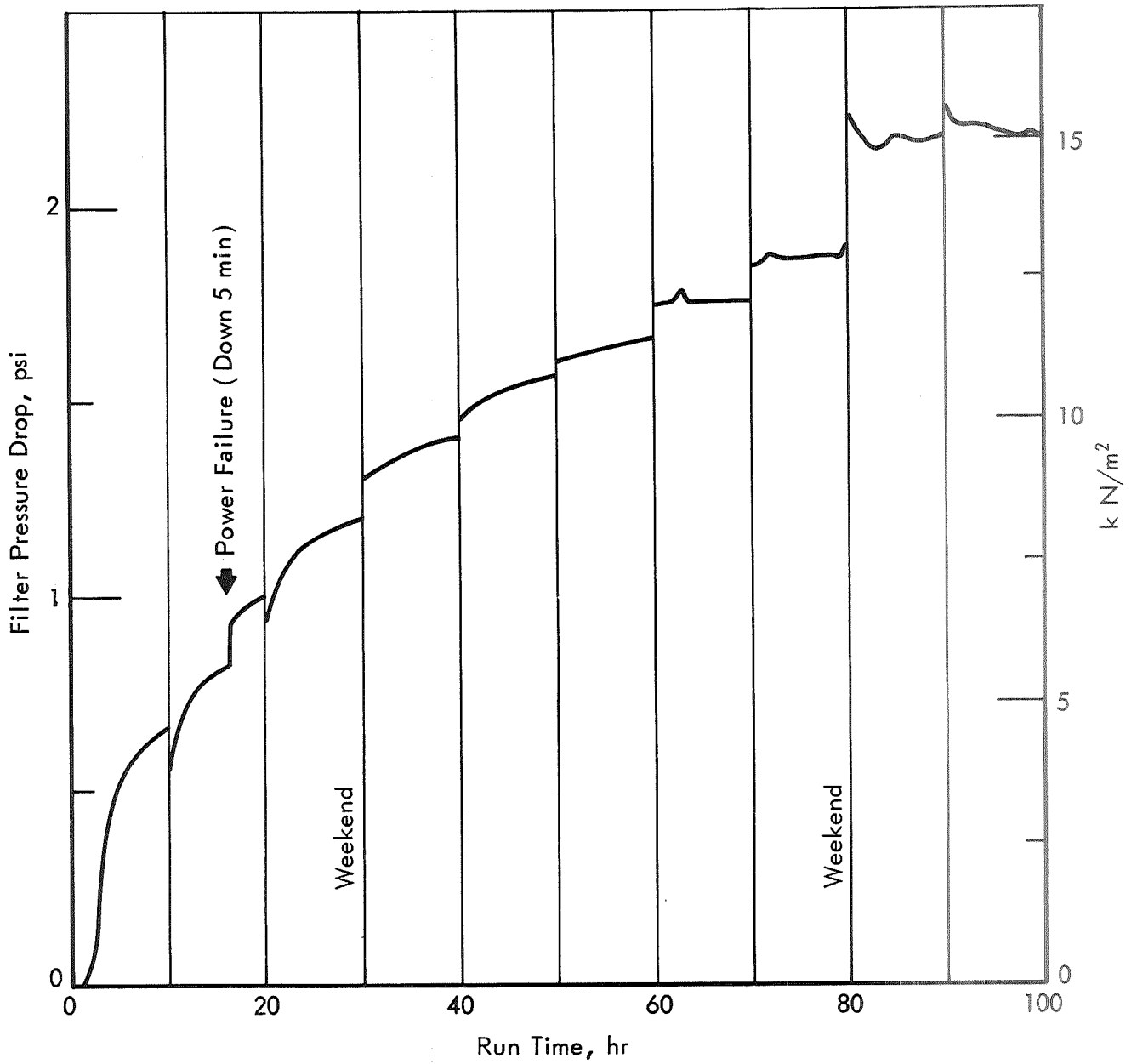
Figure 38. FILTER PRESSURE DROP DURING 100-HOUR RUN 113 WITH
AIR-SATURATED FUEL
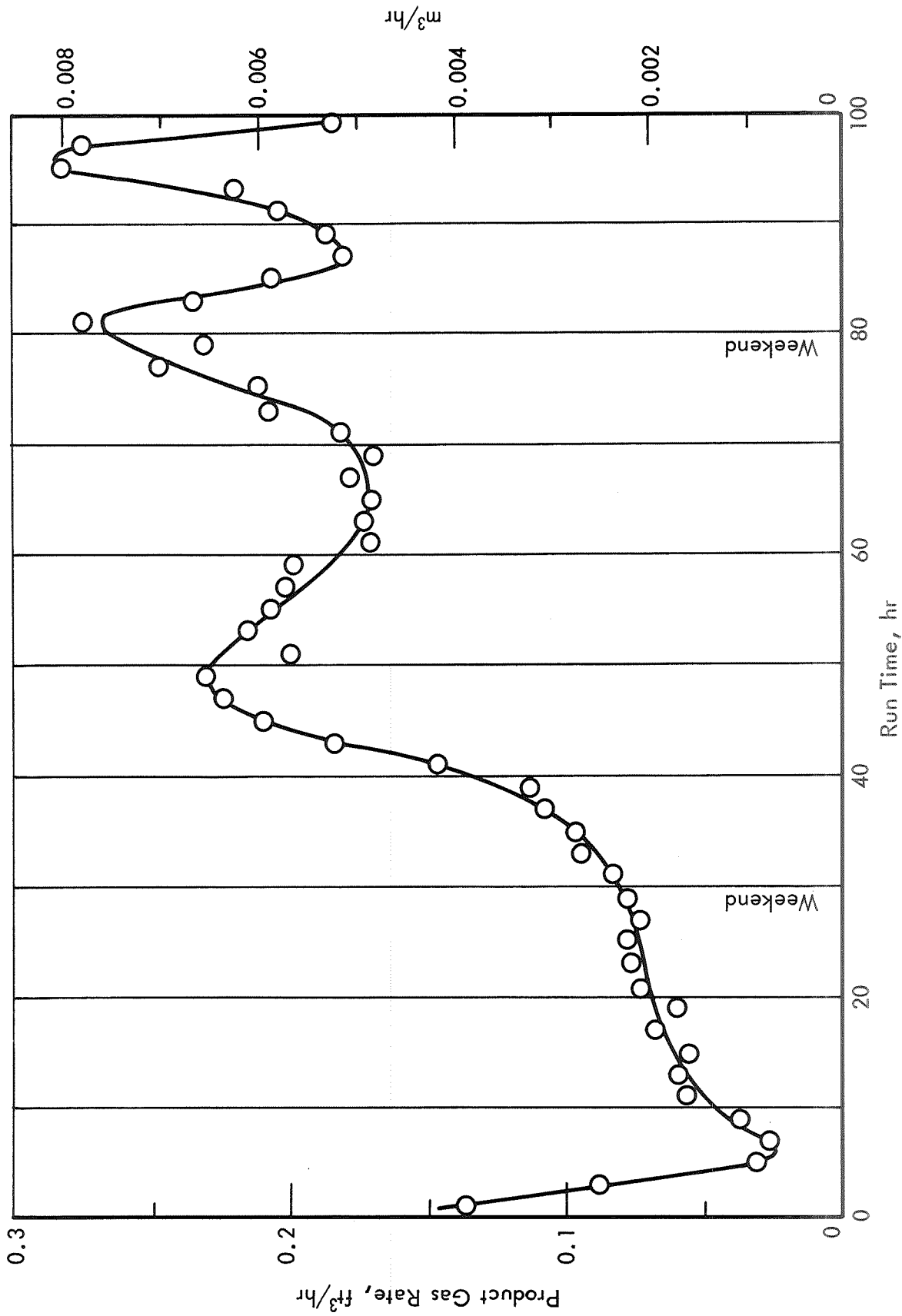
Figure 39. PRODUCT GAS RATE DURING 100-HOUR RUN 113 WITH AIR-SATURATED FUEL

S-14115
67374

Figure 40.   TUBE TEMPERATURES AND COKE DEPOSITS FOR
100-HR RUN 101 WITH DEOXYGENATED FUEL

Figure 41.   TUBE TEMPERATURES AND COKE DEPOSITS FOR
100-HR RUN 113 WITH AIR-SATURATED FUEL

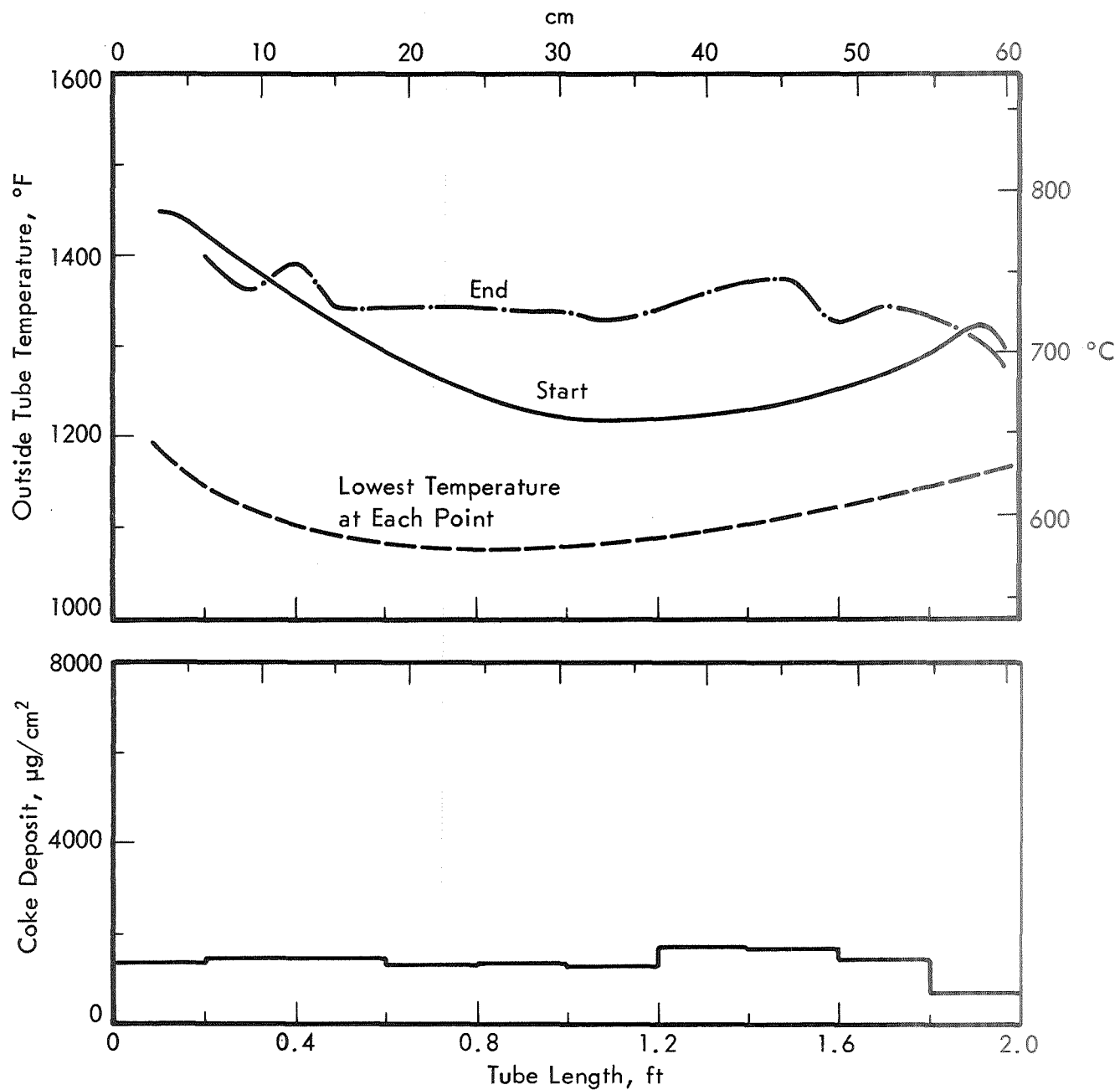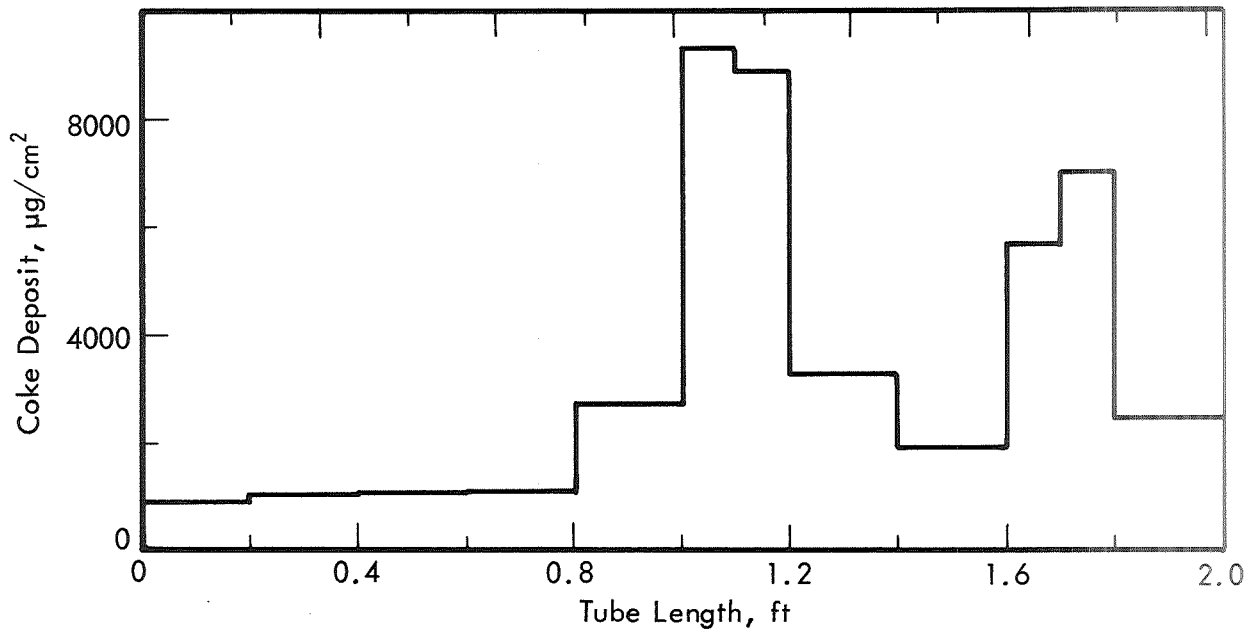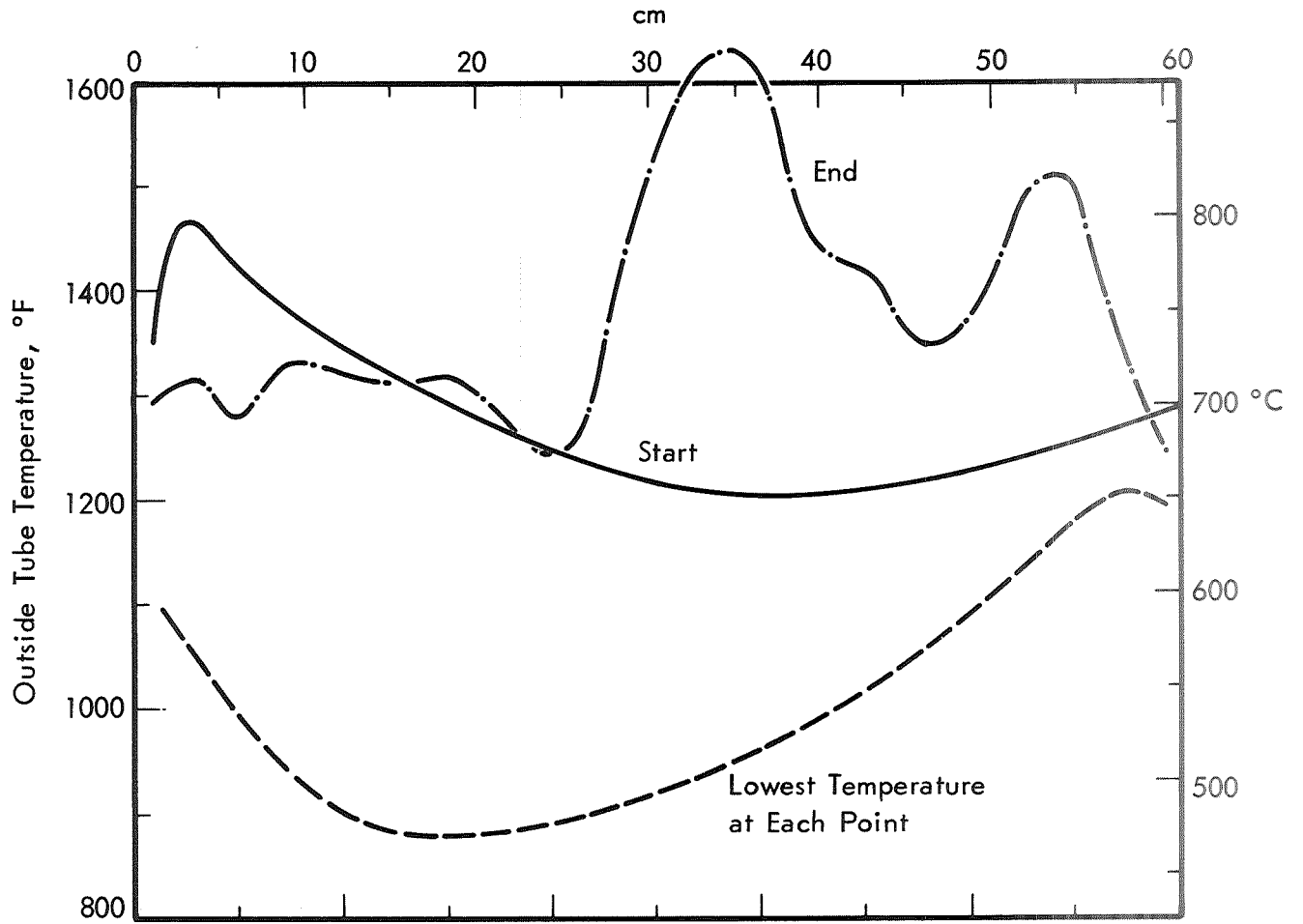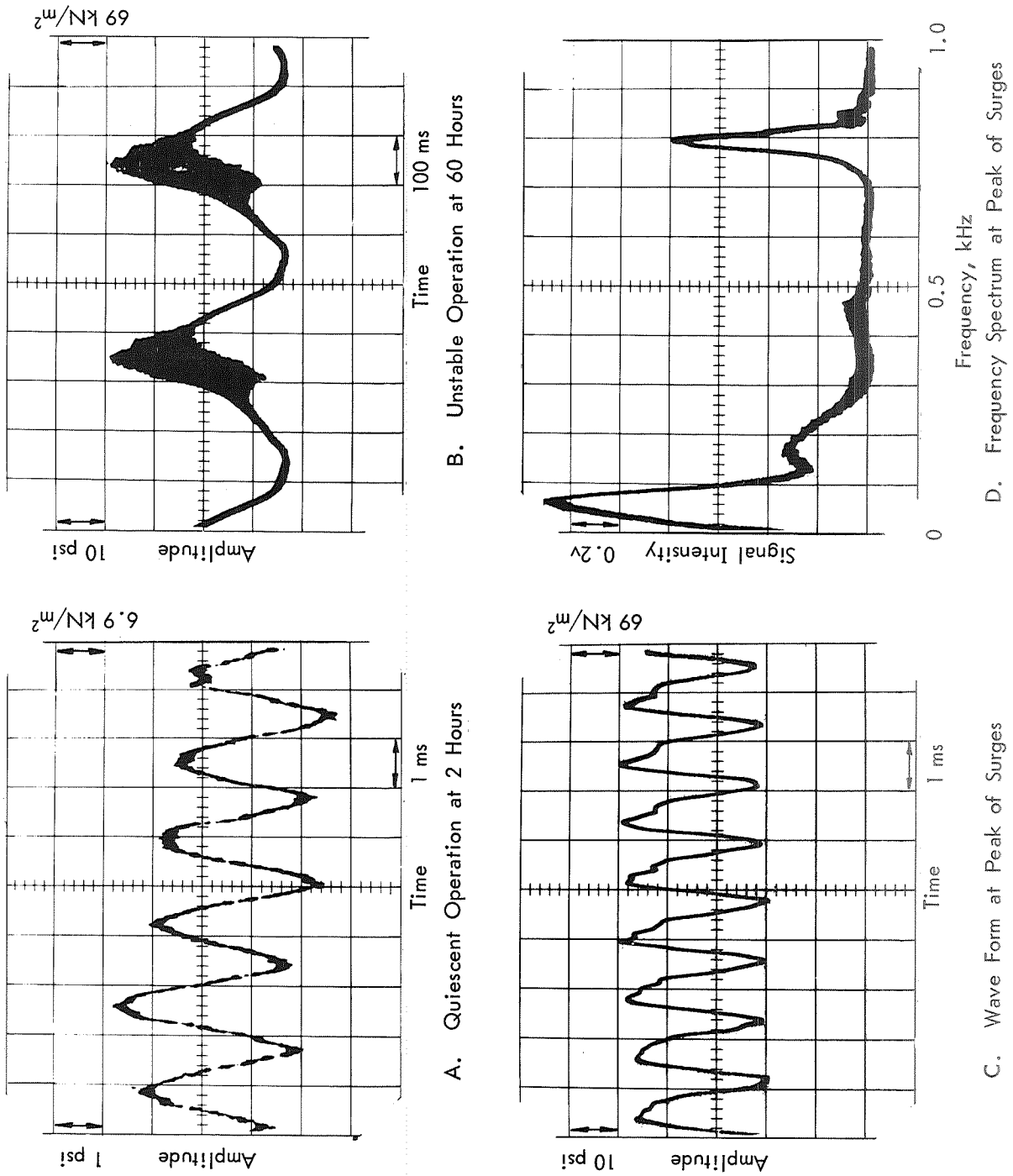Figure 42. PRESSURE PULSATIONS DURING 100-HOUR RUN 101 WITH DEOXYGENATED FUEL

A. Quiescent Operation at 2 Hours

B. Unstable Operation at 60 Hours

C. Wave Form at Peak of Surges

D. Frequency Spectrum at Peak of Surges

Discussion

Temperatures at the start of 20-hour Runs 81, 88, and 95 (Figure 24) were similar to those observed during the 5-hour Run 56. The same 50°F temperature difference between the top and bottom of the tube was observed, although this is not shown in Figure 24. Flow throughout the tubes was laminar with significant free convection to cause this temperature difference. As each test run proceeded the transition to turbulent flow, which initially occurred near the tube outlet, moved upstream. This was caused by the formation of coke on the tube surface, which presented a rougher surface to the fluid and caused earlier transition to turbulent flow. One of the curves in Figure 26 shows how this shift of the transition point upstream caused nearby tube temperatures to decrease with time. The greatest coke formation occurred at the flow transition point in each tube, since the tube temperature was generally the highest at this point. The levels of coke deposition among the three tubes differed in the same way as the relative temperatures. The flow transition point in Run 81 occurred farther downstream at a higher temperature than in Runs 88 and 95. Hence, the maximum coke deposit was greater in Run 81.

Other effects of temperature change were changes in the color of the liquid product, flow rate of the product gas, concentration of C_3 to C_8 hydrocarbons in the liquid product, and concentration of hydrocarbons in the product gas. These are all indicators of the relative extent of thermal reaction. Initially in each of the above runs there was some cracking of the fuel at the high temperatures near the tube outlet. This resulted in a liquid product which was amber. As each test proceeded the maximum tube temperature decreased, which resulted in less cracking and a liquid product that changed in color to yellow and gradually to a faint yellow tint. At the same time reduced cracking yielded less product gas, as evidenced by the lower gas flow rates. Also, the concentration of light components in the liquid product and of heavy components in the product gas decreased during the run, as illustrated by the product analyses for Run 81 (Table XXIII).

The initial temperature profiles for Runs 85, 91, and 98 (Figure 25) were similar, but this similarity ended during the runs with irregular formation of coke in each tube. The dominant behavior generally was a significant rise in tube temperature at certain points, which is illustrated by one of the curves in Figure 27. This temperature rise was in the form of a plateau in the temperature profile for Run 85 and as temperature peaks in Runs 91 and 98. The variation of coke deposits corresponded very closely with the tube temperature, the heaviest deposits occurring at the locations of the temperature maxima. These peaks did not form at the same time or rate, and even the location in different tubes varied to some extent.

The fuel flow in the above three runs was turbulent, and pressure drops across the test section were large (Figure 29). These pressure drops increased in the first few hours of a run due to the rough surface formed by the coke. Later the pressure drop generally remained at a constant value. Pressure drops across the product filter increased during each run due to filtration of particles or formation of condensable solids in the filter.

Results of the 20-hour tests showed that coke formation was irregular, and the only variable having a distinct effect on coke deposition was the tube temperature. Results for various metals did not indicate that materials have different effects on coke formation. These tests did show that coke has two effects on heat transfer. One is detrimental in that the coke acts as an insulator, which decreases the heat transfer coefficient and increases the temperature difference for a given heat flux. The second effect is beneficial in that the coke acts as a turbulence promoter to improve the convective heat transfer. This occurred in flows which initially were not fully turbulent. In laminar flow the coke even caused an earlier transition to turbulent flow.

The effect of temperature on the rate of coke deposition is illustrated dramatically by the data from the 5-hour test runs. In Figure 43 coke surface density for these runs is plotted as a function of tube temperature. The coke measurements at tube temperatures below 1340°F (727°C) are all very small, most of them less than 40 $\mu g/cm^2$. Coke deposits at temperatures above 1340°F (727°C) are much greater. The maximum observed deposit during these runs was 663 $\mu g/cm^2$ at the maximum tube temperature of 1405°F (763°C). This corresponds to an average deposition rate of 133 $\mu g/hr-cm^2$. At times the actual rate of coke deposition was greater than this. At this point and most of the other points where heavy coke deposits were determined, the temperature of the tube was greater than 1340°F (727°C) initially, but during the test run the local tube temperature decreased to some lower value. These high initial temperatures are due to low heat transfer coefficients at flow conditions that were not fully turbulent. As coke formed, more turbulence developed, which improved the heat transfer and decreased the tube temperature.

This decrease in the rate of coke formation as the temperature dropped is illustrated by the coke analyses in Table X. The coke analyses for the tube used in the 100-hour Run 101 are given along with data from a 5-hour test at the same conditions. After five hours of operation the maximum coke deposits existed in the first part of the tube, where the tube temperature was the highest. At later times during Run 101 the tube temperature near the inlet decreased due to more turbulence and better heat transfer. Hence, the rate of coke deposition at this point decreased appreciably, and coke deposits here were only 2 to 3 times as much at 100 hours as the deposits at 5 hours.

Farther downstream the tube temperature increased during the test run. The initial rate of coke deposition was low and gradually increased to a higher value as the tube temperature increased. After operating about 25 hours the outside tube temperature levelled out at 1350°F (732°C). Later on during the run the tube temperature decreased abruptly and then increased gradually to 1550°F (843°C) again. Apparently some coke was lost during a weekend shutdown. Afterwards the coke deposited on the tube as before. Profiles of the tube temperature at two points (Figure 32) illustrate these observations. There were no distinct maxima in the final coke profile, which was generally flat and matched the temperature profile at the end of the run. Rates of temperature changes at various times during this test are listed in Table XI. These were used to calculate the rates of coke deposition based on the assumptions of constant thermal conductivity of coke and that the tube temperature rise was proportional to the increase in coke deposit.

-28-   Figure 43 follows

Diameter		Pressure		Heat Flux			
				0.02	0.2	1.0	4.0 ◄─Btu/sec-in²
in.	cm	psia	MN/m²	0.0327	0.327	1.63	5.64 ◄─MW/m²
1/16	0.16	500	3.45	▽	△	☐	◇
		1000	6.90	▼	▲	■	◆
1/8	0.32	500	3.45		◇	○	
		1000	6.90	●	◆		
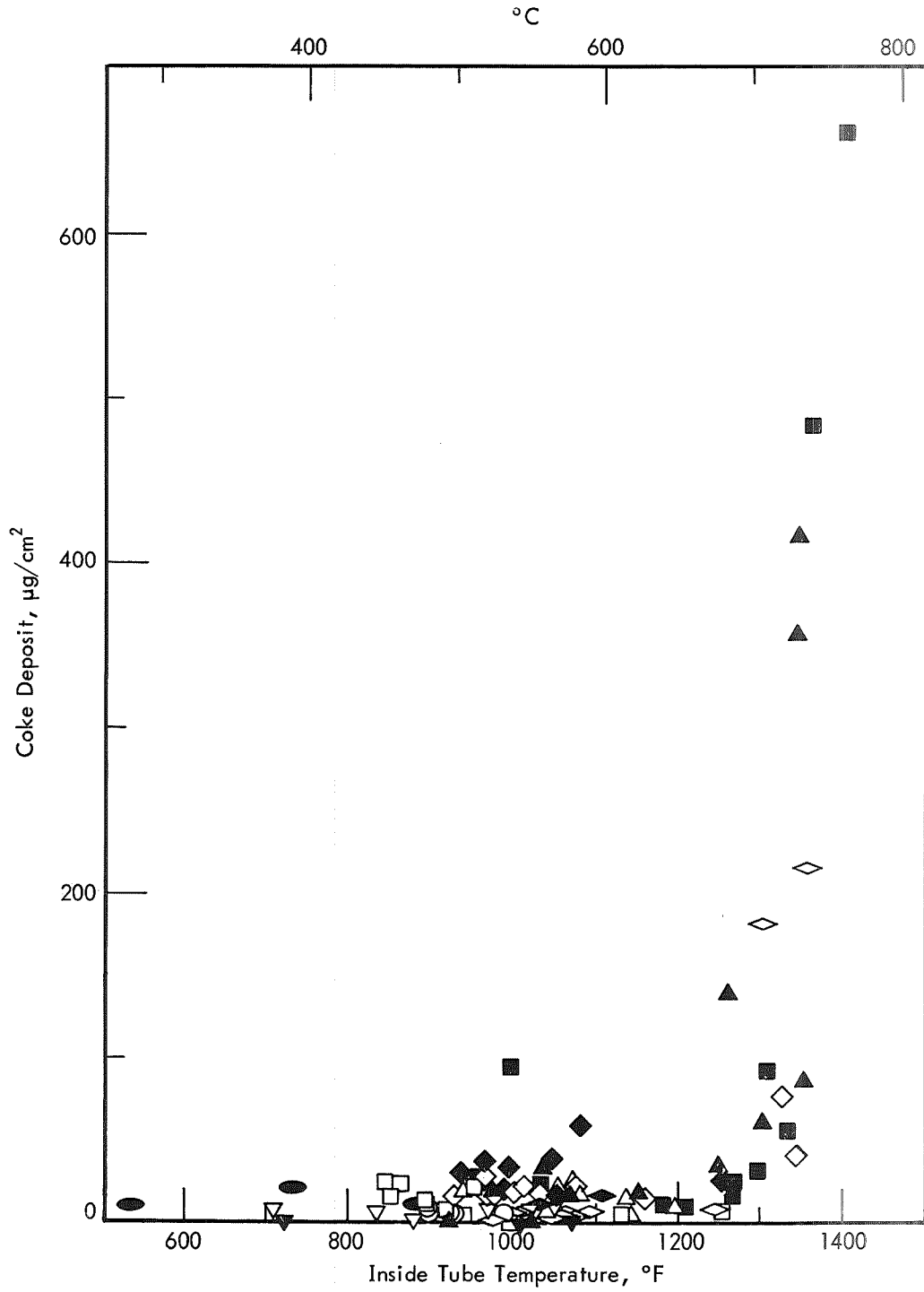
Figure 43.   COKE DEPOSITS DURING 5-HOUR RUNS

Table X. COKE ANALYSES FOR DIFFERENT RUN TIMES

Run		46	101
Run Time, hr		5	100
Tube Section		Coke Deposit, $\mu g/cm^2$	
ft	cm		
0 - 0.2	0 - 6.1	663	1365
0.2 - 0.4	6.1 - 12.2	484	1421
0.4 - 0.6	12.2 - 18.3	92	1456
0.6 - 0.8	18.3 - 24.4	26	1280
0.8 - 1.0	24.4 - 30.5	---	1351
1.0 - 1.2	30.5 - 36.6	10	1256
1.2 - 1.4	36.6 - 42.7	---	1693
1.4 - 1.6	42.7 - 48.8	11	1665
1.6 - 1.8	48.8 - 54.9	---	1431
1.8 - 2.0	54.9 - 61.0	16	658

The last test was the 100-hour Run 113 with aerated Jet A fuel. This test was run in the same manner and at the same conditions as Run 101. However, shutdowns over the weekends apparently had no effect on the coke deposits.

The profile of tube temperature in Run 113 initially was rather flat, similar to the profile in Run 101. The fuel was in transition flow in most of the tube. During the first few hours of operation coke formed on the tube surface, which presented a rough surface that increased turbulence in the fuel. This improved the heat transfer and decreased the tube temperature by 200-500°F (111-278°C) along most of the tube length. The minimum tube temperatures were reached at this time. Afterwards the deposition of coke only increased the heat transfer resistance; tube temperatures began to increase slowly. The rate of temperature increase was somewhat erratic, but the maxima in the temperature profile increased to 1400°F (760°C) in 10 hours and remained near this value up to 80 hours of operation. Later the temperatures of these peaks increased once again at a fast rate and eventually reached a maximum of 1650°F (899°C).

Figure 37 shows the change in the pressure drop across the tube during the run. Initially the pressure drop was 2.4 psi (0.017 MN/m²) and increased at a moderate rate during the test. It reached 16.4 psi (0.113 MN/m²) at 50 hours, after which it increased more rapidly until the end of the run. The increase during the last 10 hours was from 108 to 364 psi (0.74 to 2.51 MN/m²) and was due to the formation of coke which almost plugged the tube.

-29-

Table XI. RATES OF COKE DEPOSITION DURING 100-HOUR RUNS

Run	Location ft	Location m	Operating Period, hr	Rate of Temp. Increase °F/hr	Rate of Temp. Increase °C/hr	Calculated Rate of Coke Deposition, µg/hr-cm^2	Range of Inside Tube Temp.[a] °F	Range of Inside Tube Temp.[a] °C
101	0.4	0.12	5-20	11	6	70	1110-1280	599-693
			24-40	0.6	0.3	4	1300-1310	704-710
			40-50	10	6	60	1150-1250	621-677
			74-84	6	3	40	1230-1290	666-699
			84-98	0.8	0.4	5	1290-1300	699-704
101	1.5	0.46	4-20	12	7	75	1070-1270	577-688
			24-50	0.6	0.3	4	1295-1310	702-710
			53-60	9	5	55	1180-1240	638-671
			60-84	6	3	40	1145-1300	618-704
			84-100	1.5	0.8	10	1300-1325	704-718
113	0.6	0.18	5-30	3	1.7	8	880-950	471-510
			30-50	10	6	25	960-1140	516-616
			50-100	4	2	10	1140-1320	616-716
113	1.1	0.34	0-50	10	6	130	940-1400	504-760
			50-75	1	0.6	15	1400-1430	760-777
			75-100	9	5	120	1430-1650	777-899
113	1.7	0.52	0-10	30	17	600	1150-1400	621-760
			10-50	2	1	50	1400-1480	760-804
			50-70	0	0	0	1460-1470	793-799

a) Inside tube temperatures were 50-55°F (28-31°C) less than outside tube temperatures.

Figure 44 is a group of photographs showing coke deposits formed at various points in Run 113. The most extensive deposits occurred at the location of the temperature maxima, 1.1 and 1.75 ft. (0.34 and 0.53 m). At 1.1 ft (0.34 m) coke filled the tube completely (in spite of the appearance in Figure 44), which was the reason for the high pressure drop observed at the end of Run 113. Coke deposition in this run varied from 900 to 9300 $\mu g/cm^2$. The deposit profile generally followed the final profile of tube temperature. The lowest surface density of coke occurred near the tube inlet, and most of this coke formed during the first few hours of the test when tube temperatures at this point were the highest. During the run the minimum temperature was lower than in Run 101, which was probably due to a coke deposit that had a rougher surface exposed to the fuel in Run 113.

The density of coke was estimated from data in Run 113 at the two points of maximum deposits. The deposits at each end of the tube section between 1.7 and 1.8 ft (0.52 and 0.55 m) were about the same thicknesses, 5 to 6 mils (130 to 150 μm). A calculation based on this thickness and the measured surface density of the deposit yielded a coke density of 0.5 to 0.6 g/cm^3 (500 to 600 kg/m^3). The coke thickness at 1.2 ft (0.37 m) was about 10 mils (250 μm), and at 1.1 ft (0.34 m) the coke extended over the whole cross-section of the tube. Very likely the coke thickness was 10 mils (250 μm) or larger in this section of the tube. Based on a lower thickness limit of 10 mils (250 μm) the density of the coke in this section was estimated to be 0.4 g/cm^3 (400 kg/m^3) or less. These calculated densities correspond to the bulk density of coke, 0.37 to 0.51 g/cm^3 (370 to 510 kg/m^3), which means that the coke deposits were quite porous.

Thicknesses of coke deposits in all other runs, including Run 101, were very small and generally could not be measured. The greatest deposit thickness in these runs was less than 1 mil (25 μm) in Run 101. The fuel used in these runs was deoxygenated Jet A fuel. Hence, it is very desirable to use fuel as a coolant with an oxygen concentration as low as possible.

Efforts were made to estimate the thermal conductivity of the coke deposits. Figure 45 is a plot of the increase in tube temperature versus the amount of coke deposit. Curves were drawn for assumed thermal conductivities and an assumed deposit density of 0.5 g/cm^3 (500 kg/m^3). The data for the deposits, especially for Run 113, are quite scattered but do fall in the range of the bulk thermal conductivity for a mixture of coke particles, 0.11 Btu/hr-ft-°F (0.19 W/m·°C) for powdered coke and 0.55 Btu/hr-ft-°F (0.95 W/m·°C) for 20-100 mesh coke particles. The scatter of the data was expected, since the coke deposits do not form uniformly but present quite irregular surfaces as shown in Figure 44.

The temperature profiles shown in Figures 32 and 36 and the deposit measurements were used to estimate rates of coke deposition at various times during the 100-hour runs. These calculated rates are listed in Table XI. In Run 101 the rate of deposition at 5-20 hours, about 50 $\mu g/hr-cm^2$, was fairly high. When the inside tube temperature reached 1300°F (704°C), the rate decreased by an order of magnitude to 5 $\mu g/hr-cm^2$. There was no apparent reason for this change. Perhaps the temperature at the surface of the deposit had decreased, but there was no indication of this. Since the temperature profile was generally flat, deposition rates throughout the tube apparently were similar with the deoxygenated fuel in Run 101.

Figures 44 and 45 follow

In Run 113 the deposition rate was less predictable. The rate was variable throughout the tube with rapid deposition at some locations, where temperature maxima occurred, and slow at other places. The temperature maxima did remain in the vicinity of 1400°F (760°C) for 70 hours but eventually increased at a rapid rate before the end of the run. Much faster deposition rates and heavier deposits were characteristic of the aerated fuel.

Carburization was detected only on the inside surface of the tube used in Run 113 (Table IX). Photographs of specimens from tubes used in the 100-hour runs are shown in Figure 46. The depth of carburization, approximately 2.4 mils (60 μm), is clearly visible in the photograph for Run 113.

Because of the extent of coke deposition during Run 113, the inside tube temperature reached 1610°F (877°C). In the other 100-hour test (Run 101) the surface temperature reached only 1330°F (721°C), which was too low to cause carburization. In the 20-hour tests the inside tube temperatures were somewhat higher with a maximum of 1385°F (752°C), but no carburization was detected. Although the run times for these tests were only 20 hours, the tubes were exposed to the highest temperatures during much of this time. This should have been sufficient for any carburization to occur and later be detected.
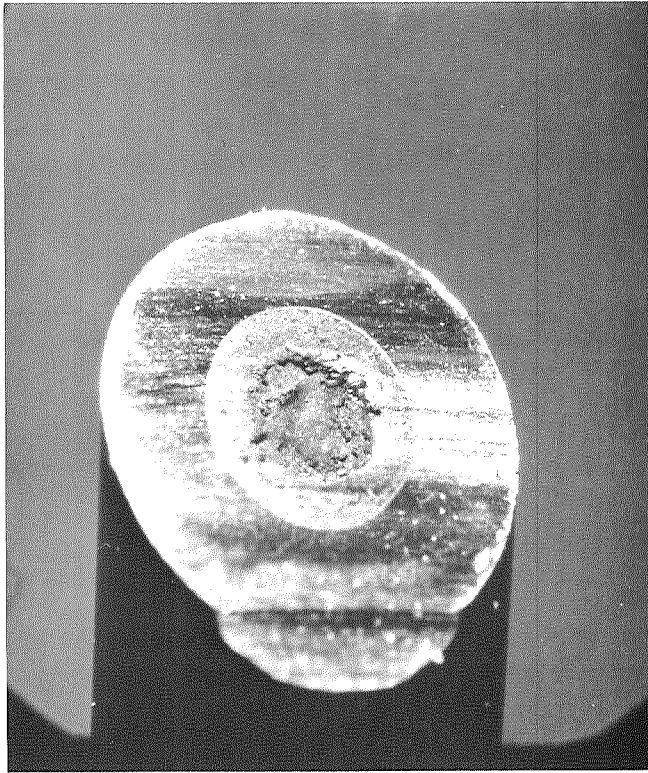
Based on these analyses, carburization of Hastelloy C occurs at a fast rate at 1600°F (871°C) and has a threshold temperature between 1400 and 1600°F (760 and 871°C). Stainless steel type 316 and L-605 (Haynes 25) alloy do not carburize at surface temperatures up to 1400°F (760°C).

HIGH FREQUENCY PRESSURE PULSATION

Pressure oscillations severe enough to cause an audible whistling noise were detected at the two test conditions listed in Table XII. The conditions for Runs 85, 91, and 98 were duplications of the 5-hour Run 32, during which the whistle was not heard. During the 20-hour tests the whistle could not be detected at the start of each run but became audible after a few hours of operation.

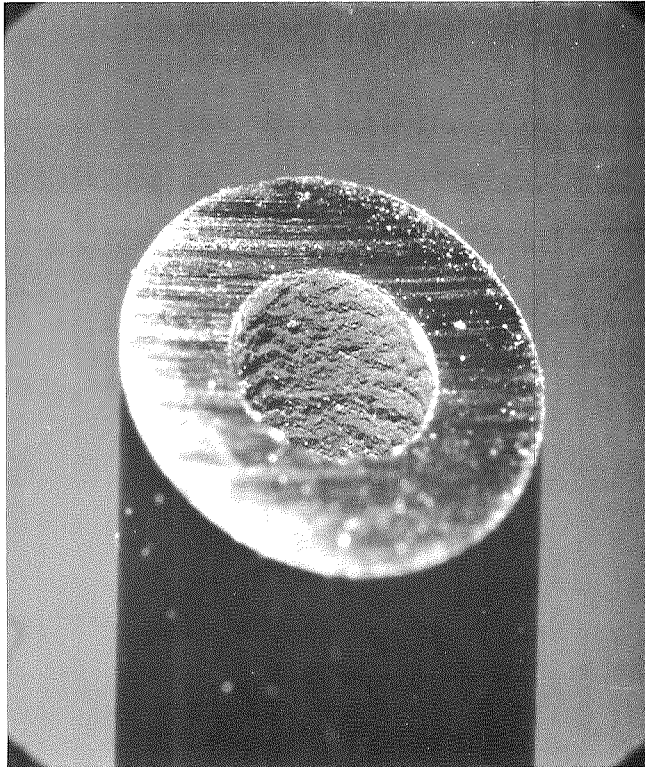Table XII. CONDITIONS FOR AUDIBLE PRESSURE OSCILLATIONS

Run	Outside Tube Diameter		Run Time, hr	Heat Flux		Outlet Fuel Temperature		Inlet Pressure	
	inch	cm		Btu/sec-in²	MW/m²	°F	°C	psia	MN/m²
42	1/8	0.32	5	1	1.63	800	427	500	3.45
79	3/16	0.48							
85									
91	1/8	0.32	20	4	6.54	1000	538	1000	6.90
98									

Figure 46 follows

S-14115

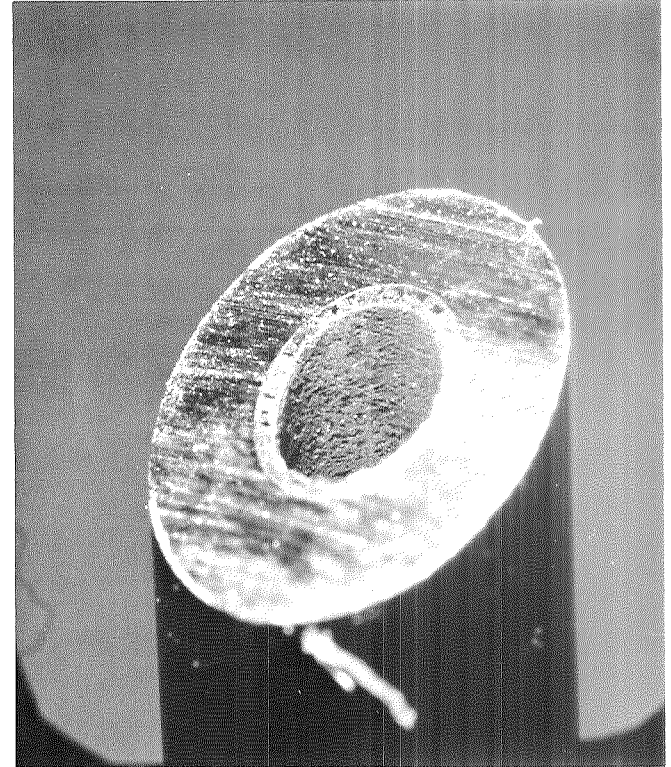A.   1.1 ft (0.34 m)   B.   1.2 ft (0.37 m)

C.   1.6 ft (0.49 m)   D.   1.7 ft (0.52 m)

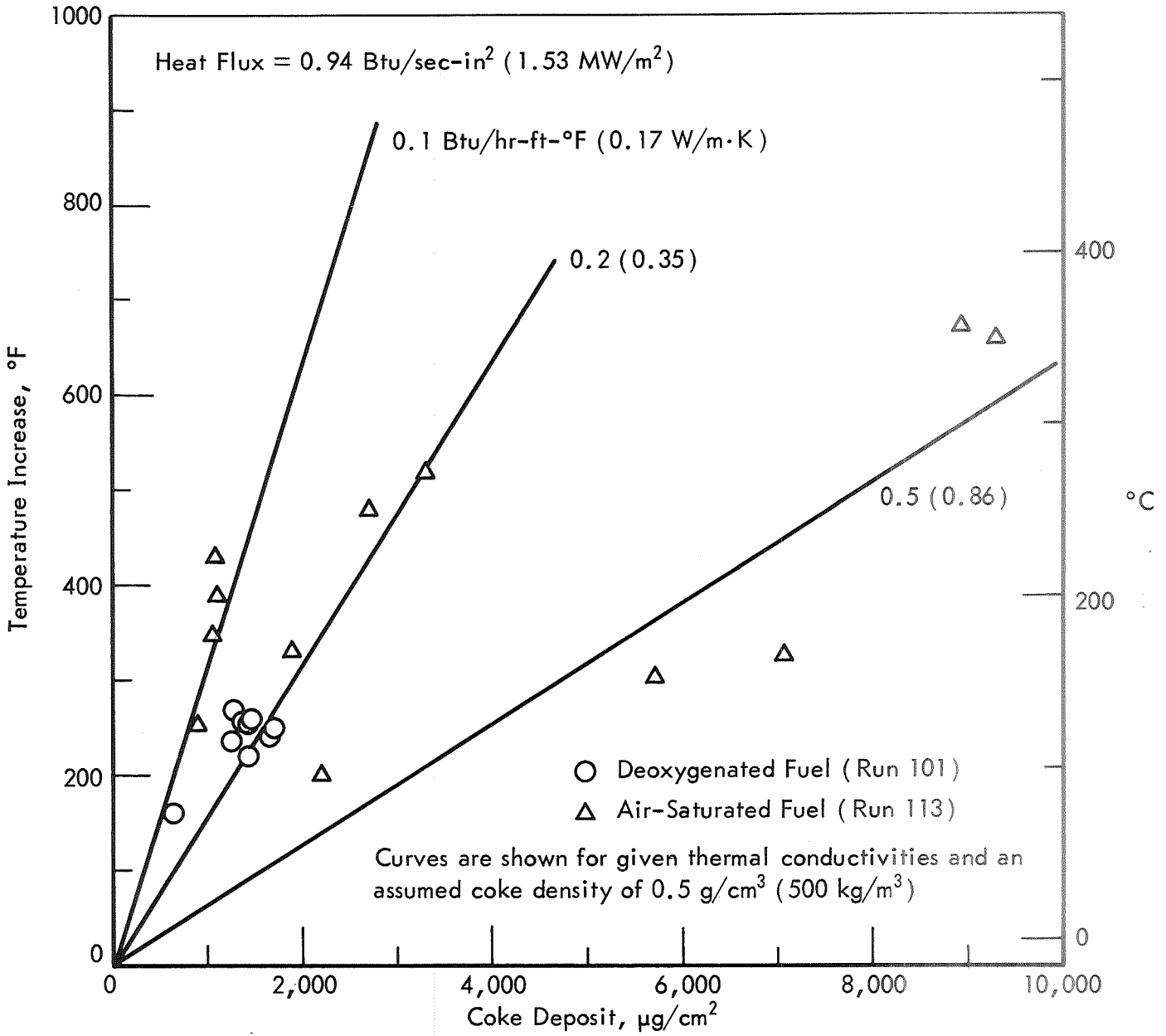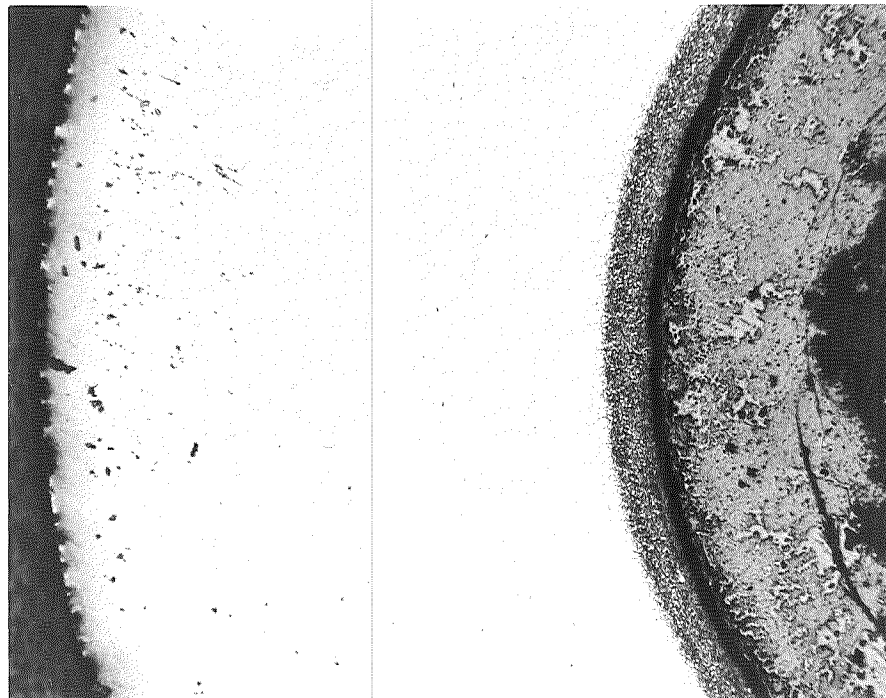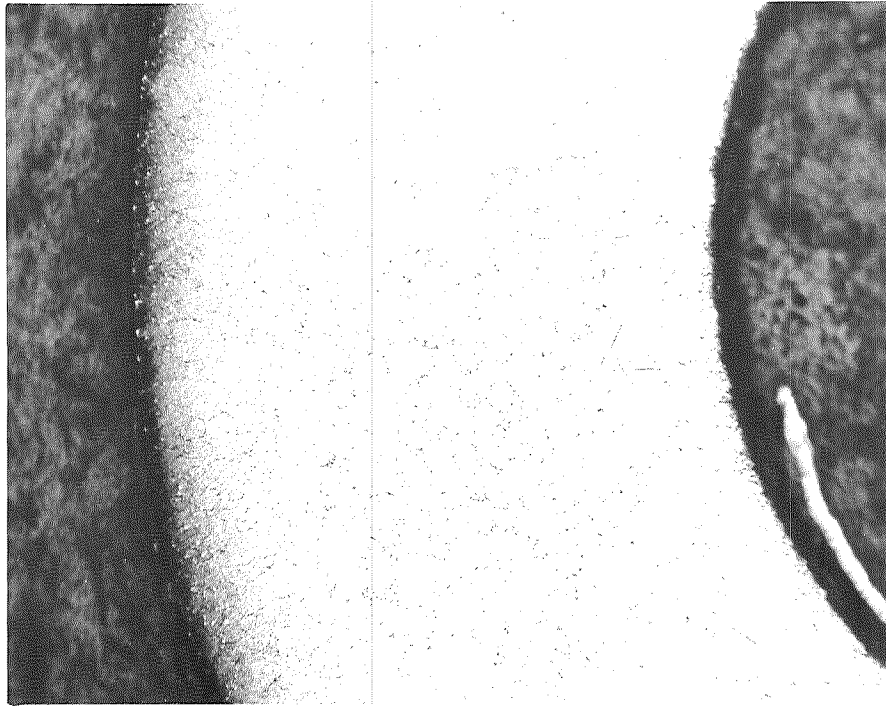Figure 44.   COKE DEPOSITS IN RUN 113 WITH AIR-SATURATED FUEL
Magnification: 17X

S-14115
67225

Figure 45. CORRELATION OF TEMPERATURE RISE WITH COKE DEPOSIT IN 100-HOUR RUNS

31.7 mils
(805 μm)

A. Run 113
1.1 ft (0.34 m)
Maximum Surface Temperature, 1610°F (877°C)

B. Run 101
1.5 ft (0.46 m)
Maximum Surface Temperature, 1330°F (721°C)

31.7 mils
(805 μm)

2.4 mils
(60 μm)

Figure 46.   CARBURIZATION OF HASTELLOY C TUBE
Magnification: 100X

Figure 47 shows photographs of oscilloscope traces taken during the 20-hour tests. Photograph A shows the wave form of the pressure fluctuation with an amplitude about 150 psi (1.0 MN/m²). Photographs B and C show the frequency spectrum of the pressure oscillations with well-defined peaks at 4300 and 8500 Hz. There also was much high frequency noise between 15,000 and 40,000 Hz.

Runs 42 and 79 were made at the same conditions with tubes of different diameters, and whistling was heard during both runs. Figure 48 shows the sensor output signal and frequency spectrum obtained while using the smaller tube (Run 42), and Figure 49 shows similar results for the larger tube (Run 79). The frequency spectra were quite similar for the two cases with a major peak at 1500 Hz and smaller peaks at frequencies of 5000 and 7000 Hz. However, the amplitudes of the pulsations differ appreciably: 100 psi (0.7 MN/m²) for the smaller tube and 350 psi (2.4 MN/m²) for the larger tube. The steady 350-psi (2.4 MN/m²) pulsation was interrupted for short periods at intervals of 1 to 10 minutes by a low frequency surge. Oscilloscope traces taken during a period of this surging operation and 5 minutes later during a period of steady pulsation are shown in Figure 50. The surging operation was characterized by a high frequency burst every 0.4 second   This high frequency burst was similar to the steady oscillation observed during most of this test. During half of each low frequency cycle the oscillation was very low with an amplitude about 15 psi (0.1 MN/m²). These low frequency oscillations were similar to the ones observed during the unsteady operation of the 100-hour Run 101.

While the whistling noise was heard at only two operating conditions, a whistle was heard frequently while heating the unit to operating temperature or while shutting down at the end of a run. This generally occurred when the outlet fuel temperature was near or slightly above the pseudocritical temperature of the fuel. When the whistle was heard during startup or shutdown the conditions in the tube were changing, so that the whistle was changing in pitch and intensity. Figure 51 is an illustration of the wave form (Photograph A) and frequency spectrum (Photograph B) observed during one of these shutdowns. Conditions for the results shown in the photographs were approximately:

Heat Flux	1.8 Btu/sec-in²	2.94 MW/m²
Outlet Fuel Temperature	580°F	304°C
Inlet Pressure	1000 psia	6.90 MN/m²
Outside Tube Diameter	1/8 inch	0.32 cm
Stainless Steel Type 316 Tube		

This particular whistle was a very clear tone, and its wave form was particularly sharp. The whistle apparently had a primary frequency at 3000 Hz and a secondary frequency at 5500 Hz; its amplitude was 18 psi (0.12 MN/m²).

These pressure fluctuations are thought to be flow instabilities which were caused by rapid changes in the fluid properties during heat transfer. The following description is a possible explanation of these instabilities.

S-14115

The fuel at the tube outlet generally was near its pseudocritical point. As heat was transferred to the fuel there were rapid changes in its physical properties, especially a sudden decrease in viscosity. This decrease in viscosity caused a thinning in the heat transfer boundary layer and an increase in the heat transfer coefficient, which in turn caused a decrease in the film temperature of the fuel and a resultant increase in its viscosity. Because of this change in viscosity, the boundary layer then increased, and the cycle repeated itself. This phenomenon is similar to the instability caused by boiling and could be considered as pseudoboiling heat transfer. Observations of pressure fluctuations were more frequent at 500 psia (3.45 MN/m^2) than at 1000 psia (6.90 MN/m^2). At the greater pressure changes in fuel properties were less severe; hence, there was less tendency for flow instability to occur.

CONCLUSIONS

Heat transfer to Jet A fuel was investigated in both turbulent and laminar flow. Considerable free convection occurred in laminar flow, which greatly enhanced the heat transfer rates. Temperature differences between the top and bottom of the tubes were as great as 150°F (83°C) in tubes of 1/8-inch (0.32 cm) inside diameter. Observed Nusselt numbers in some cases were several times the theoretical value for Poiseuille flow. The laminar flow apparently was stabilized by the free convection, in some cases at Reynolds numbers up to 15,000 for high Grashof numbers. For these Grashof numbers turbulent flow occurred at higher Reynolds numbers and in some cases at Reynolds numbers down to 5000. For low Grashof numbers turbulent flow was observed at Reynolds numbers above 2200.

Correlations were developed for predicting heat transfer coefficients in the two flow regimes. The Grashof number was found to be the most important independent variable for laminar flow heat transfer enhanced by free convection. Other significant variables were the Prandtl number and the ratio of the bulk fuel density to the fuel density at wall conditions. In turbulent flow the Reynolds and Prandtl numbers were significant variables which correlated with the Nusselt number. The ratio of the bulk fuel temperature to the wall temperature improved this correlation.

A large number of metals and alloys were screened in coker tests with aerated fuel to determine the influence of tube material on coke deposition. Although the deposition rate varied for different materials, there was no obvious relationship between coking tendency and tube composition. Deposit measurements on all materials were found to be small or moderate, and there were no heavy deposits on any metal. Further testing with deoxygenated fuel in the heat transfer test rig at more severe conditions yielded similar results for different metals. Coking at conditions of laminar flow with free convection was mild and not extremely different for each tube material. In turbulent flow coke deposition was irregular, and the results did not indicate clearly any relationship between coking tendency and tube material. The primary factor affecting deposit formation was the tube temperature. Test runs showed that the deposition rate was significant at surface temperatures above 1340°F (727°C).
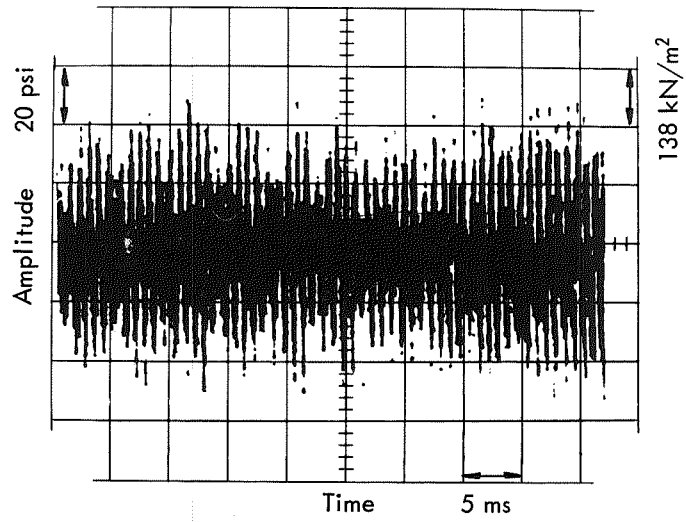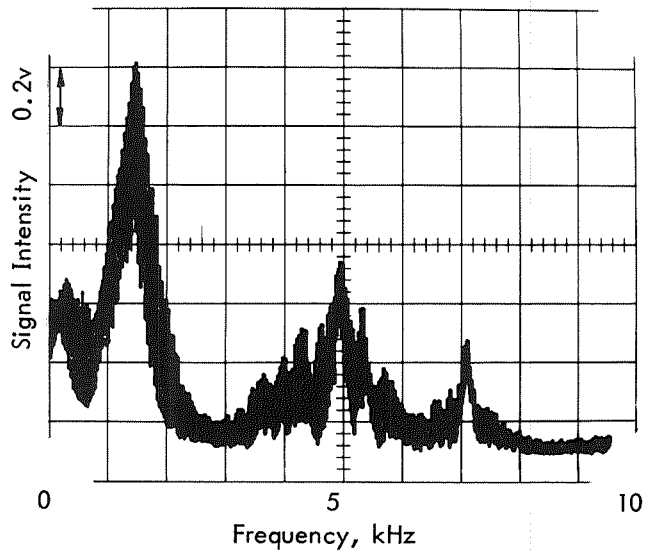
-34-
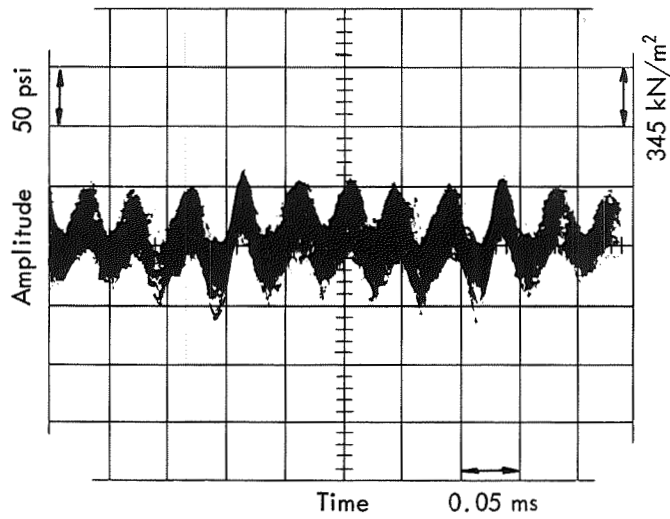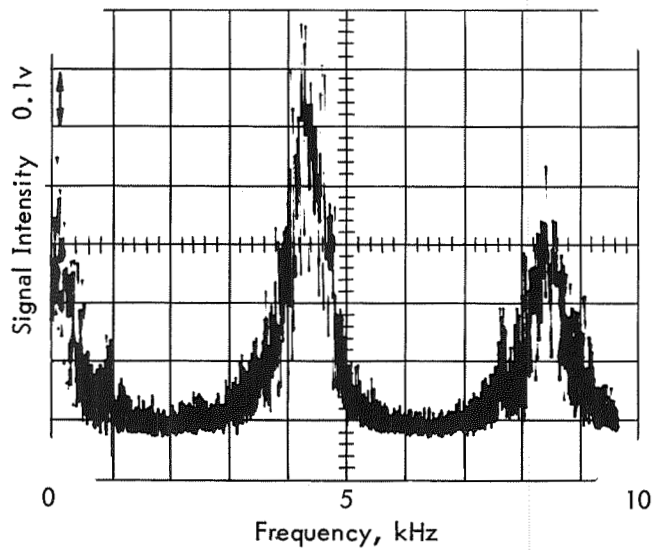
A. Wave Form

B. Frequency Spectrum
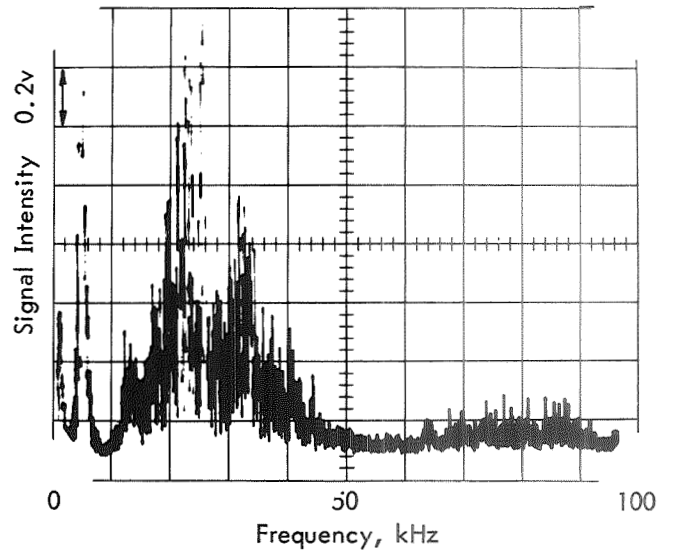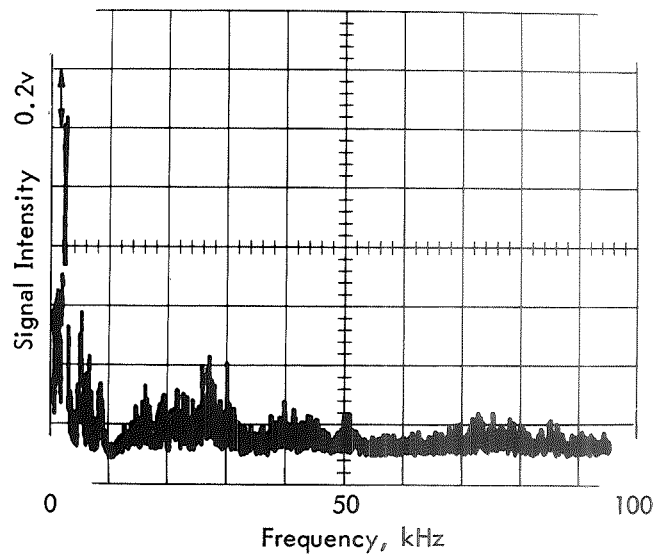
C. High Frequency Spectrum

Figure 47. PRESSURE PULSATIONS DURING 20-HOUR RUNS 85, 91 AND 98

A. Wave Form

B. Frequency Spectrum C. High Frequency Spectrum

Outside Tube Diameter = 1/8 in (0.32 cm)

Figure 48. PRESSURE PULSATIONS DURING RUN 42

A. Wave Form
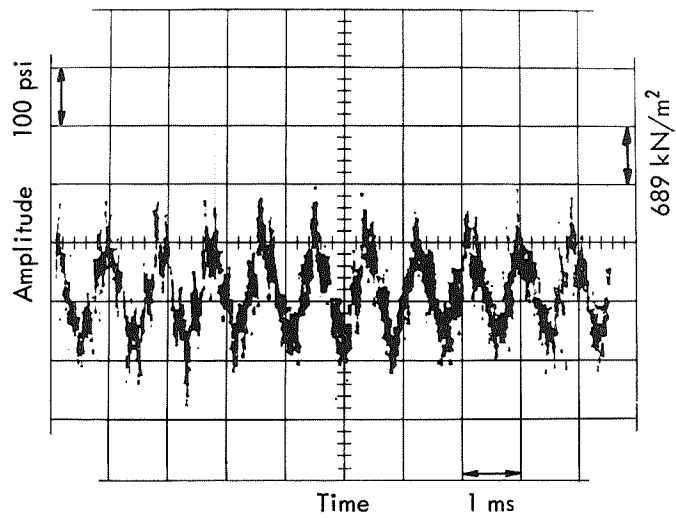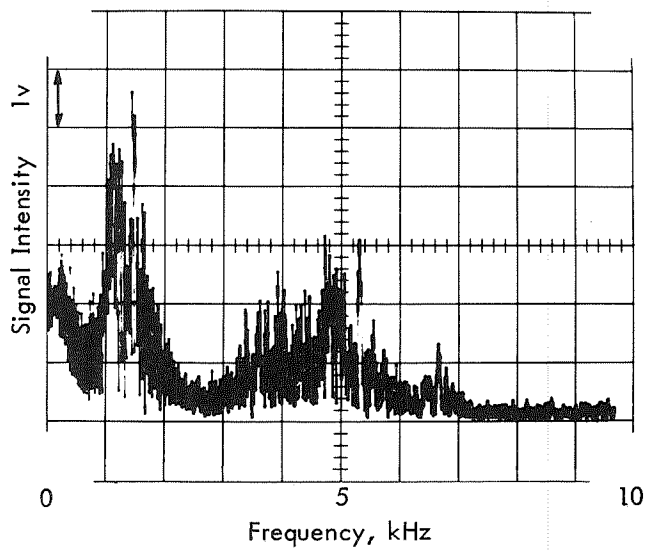
B. Frequency Spectrum   C. High Frequency Spectrum
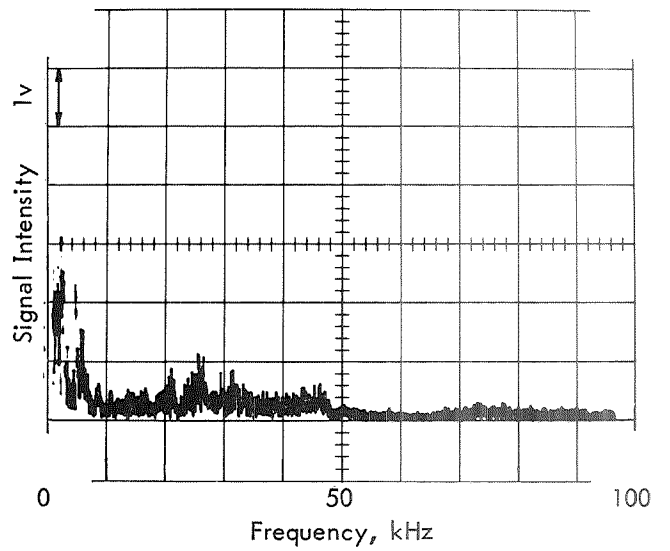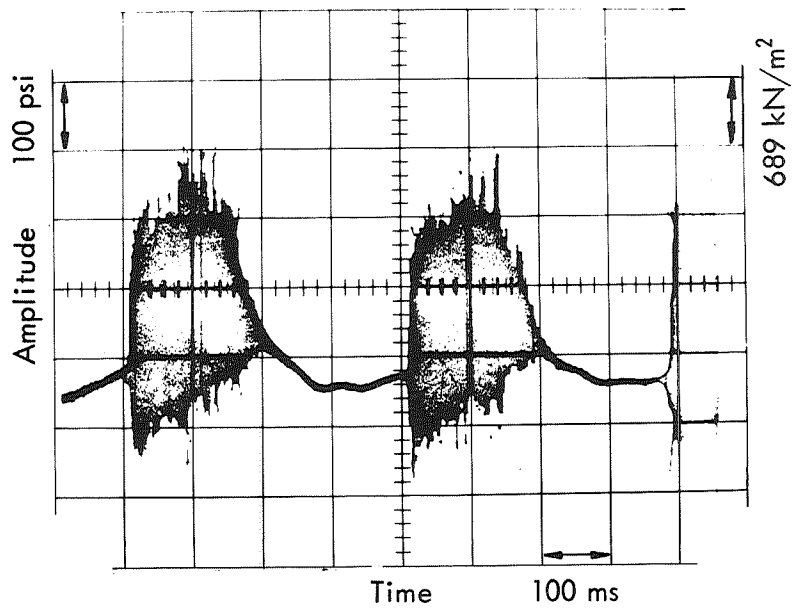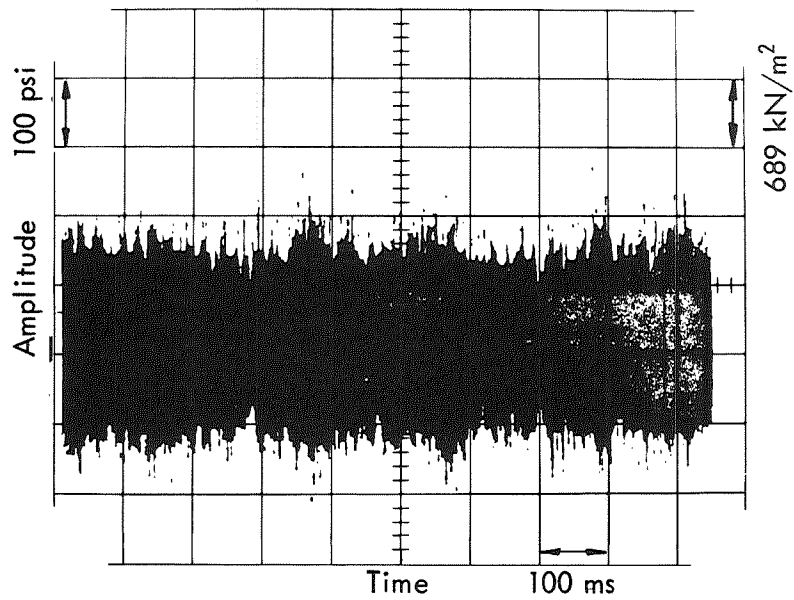
Outside Tube Diameter = $\frac{3}{16}$ in (0.48 cm)

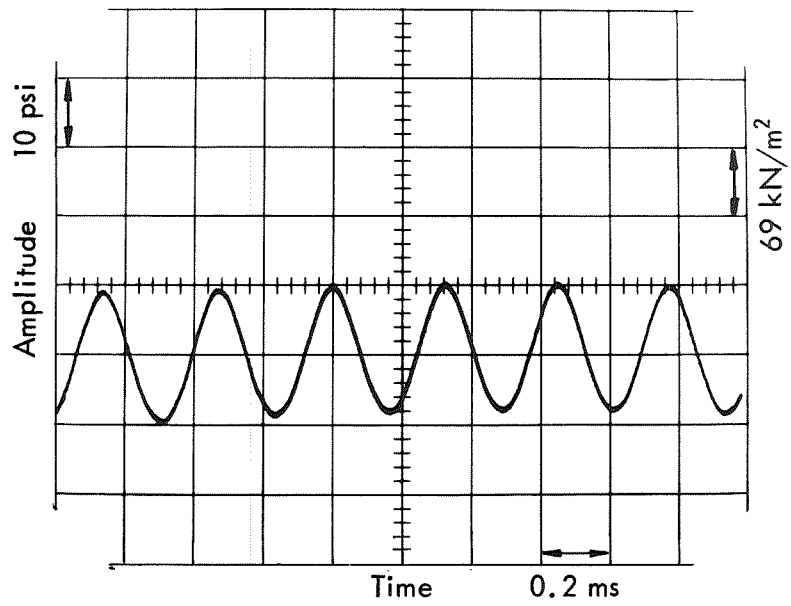Figure 49. PRESSURE PULSATIONS DURING RUN 79

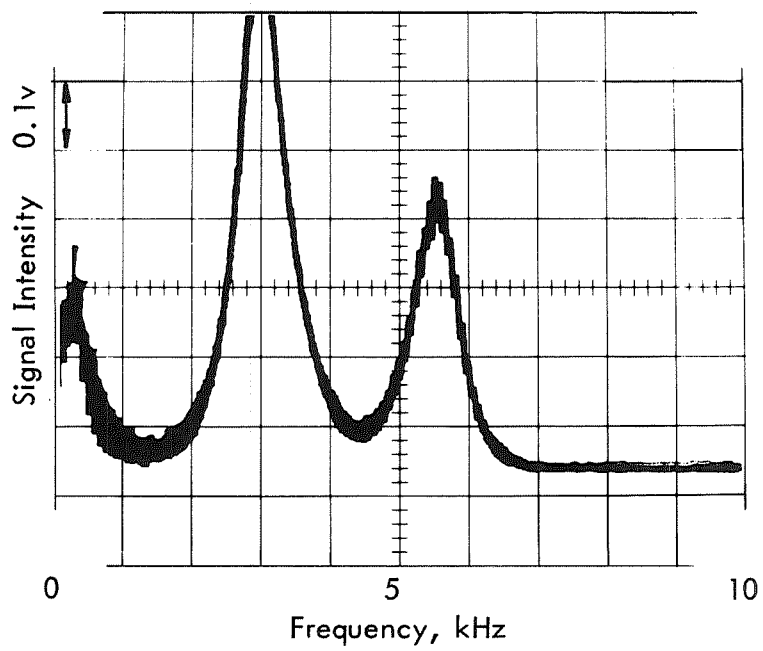S-14115
67374

A. Surging Operation

B. Non-Surging Operation

Outside Tube Diameter = $\frac{3}{16}$ in (0.48 cm)

Figure 50. PRESSURE PULSATIONS DURING SURGING OPERATION OF RUN 79

A. Wave Form

B. Frequency Spectrum

Figure 51. PRESSURE PULSATIONS DURING SHUTDOWN OF RUN 91

There were two effects of coke deposition on heat transfer. At the start of many tests the formation of a rough coke surface increased the fluid turbulence and the convective heat transfer coefficient to those for fully turbulent flow. Only a very thin deposit was necessary to achieve this effect. This phenomenon had the additional benefit of reducing the rate of coke deposition. On the other hand, the resistance to heat transfer increased as coke formed. This effect on heat transfer was insignificant for thin deposits.

Experiments also showed that oxygen had a strong influence on coke deposition, which affected the heat transfer. Deposits formed from deoxygenated fuel were relatively thin, less than 1 mil (25 μm). The use of aerated fuel resulted in faster rates of deposit formation and much heavier deposits, which almost plugged a tube of 1/16-inch (0.16 cm) inside diameter. Heat transfer resistances of deposits formed from the aerated fuel were greater, and surface temperatures of the tube reached a maximum of 1610°F (877°C). This was high enough for carburization of the tube to occur.

Deposit formation was the result of thermal reaction of the fuel, which also produced other changes in the fuel. Thermal cracking occurred and yielded light hydrocarbons and hydrogen. This also resulted in a color change of the fuel from water-white to yellow or amber. The extent of cracking during the thermal reaction was small; hence, cracking was an insignificant contribution to the heat sink of the fuel. However, some of the reaction products must have enhanced the rate of coke formation.

Pressure oscillations were audible at certain turbulent flow conditions when the exit fuel was near the pseudocritical temperature. Amplitudes of these pressure fluctuations ranged up to 350 psi (2.4 MN/m^2) in tubes of 1/8-inch (0.32 cm) inside diameter and 150 psi (1.0 MN/m^2) for 1/16-inch (0.16 cm) inside diameter. Primary frequencies varied from 1000 to 5000 Hz. The noise was heard at both 500 and 1000 psia (3.45 and 6.90 MN/m^2), but it was more common and its amplitudes were greater at the lower pressure. These oscillations apparently are analogous to boiling heat transfer, and the effect of pressure is probably due to greater changes in the fuel viscosity and density at lower pressures.

In these tests coke deposits were light in the deoxygenated fuel, even after extended test runs of 20 and 100 hours at a heat flux of 1.0 Btu/hr-ft^2 (1.63 MN/m^2). Aerated fuel was tested for 100 hours, and, although coke formation was faster in this fuel, most of the coke deposition occurred near the end of the test. Increases in the pressure drop across the test section were small with the deoxygenated fuel and only slightly higher during most of the run with the aerated fuel. Experimental results with both fuels showed that a thin layer of coke was beneficial in promoting more turbulence to enhance the convective heat transfer coefficient.

RECOMMENDATIONS

This study has been fruitful in providing information on heat transfer and coking when Jet A fuel is used as a coolant. Additional testing can furnish more data on coking, and the following points are suggested for future work.

S-14115

Additional heat transfer and coking tests of 100-hour duration are desirable. Although tube temperature is a primary factor affecting the rate of coke deposition, tube temperature is determined by other factors such as heat flux, tube diameter, and flow conditions. The relation between these variables and tube temperature is complicated by the presence of coke, and data from extended tests at other heat fluxes and tube diameters would be useful.

Other long coking tests at oxygen concentrations between 0.5 and 66 ppm would provide useful data. There is an enormous benefit achieved by maintaining a low oxygen concentration, as illustrated in the reported tests. However, these tests were run under laboratory conditions, and it may not be possible to achieve such a low concentration at all times in actual use. Hence, data at other concentrations which are considered to be easily reached and maintained in actual use would be desirable.

Repetitive experiments of extended duration are desirable to determine the reproducibility of coke deposits, since coke formation is irregular and its rate is difficult to predict.

Experience from these tests indicate that cracking and coking in the fuel should cause no difficulty in the fuel system downstream of a heat exchanger. Also, the effect on ignition and combustion of the fuel should be very slight. Nevertheless, system studies would be useful to verify this expected behavior, and there may be some slight effect on combustion efficiency and some differences in the production of smoke or undesirable combustion products.

S-14115

APPENDIX

(This page is blank.)

Modified Jet Fuel Thermal Oxidation Tester

The Jet Fuel Thermal Oxidation Tester (JFTOT) was designed as a reduced version of the standard CRC-ASTM fuel coker. A basic objective of the design was to reduce the volume of test fuel from the 5 gallons ($0.02 \ m^3$) required for the standard coker to about 1 quart ($0.001 \ m^3$). Accordingly, the entire system was scaled down by a factor of about 20, without changing the basic flow and heat transfer characteristics of the test. For example, in the JFTOT the fuel residence time in the preheater at the established flow rate of $3.0 \ cm^3/min$ ($0.05 \ cm^3/s$) is about 12 seconds. In the standard coker the residence time is about 10.4 seconds at a flow rate of 5 lb/hr ($0.63 \ g/s$). Tests in both cokers have a 5-hour duration. Comparisons of maximum visual ratings of two different Jet A fuels in the JFTOT with ratings on the same fuels in the ASTM Coker showed good agreement (Table XIII). The difference in ratings are within the reproducibility of the two tests.

A schematic diagram of the JFTOT fuel system is shown in Figure 52. The essential elements of this test rig were modified somewhat to withstand 1000°F (538°C) and 1000 psig ($7.0 \ MN/m^2$) compared to the standard 300 psig ($2.1 \ MN/m^2$). This modification required a stronger fuel reservoir and fuel flow indicator.

In preparing the system for operation the fuel charge is placed in the bottom of the cylindrical stainless steel reservoir. An aluminum piston with a rubber V-seal is placed on top of the fuel, and a flange cover is bolted to the reservoir. Nitrogen pressure is supplied through a regulator to the top side of the piston to establish the system pressure. Fresh fuel is pumped through the system from the bottom of the reservoir back to the top of the reservoir above the piston. The V-seal on the piston prevents intermixing of the fresh and spent fuels.

As the fresh fuel is forced from the reservoir, it passes through a membrane filter at the reservoir outlet. The fuel then enters the bottom of an annular heater tube section and flows up around an inner tube, which is heated directly by resistance heating. A movable thermocouple inside of this heater tube is used to measure its temperature profile during the test. At the outlet of the heater section the fuel passes through a test filter. The pressure drop across this filter is measured by a differential pressure transducer and printed on a recorder. The spent fuel then passes through a cooler and enters a Zenith metering pump, after which it is returned to a fuel flow drip indicator to the top of the reservoir. Hence, the fresh fuel is never exposed to the pump.

During a run in the JFTOT the tube temperatures are measured by the movable thermocouple and printed by a recorder as a profile along the tube length. Also, the liquid outlet temperature is measured by a thermocouple and printed. Our unit is supplied with a Minarek Electric variable speed and torque control on the pump to permit compensation for flow changes due to the effects of flow resistance or pump wear, whereas the commercial version has a fixed pumping speed. System pressure is indicated on a Heise gauge with a range of 0-2000 psig ($0 - 13.8 \ MN/m^2$).

Figure 52 follows

S-14115

Table XIII. COMPARATIVE RATINGS ON THE JFTOT AND ASTM COKERS

5-hour Tests with Jet A Fuels

Fuel Designation	Test Method	Fluid Temperature		Maximum Code Rating
		°F	°C	
F-185	JFTOT	418	214	4
F-185	ASTM	417	214	4
F-185	ASTM	420	216	4
F-187	JFTOT	410	210	2
F-187	ASTM	410	210	1
F-187	JFTOT	415	213	2
F-187	ASTM	415	213	2.5
F-187	JFTOT	422	217	2.5
F-187	ASTM	420	216	3.5

The heater tube section is dismantled following a test and the inner tube removed, washed with normal heptane, and rated for deposits.
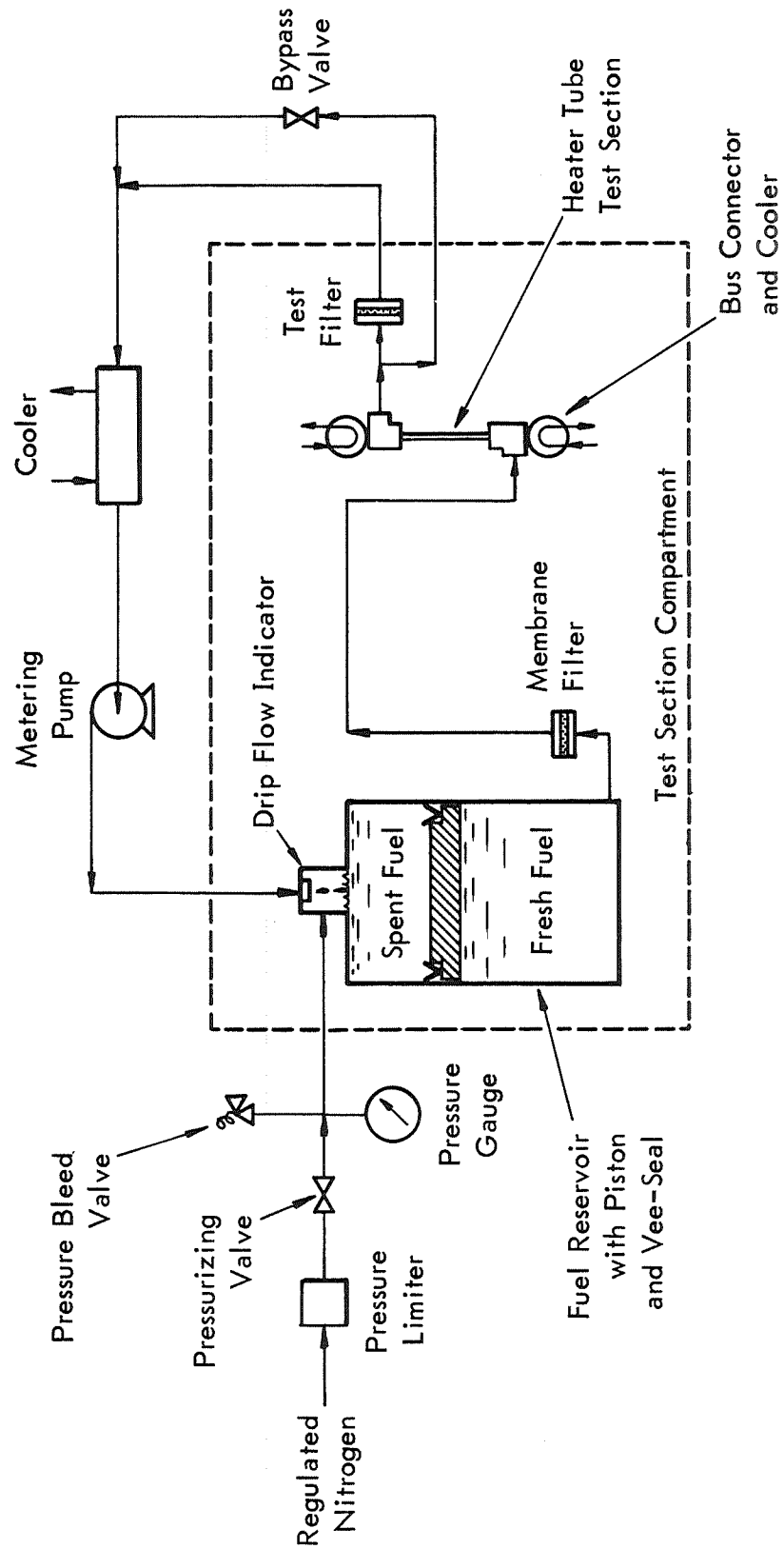
Figure 52. FLOW DIAGRAM OF JFTOT COKER

Beta-Ray Deposit Rater[a)]

The Beta-Ray Deposit Rater (BDR) is an instrument used for measuring deposits on coker tubes. In measuring the deposits in the BDR a beam of low energy electrons impinges on the deposit and tube surface, from which back-scatter of the electrons occurs. A detector is used to measure the intensity of electron backscatter, and the signal from the detector is recorded. The extent of backscatter is related to the surface density and atomic number of the deposit and the average atomic number of the substrate metal. Calibration data for organic films on various metals and alloys are used to interpret the detector signal and determine the amount of coke deposit. A scanning mechanism is used to translate and rotate the tube past the detector so as to measure coke deposition over all the tube surface.

The instrument is shown in Figure 53 and consists of the following functional units: (1) vacuum system, (2) scanning mechanism, (3) beta-ray source, and (4) detection system.

The vacuum system consists of a chamber made from a 3-ft (0.9 m) length of 6-inch (15 cm) Schedule 40 steel pipe. End plates are attached and sealed by O-rings. One end plate is removable and provides access for insert-ing a coker tube; the drive mechanism is connected through the other end plate. Vacuum in the system is achieved by a Welch 1402B fore pump. The suction side of the pump is connected by rubber tubing to a pipe nipple welded to the vacuum chamber. The remainder of the vacuum system consists of a thermocouple gage and a bleed valve for pressure regulation.

The scanning mechanism serves to translate and rotate the coker tube past the source and detector. It consists of a track fastened to the inside of the vacuum chamber on which a carriage rides. The carriage holds the coker rod and is driven by a shaft and lead screw arrangement attached to the end plate of the vacuum system. The drive shaft in the test chamber is connected through a vacuum seal to a variable speed reversible motor.

The beta-ray source is contained in a block which is mounted on the face of the detector. The source material is tritium, which was obtained from the target of a Texas Nuclear neutron generator. The block consists of layers of brass with two milled slots to direct the beta-ray beam to the coker tube, which is located at the intersection of the beams. Between these two slots is a third slot which is aligned with the opening in the detector. Backscat-tered radiation passes through this slot and is measured by the detector.

The detection system measures the radiation that is backscattered from the coker tube and presents the count rate on a strip chart recorder. The detector is a flow proportional counter with an ultrathin window and operates on P-10 gas (90% argon and 10% methane). The window is a thin film of cellulose nitrate. It is supported by a Buckbee Meers Company nickel screen of 70% transmission. The detector is attached to a flange that provides a vacuum seal and can be moved while under vacuum to position the opening relative to the coker tube in order to focus the radiation.

a) The Beta-Ray Deposit Rater was developed under Air Force Contract F33615-70-C-1038 for the Air Force Aero Propulsion Laboratory, Air Force Systems Command, United States Air Force, and is more completely described in Semiannual Progress Report No. 2 (Shell Development Company Report No. S-14114, April 1971).

-41-   Figure 53 follows

The rest of the detection system is outside the vacuum chamber and consists of a high voltage power supply for the proportional counter, a low noise preamplifier, a linear amplifier, a count rate meter, and a strip chart recorder with an offset zero adjustment.

The readout signal on the strip recorder is calibrated in beta radiation counts/second, which may be converted to deposit surface density by using calibration curves such as that illustrated in <u>Figure 54</u>. A family of curves is shown for deposits of average atomic number 5, 6, and 7 on an Inconel 600 tube of 5/8-inch (0.16 cm) OD. A different family of curves is required for each metal substrate. The general expression describing these curves is as follows:

$$
\begin{aligned}
I = A & \left\{ 1 - \exp\left[-1.8 \times 10^4 \left(\frac{331 + Z_1}{106 + Z_1} \right) X \right] \right\} \\
& + B \exp\left\{ -1.8 \times 10^4 \left[1 + \left(\frac{225}{106 + Z_2} \right) \left(\frac{Z_1}{Z_2} \right)^{1/3} \right] X \right\}
\end{aligned}
\tag{7}
$$

where
I = observed count rate for deposit on the tube, counts/second
A = observed count rate for pure deposit, counts/second
B = observed count rate for clean tube, counts/second
Z_1 = average atomic number of deposit
Z_2 = average atomic number of tube
X = deposit surface density, g/cm^2

Figure 54 follows
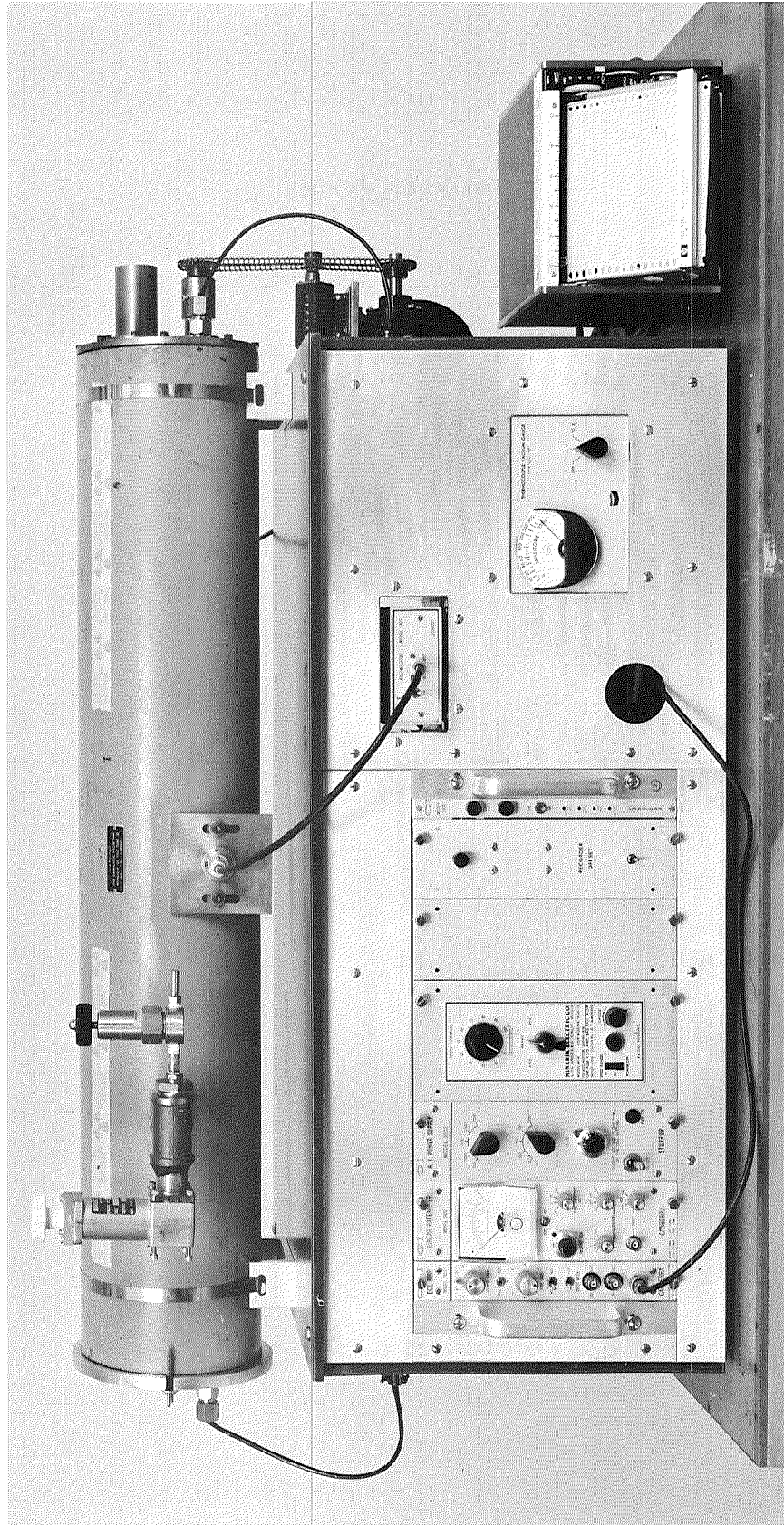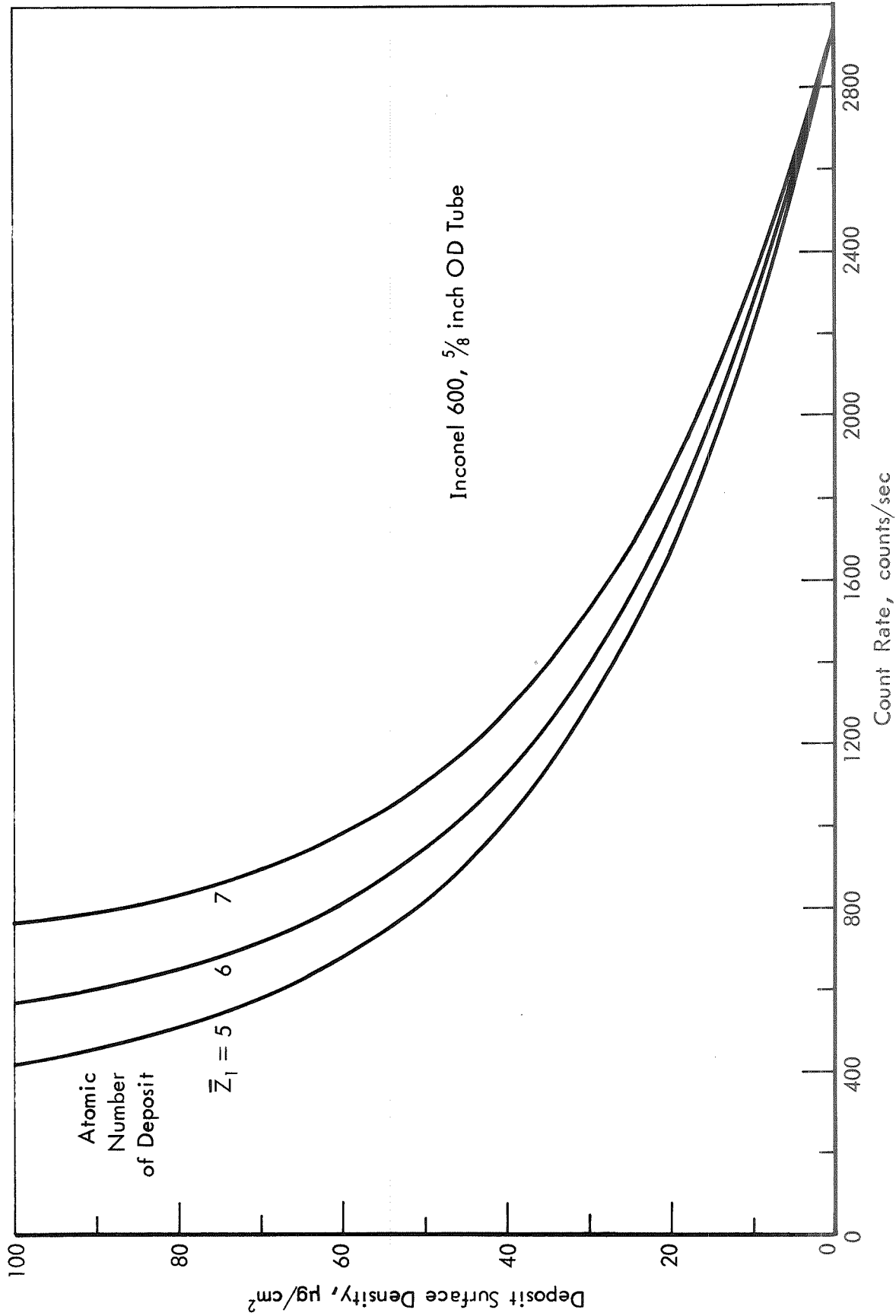
Figure 53. BETA-RAY DEPOSIT RATER

Figure 54.   CALIBRATION CURVES FOR BETA-RAY DEPOSIT RATER

Table XIV. SPECIFICATIONS FOR AVIATION
TURBINE FUEL TYPE A[a]

Property	Specification	ASTM Test Method
Gravity, max, °API	51	D 287
Gravity, min, °API	39	D 287
Distillation Temperature, °F:		D 86
10% Evaporated, max	400	
50% Evaporated, max	450	
Final Boiling Point, max, °F	550	
Distillation Residue, max, %	1.5	
Distillation Loss, max, %	1.5	
Flash Point, min, °F	110 or legal	D 56
Flash Point, max, °F	150	D 56
Pour Point, max, °F	-40	D 97
Freezing Point, max, °F	-40	D 1477
Viscosity at -30°F, max, cs	15	D 445
Net Heat of Combustion, min, BTU/lb	18,400	D 1405 or D 240
Net Heat of Combustion, BTU/gal	None	
Copper Strip Corrosion, 3 hr at 122°F, max	No. 1	D 130
Total Acidity, max, mg KOH/gram	0.1	D 974
Sulfur, max, %	0.3	D 1266
Mercaptan Sulfur, max, %	0.003	D 1323 or D 1219
Water Tolerance, vol change, not to exceed, ml	$\pm$1	D 1094
Existent Gum, max, mg/100 ml	7	D 381
Total Potential Residue, 16 hr, max, mg/100 ml	14	D 873
Thermal Stability at 300 to 400°F:		
Filter Press Drop, max, in Hg	12	D 1660
Preheater Deposit less than	Code 3	
Combustion Properties. One of the following requirements shall be met:		
(1) Luminometer Number, min	45	D 1740
or		
(2) Smoke Point, min	25	D 1322
or		
(3) { Smoke Point, min	20	D 1322
{ Burning Test, 16 hr	--[a]	D 187
or		
(4) { Smoke Point, min	20	D 1322
{ Naphthalenes, max, %	3	D 0000
or		
(5) Smoke Volatility Index, min	None	D 1322 and D 86
Aromatics, vol, max, %	20	D 1319
Additives	--[a]	...

a) ASTM D 1655-61 T.

S-14115

Table XV. INSPECTION DATA FOR JET A FUEL (F-187)

Property	Measurement
Gravity, °API	39.8
Color, Saybolt	30+
Flash, Tag c.c., °F	136
Pour Point, °F	B-60
Viscosity, cs at 30°F	10.24
Copper Strip Corrosion at 122°F	1
Copper Strip Corrosion at 212°F	1
Corrosion, Silver Strip	0
Mercaptan Sulfur, % wt	0.0001
Odor	ok
Smoke Point, mm	20
Aromatics, % vol	14.1
Freezing Point, ASTM °F	B-58
Water Reaction, Inc. or Dec., ml	0.5
Interface Rating	1
ASTM Distillation, °F:	
I.B.P.	344
10% Evaporated	365
50% Evaporated	419
90% Evaporated	478
95% Evaporated	491
End Point	504
Recovery, % vol	98
Residue, % vol	1.0
Loss, % vol	1.0
Aniline Gravity Constant	5532
Net Heat of Combustion, Btu/lb (Calc)	18,500
Gum, Existent, Steam Jet, mg	1
Gum, Potential, Steam Jet, mg	1
Total Acid Number, Colorimetric	Neutral
Strong Acid Number, Colorimetric	Nil
Olefins, % vol	0.7
Naphthalenes (Diaromatics)	0.31
Water Separometer Index Mod	98
Luminometer Number	47.3
Thermal Stability, ASTM-CFR	
Pressure Drop, in Hg	0.05
Preheater Deposit Rating	0

Table XVI. ANALYSES OF JET A FUEL (F-187)

Gum, Steam Jet: 0.1 mg/100 ml

Fluorescent Indicator Analysis

Component	Concentration, % vol
Saturates	84
Olefins	1
Aromatics	15

Mass Spectrometer Ring Analysis

Number of Rings	Concentration, % vol
0	38
1	33
2	25
3	4

Trace Impurities

Component	Concentration, ppb
Sulfur	10,000
Lead	500
Nickel	13
Copper	7
Iron	7

ASTM D86 Distillation

Distilled, %	Temperature, °F
I.B.P.	334
5	354
10	363
15	369
20	375
30	388
40	402
50	417
60	431
70	444
80	458
90	475
95	490
E.P.	498
Recovery	98.5% vol
Residue	1.5% vol
Pressure	766.4 mm Hg

Hydrocarbon Type Analysis
(High Resolution Mass Spectrometer)

Type	Concentration, % vol	Avg. C Number
C_nH_{2n+2}	35	12.1
C_nH_{2n}	27	11.5
C_nH_{2n-2}	21	12.2
C_nH_{2n-4}	5.1	12.7
C_nH_{2n-6}	5.5	10.7
C_nH_{2n-8}	3.9	12.2
C_nH_{2n-10}	1.1	11.9
C_nH_{2n-12}	0.27	11.8
C_nH_{2n-14}	0.25	13.7
C_nH_{2n-16}	0.11	12.3
C_nH_{2n-18} to C_nH_{2n-20}	0	

Avg. Molecular Weight: 166

Carbon Number
(Chromatographic Analysis)

Carbon Number	Concentration, % wt
8	0.1
9	4.3
10	13.3
11	14.4
12	19.5
13	18.8
14	14.2
15	10.6
16	3.3
17	0.8
18	0.4
19	0.2
> 19	0.1

S-14115

Table XVII. EXPERIMENTAL PHYSICAL PROPERTIES OF JET A FUEL (F-187)

Temperature		Density	
°F	°C	g/ml	kg/m³
32	0	0.834	834
100	38	0.809	809
200	93	0.768	768
300	149	0.725	725
		Viscosity	
		cp	μN·s/m²
-40	-40	11.35	11350
32	0	2.74	2740
100	38	1.28	1280
210	99	0.587	587
348	176	0.303	303
		Thermal Conductivity	
		cal/sec-cm-°C	mW/m·K
77	25	0.000328	137
		Vapor Pressure	
		mm Hg	kN/m²
100	38	1.8	0.24
150	66	7.0	0.93
200	93	23.	3.1
		Refractive Index	
59	15	1.4561	
68	20	1.4542	

Table XVIII. LIQUID PROPERTIES OF JET A FUEL

Average Molecular Weight   170.1
Pseudocritical Pressure   265 psia $1.82 \ MN/m^2$
Pseudocritical Temperature 721°F   383°C
Pseudocritical Density $14.8 \ lb/ft^3$ $237 \ kg/m^3$

Temp.		Density		Enthalpy		Specific Heat at Constant Pressure	
°F	°C	lb/ft^3	kg/m^3	Btu/lb	kJ/kg	Btu/lb-°F	kJ/kg·°C
0	-18	52.8	845	0	0	0.440	1.84
100	38	50.5	809	47	110	0.508	2.13
200	93	48.0	769	101	236	0.575	2.41
300	149	45.3	725	161	375	0.644	2.69
400	204	42.2	677	227	528	0.719	3.01
500	260	38.6	619	298	693	0.807	3.38
600	316	33.9	543	375	872	0.943	3.94
700	371	25.2	403	465	1081	1.531	6.41

Temp.		Viscosity		Thermal Conductivity	
°F	°C	lb/ft-hr	$\mu N \cdot s/m^2$	Btu/hr-ft-°F	mW/m·°C
0	-18	11.73	4850	0.1014	175
100	38	3.07	1270	0.0907	157
200	93	1.43	591	0.0814	141
300	149	0.889	368	0.0732	127
400	204	0.650	269	0.0658	114
500	260	0.404	167	0.0588	102
600	316	0.221	91	0.0523	90
700	371	0.111	46	0.0522	90

(This page is blank.)

Tables XIX through XXIII follow

Table XIX. GAS PROPERTIES OF JET A FUEL

Density, lb/ft³ (kg/m³)

Temp., °F (°C)	Pressure, psia (MN/m²)		
	0 (0)	500 (3.45)	1000 (6.90)
750 (399)	0	21.5 (345)	27.9 (446)
800 (427)	0	17.6 (282)	25.5 (408)
850 (454)	0	13.88 (222)	23.1 (370)
900 (482)	0	11.04 (177)	20.9 (334)
950 (510)	0	9.14 (146)	18.7 (300)
1000 (538)	0	7.88 (126)	16.7 (268)

Compressibility Factor

Temp., °F (°C)	Pressure, psia (MN/m²)		
	0 (0)	500 (3.45)	1000 (6.90)
750 (399)	1	0.305	0.470
800 (427)	1	0.357	0.494
850 (454)	1	0.436	0.524
900 (482)	1	0.528	0.559
950 (510)	1	0.615	0.601
1000 (538)	1	0.689	0.650

Specific Heat at Constant Pressure, Btu/lb-°F (kJ/kg-°C)

Temp., °F (°C)	Pressure, psia (MN/m²)		
	0 (0)	500 (3.45)	1000 (6.90)
750 (399)	0.730 (3.06)	0.945 (3.95)	0.894 (3.74)
800 (427)	0.748 (3.13)	0.965 (4.04)	0.896 (3.75)
850 (454)	0.765 (3.20)	0.973 (4.07)	0.899 (3.76)
900 (482)	0.781 (3.27)	0.948 (3.97)	0.902 (3.77)
950 (510)	0.797 (3.34)	0.917 (3.84)	0.905 (3.79)
1000 (538)	0.812 (3.40)	0.899 (3.76)	0.908 (3.80)

Enthalpy, Btu/lb (kJ/kg)

Temp., °F (°C)	Pressure, psia (MN/m²)		
	0 (0)	500 (3.45)	1000 (6.90)
750 (399)	565 (1313)	495 (1149)	489 (1136)
800 (427)	602 (1400)	542 (1260)	533 (1240)
850 (454)	640 (1488)	591 (1373)	578 (1344)
900 (482)	679 (1577)	639 (1485)	623 (1449)
950 (510)	718 (1669)	686 (1593)	669 (1554)
1000 (538)	758 (1763)	731 (1699)	714 (1659)

Thermal Conductivity, Btu/hr-ft-°F (mW/m·°C)

Temp., °F (°C)	Pressure, psia (MN/m²)		
	0 (0)	500 (3.45)	1000 (6.90)
750 (399)	0.0231 (39.9)	0.0344 (59.4)	0.0407 (70.3)
800 (427)	0.0246 (42.5)	0.0328 (56.7)	0.0395 (68.4)
850 (454)	0.0260 (45.0)	0.0318 (55.0)	0.0387 (67.0)
900 (482)	0.0275 (47.6)	0.0317 (54.8)	0.0383 (66.2)
950 (510)	0.0291 (50.3)	0.0322 (55.3)	0.0381 (65.9)
1000 (538)	0.0306 (52.9)	0.0332 (57.4)	0.0382 (66.0)

Viscosity, lb/ft-hr (μN·s/m²)

Temp., °F (°C)	Pressure, psia (MN/m²)		
	0 (0)	500 (3.45)	1000 (6.90)
750 (399)	0.0256 (10.6)	0.0886 (36.6)	0.1333 (55.1)
800 (427)	0.0266 (11.0)	0.0696 (28.8)	0.1148 (47.4)
850 (454)	0.0276 (11.4)	0.0559 (23.1)	0.1003 (41.5)
900 (482)	0.0285 (11.8)	0.0481 (19.9)	0.0879 (36.3)
950 (510)	0.0295 (12.2)	0.0442 (18.3)	0.0775 (32.0)
1000 (538)	0.0305 (12.6)	0.0423 (17.5)	0.0695 (28.7)

Table XX. DATA SUMMARY FOR 5-HOUR TEST RUNS

Heat Exchange Tubes: Runs 24 through 70, 84; Hastelloy C - 0.1268-in OD x
0.0317-in Wall x 2-ft Length
(0.03325-ft² Inside Surface)

Runs 73 through 79; Hastelloy C - 0.1908-in OD x
0.032-in Wall x 2-ft Length
(0.06641-ft² Inside Surface)

Fuel: Jet A, Oxygen Content < 0.5 ppm

Run Number	24	30	34	26	28[a]	84[a]	32	36	42	44	38	40	46	50	54	58	48	52	56	62	66	70	60	64	68	73	75	77[b]	79	9
Nominal Run Conditions																														
Heat Flux, Btu/sec-in²	4	4	4	4	4	4	4	1	1	1	1	1	1	.2	.2	.2	.2	.2	.2	.02	.02	.02	.02	.02	.02	.02	.2	.2	.2	1
Inlet Pressure, psia	500	500	500	1000	1000	1000	1000	500	500	500	1000	1000	1000	500	500	500	1000	1000	1000	500	500	500	1000	1000	1000	1000	500	1000	500	500
Exit Fluid Temp., °F	500	800	1000	500	800	800	1000	500	800	500	500	800	1000	500	800	1000	1000	800	1000	500	500	1000	800	800	1000	1000	500	1000	500	800
Actual Run Conditions (Time Avg.)																														
Feed Rate, lb/hr	294	144	104	292	149	147	112	72.4	35.8	26.6	72.3	36.7	28.0	14.4	7.08	4.88	14.4	7.02	5.15	1.47	.718	.504	1.47	.708	.504	1.10	.2	.2	.2	71.2

a) Run 84 was a brief test at conditions of Run 28 to obtain improved heat transfer data.
b) Measured exit fuel temperatures for low flow rate runs were low due to rapid cooling of fuel before reaching the temperature measuring point.
c) Calculated from power input, flow rate, and heat capacity data corrected for losses.
d) Corrected for heat losses.
e) T.C. No. refers to order of printout on 24-pt recorder. Location is measured from start of heated tube section.
f) T and B refer to position of T.C. junction on Top or Bottom of horizontal test section.
g) Less than 0.001 psi.

S-14115
67374

Table XXI. DATA SUMMARY FOR 20-HOUR TEST RUNS

Heat Exchange Tubes: Runs 81 and 85; Hastelloy C - 0.1268-in OD x 0.0317-in Wall x 2-ft Length (0.03325-ft² Inside Surface)
Runs 88 and 91; Stainless Steel Type 316 - 0.1260-in OD x 0.026-in Wall x 2-ft Length (0.03875-ft² Inside Surface)
Runs 95 and 98; L-605 (Haynes 25) - 0.1278-in OD x 0.0313-in Wall x 2-ft Length (0.03409-ft² Inside Surface)

Fuel: Jet A, Oxygen Content < 0.5 ppm

Run Number		81					88					95					85				91				98				
Nominal Run Conditions																														
Heat Flux, Btu/sec-in²				.2					.2					.2					4					4				4		
Inlet Pressure, psia				1000					1000					1000					1000					1000				1000		
Exit Fluid Temp., °F				1000					1000					1000					1000					1000				1000		
Actual Run Conditions (Time Avg.)																														
Feed Rate, lb/hr				5.09					6.05					5.42					106					123				107		
Inlet Pressure, psia				1005					1000					1000					1010					1000				1005		
Fluid Temp., °F — In (Measured)[a]				100					100					100					100					100				100		
Out (Measured)[a]				950					973					970					1006					1006				1000		
Out (Calc.)[b]				1041					1008					1036					998					1010				996		
Power Supplied, Btu/hr x 10⁻³				3.73					4.23					3.93					68.8					81.7				69.3		
Net Heat to Fuel[c] — Btu/hr x 10⁻³				3.50					3.97					3.70					68.5					81.4				69.0		
Btu/lb				688					656					683					648					660				646		
Net Heat Flux, Btu/sec-in²[c]				.205					.198					.209					3.98					4.05				3.90		

Outside Wall Temp., °F

T.C. No.	Location, ft[d]		81 (.1)	81 (.8)	81 (4.7)	81 (9.6)	81 (19.8)	88 (.1)	88 (.7)	88 (4.9)	88 (9.8)	88 (20.0)	95 (.1)	95 (.9)	95 (4.7)	95 (9.8)	95 (20.0)	85 (.3)	85 (5.0)	85 (9.8)	85 (20.0)	91 (.3)	91 (4.9)	91 (9.9)	91 (19.7)	98 (.3)	98 (4.8)	98 (6.5)	98 (9.9)	98 (20.0)
14	0.05	T	716	728	742	730	748	686	707	700	699	699	645	646	640	650	660	1389	1294	1301	-	1343	1320	1299	1320	1495	1348	1355	1248	1287
2	.125	B	854	868	882	901	911	835	840	840	831	835	854	838	844	860	898	1334	1329	1305	1289	1335	1328	1297	1310	1435	1280	1257	1230	1288
15	.2	T	900	907	920	913	933	867	883	875	870	872	888	885	884	900	926	1257	1238	1222	1200	-	-	-	-	1377	1290	1275	1251	1258
3	.3	T	980	991	1001	983	1001	964	967	973	962	966	980	958	961	979	1012	-	-	-	-	1223	1228	1190	1184	1273	1315	1410	1171	1232
16	.4	T	1024	1030	1039	1023	1035	999	1020	1015	1004	1008	1009	1002	1001	1016	1050	1295	1350	1361	1372	-	1241	1208	1195	1273	1316	1437	1473	1385
4	.5	B	1010	1017	1025	1007	1051	973	984	989	976	985	1019	993	995	1012	1080	-	-	-	-	1218	1491	1527	1465	1208	1336	1465	1511	1502
17	.6	B	1041	1045	1055	1047	1152	1005	1019	1020	1000	1028	1037	1028	1027	1042	1152	1254	1292	1333	1380	1230	1369	1323	1238	1172	1332	1454	1518	1561
5	.7	T	1112	1119	1132	1119	1218	1087	1004	1112	1099	1130	1120	1094	1095	1118	1197	1283	1326	1358	1400	1243	1342	1353	1302	1232	1321	1415	1520	1569
18	.8	T	1141	1151	1171	1176	1245	1126	1145	1150	1134	1162	1147	1134	1130	1147	1182	1282	1298	1336	1400	1259	1303	1278	1247	1210	1297	1371	1464	1506
6	.9	B	1124	1136	1178	1180	1200	1110	1115	1124	1115	1155	1141	1118	1115	1118	1162	-	-	-	-	1247	1240	1238	1202	1190	1243	1278	1302	1206
19	1.0	B	1158	1170	1162	1162	1165	1130	1153	1154	1129	1151	1170	1154	1150	1143	1159	1285	1272	1309	1373	1208	1222	1221	1221	1208	1210	1228	1225	1210
7	1.1	T	1255	1249	1229	1202	1206	1248	1253	1250	1209	1220	1225	1202	1179	1179	1188	1316	1291	1342	1405	1319	1314	1368	1498	1233	1217	1212	1229	1291
20	1.2	T	1266	1279	1279	1243	1232	1268	1291	1282	1128	1140	1280	1264	1223	1233	1138	1325	1275	1270	1231	1327	1374	1440	1490	1270	1307	1342	1358	1330
8	1.3	B	1247	1261	1263	1223	1195	1254	1255	1222	1073	1004	1270	1239	1191	1220	1028	1316	1273	1279	1284	1342	1381	1398	1355	1286	1339	1362	1304	1297
21	1.4	B	1279	1289	1295	1257	1120	1268	1294	1017	1041	1061	1298	1245	1152	1161	1085	1558	1323	1516	1307	1381	1393	1396	1387	1296	1373	1437	1297	1306
9	1.5	T	1343	1356	1360	1320	1061	1370	1359	977	999	1064	1367	1332	1116	1055	1066	1432	1436	1423	1395	1336	1493	1500	1329	1316	1453	1500	1329	1339
22	1.6	T	1370	1379	1387	1202	1084	1384	1052	1034	1032	1083	1376	1296	1092	1084	1108	1396	1390	1368	1361	1460	1481	1457	1415	1336	1493	1532	1370	1378
10	1.7	B	1341	1334	1330	1159	1095	1552	1060	1045	1096	1103	1321	1117	1076	1116	1141	1411	-	-	-	1439	1475	1432	1452	1350	1423	1474	1354	1340
23	1.8	B	1340	1260	1223	1195	1165	1350	1147	1172	1160	1142	1302	1158	1151	1130	1148	-	-	-	-	1489	1460	1435	-	1363	1378	1399	1377	1380
11	1.875	B	1362	1195	1207	1160	1165	1403	1191	1209	1140	1158	1240	1202	1170	1150	1162	1466	1465	1457	1463	1539	1486	1462	1439	1412	1411	1400	1417	1425
12,24	1.95	T	1296	1189	1166	1168	196	1336	1190	1209	1199	1166	1173	1192	1161	1163	1182	1476	1471	1473	1468	1539	1482	1458	1437	1429	1453	1432	1441	1453
Tube Pressure Drop, psi			.13	.13	.17	.31	.39	.10	.20	1.10	.88	.17	.14	.15	.19	.23	.33	52	66	64	71	27	40	40	46	40	64	65	59	57
Filter Pressure Drop, psi			e)	e)	e)	e)	e)	e)	e)	e)	e)	e)	e)	e)	e)	e)	e)	.07	.80	.50	1.45	.10	1.35	2.15	3.17	.06	.59	.67	.92	1.61
Product Gas Rate, SCFH			1.11	1.11	1.07	.21	.12	1.25	.50	.16	.03	.06	.75	.50	.17	.08	.06	-	-	-	-	-	.32	.45	.41	.23	.24	-	-	.22

	81	88	95	85	91	98
Coke on Filter, mg	5.7	7.6	5.5	39.9[f]	59.4	86.0
Filter Temp., °F	600	570	550	860	830	850
Coke Deposit in Tube, µg/cm² — Tube Section, ft						
0.2 - 0.4	3	12	1	27	12	14
0.4 - 0.6					357	725
0.6 - 0.8	11	8	4	55	21	841
0.8 - 1.0						
1.0 - 1.2	96	121	98	45	445	4
1.2 - 1.4	335	381	308			
1.4 - 1.6	745	289	245	13	26	134
1.6 - 1.8	293	160	89			60
1.8 - 2.0	92	105	34	42	116	13

a) Measured exit fuel temperatures for low flow rate runs were low due to rapid cooling of fuel before reaching the temperature measuring point.
b) Calculated from power input, flow rate, and heat capacity data corrected for losses.
c) Corrected for heat losses.
d) T.C. No. refers to order of printout on 24-pt recorder. Location is measured from start of heated section. T and B indicate junction on Top or Bottom of test section.
e) Less than 0.001 psi.
f) New filter installed after initial 5-hr period. 9.6 mg on filter during 0-5 hr, 30.3 mg during 5-20 hr.

Table XXII. DATA SUMMARY FOR 100-HOUR TEST RUNS

Heat Exchange Tubes: Hastelloy C – 0.1268-in OD x 0.0317-in Wall x 2-ft Length (0.03325-ft² Inside Surface)

Fuel: Run 101 – Jet A with < 0.5 ppm Oxygen
Run 113 – Air-Saturated Jet A

Run Number	101	113
Nominal Run Conditions		
Heat Flux, Btu/sec-in²	1	1
Inlet Pressure, psia	1000	1000
Exit Fluid Temp., °F	1000	1000
Actual Run Conditions (Time Avg.)		
Feed Rate, lb/hr	26.7	26.7
Inlet Pressure, psia	1000	1010
Fluid Temp., °F In (Measured)	100	100
Out (Measured)	948	952
Out (Calc)[a]	957	957
Power Supplied, Btu/hr x 10⁻³	17.6	16.5
Net Heat to Fuel[b] Btu/hr x 10⁻³	17.3	16.2
Net Heat Flux, Btu/sec-in²[b]	645 / .999	606 / .939
	16.4 / 16.2 / 605 / .957	

Run 101 — Outside Wall Temp., °F

T.C. No.[e]	Location, ft[f]	.2	1.25	2.0	3.0	4.05	5.08	6.08	7.0	8.0	9.10	10.0	20.0	30.0	40.2ᶜ	50.0	65.0ᵈ	74.2	80.0	90.0	100
14 T	0.05	1449	1460	1456	1470	1465	1230	1319	1323	1303	1293	1275	1173	1217	1165	1215	–	–	–	–	–
2 B	.125	1433	1413	1413	1422	1384	1236	1350	1240	1223	1215	1213	1253	1357	1372	1343	–	–	–	–	–
15 T	.2	1435	1389	1359	1280	1280	1175	1172	1158	1176	1200	1207	1288	1361	1361	1300	–	–	–	–	–
16 T	.3	1379	1359	1359	1153	1225	1173	1135	1152	1291	1192	1214	1328	1356	1355	1299	–	–	–	–	–
4 T	.4	1355	1285	1298	1298	1117	1117	1153	1177	1256	1163	1200	1306	1352	1353	1271	–	–	–	–	–
17 T	.5	1327	1265	1203	1203	1143	1143	1133	1139	1152	1147	1176	1277	1342	1341	1270	–	–	–	–	–
5 B	.6	1302	1193	1092	1087	1116	1101	1119	1123	1135	1150	1157	1264	1352	1349	1275	–	–	–	–	–
18 T	.7	1275	1104	1079	1083	1088	1088	1108	1116	1142	1157	1164	1277	1342	1341	1174	–	–	–	–	–
6 B	.8	1259	1090	1080	1093	1095	1108	1119	1129	1150	1160	1161	1264	1342	1342	1176	–	–	–	–	–
19 T	.9	1250	1085	1085	1101	1101	1115	1123	1135	1160	1170	1170	1255	1342	1341	1176	–	–	–	–	–
7 T	1.0	1221	1101	1105	1115	1112	1123	1132	1149	1166	1171	1171	1255	1334	1347	1180	–	–	–	–	–
20 B	1.1	1219	1097	1107	1105	1114	1132	1136	1150	1152	1179	1184	1280	1333	1348	1219	–	–	–	–	–
8 B	1.2	1224	1101	1101	1109	1111	1111	1149	1150	1160	1178	1184	1280	1350	1350	1290	–	–	–	–	–
21 B	1.3	1222	1112	1105	1111	1117	1136	1150	1152	1160	1178	1178	1301	1349	1355	1339	–	–	–	–	–
9 T	1.4	1223	1112	1118	1125	1119	1119	1156	1156	1160	1190	1192	1311	1346	1355	1339	–	–	–	–	–
22 T	1.5	1245	1135	1139	1135	1125	1125	1156	1160	1170	1197	1190	1320	1348	1349	1326	–	–	–	–	–
10 T	1.6	1275	1168	1156	1145	1147	1150	1148	1158	1140	1149	1165	1250	1345	1350	1346	–	–	–	–	–
23 B	1.7	1285	1201	1195	1184	1150	1137	1158	1160	1149	1146	1146	1189	1321	1341	1291	–	–	–	–	–
11 T	1.875	1317	1246	1203	1167	1180	1178	1176	1164	1178	1174	1175	1226	1288	1331	1271	–	–	–	–	–
12,24 T	1.95	1308	1229	1210	1169	1181	1181	1187	1180	1187	1183	1183	1199	1223	1287	1259	–	–	–	–	–
Tube Pressure Drop, psi		2.6	3.4	4.1	4.2	4.2	4.3	4.3	4.4	4.4	4.4	4.4	5.4	5.6	5.0	6.0	5.5	5.4	5.8	6.4	6.6
Filter Pressure Drop, psi		.001	.001	.002	.005	.011	.017	.022	.029	.035	.041	.046	.042	.130	.423	1.22	.15ᶠ	.29	.35	.60	.99
Product Gas Rate, SCFH		.16	.14	.12	.09	.06	.03	.00	.00	.00	.01	.02	.04	.15	.03	.12	.05	.07	.10	.22	.22

Coke on Filter, mg: 61.5 (0 – 52 hr)   41.1 (52 – 100 hr)
Filter Temp., °F: 720

Run 113 — Outside Wall Temp., °F

T.C. No.[e]	Location, ft[f]	.05	1.0	2.0	3.0	4.0	5.0	6.0	7.0	8.0	9.0	10.0	20.0	30.0	40.0	50.0	60.0	70.0	80.0	90.0	100
14 T	0.05	1381	1389	1293	1251	1181	1142	1112	1100	1109	1121	1143	1174	1212	1271	1297	1295	1290	1290	1280	1298
2 B	.125	1460	1451	1461	1456	1403	1260	900	977	977	945	950	1221	1219	1221	1272	1282	1287	1282	1282	1315
15 T	.2	1465	1420	1413	1350	1165	1074	1010	1018	1020	1035	1056	1128	1153	1150	1280	1298	1303	1295	1295	1280
16 T	.3	1349	1331	1348	1348	1055	1020	979	971	985	1000	1019	1140	1180	1140	1283	1263	1263	1299	1299	1334
4 T	.4	1331	1187	1002	940	1002	921	913	904	905	906	971	1028	1142	1180	1210	1257	1271	1285	1302	1324
17 T	.5	1319	1151	1073	909	885	909	888	889	894	900	905	973	943	945	1033	1120	1162	1243	1267	1313
5 B	.6	1294	1073	963	970	903	890	885	880	888	889	891	926	943	1029	1135	1165	1243	1290	1290	1320
18 T	.7	1252	1129	977	919	900	919	888	885	890	890	929	953	1041	1151	1222	1258	1281	1281	1284
6 B	.8	1258	1111	952	917	900	901	907	913	974	921	974	1010	1095	1204	1252	1262	1298	1298	1246
19 T	.9	1228	1085	945	963	941	953	952	957	982	1084	982	1110	1226	1262	1305	1374	1466	1532	1359
7 T	1.0	1210	1016	936	948	962	980	969	970	1016	1084	1062	1130	1330	1406	1478	1466	1532	1532
20 B	1.1	1210	1002	985	978	988	999	1001	1013	1029	1062	1158	1330	1406	1479	1546	1608	1628
8 B	1.2	1215	1060	1021	1021	1009	1018	1015	1019	1051	1050	1055	1122	1272	1393	1400	1450	1608
21 B	1.3	1216	1018	1054	1077	1029	1040	1045	1053	1118	1122	1190	1257	1343	1344	1350	1422	1450
9 T	1.4	1242	1074	1115	1089	1077	1057	1040	1044	1132	1190	1132	1257	1310	1342	1352	1373
22 T	1.5	1242	1080	1115	1216	1205	1115	1313	1245	1282	1308	1319	1356	1349	1336	1352	1373	1362
10 T	1.6	1242	1152	1190	1216	1246	1137	1165	1261	1371	1381	1388	1410	1450	1471	1470	1465	1504
23 B	1.7	1263	1106	1251	1216	1198	1189	1243	1285	1261	1282	1243	1279	1349	1375	1379	1482	1429	1346	1385
11 T	1.875	1268	1205	1236	1253	1226	1269	1245	1255	1284	1279	1278	1280	1251	1310	1332	1346	1346	1364	1271
12,24 T	1.95	1205	1205	1257	1253	1277	1283	1287	1287	1284	1280	1278	1297	1268	1268	1276	1270	1271	1272	1274
Tube Pressure Drop, psi		2.4	4.0	5.4	6.2	6.8	7.2	7.5	7.8	8.0	8.3	8.5	10.2	11.6	13.7	16.4	22.0	30.2	50	108	364
Filter Pressure Drop, psi		.002	.005	.05	.26	.43	.52	.57	.60	.63	.65	.67	1.00	1.21	1.11	1.58	1.66	1.75	1.94	2.18	2.13
Product Gas Rate, SCFH		.15	.13	.10	.08	.05	.03	.03	.04	.04	.04	.04	.06	.08	.12	.23	.17	.17	.23	.17	.17

Coke on Filter, mg: 30.5
Filter Temp., °F: 720

Coke Deposit, in Tube, μg/cm²

Tube Section, ft	101	113
0 – 0.2	1365	925
0.2 – 0.4	1421	1062
0.4 – 0.6	1456	1086
0.6 – 0.8	1280	1113
0.8 – 1.0	1351	1113
1.0 – 1.2	1256	2706
1.2 – 1.4	1695	(1.0 – 1.1 ft) 9341 / (1.1 – 1.2 ft) 6915
1.4 – 1.6	1665	3269
1.6 – 1.8	1431	1930
1.8 – 2.0	658	(1.6 – 1.7 ft) 5695 / (1.7 – 1.8 ft) 7043
		2205

a) Calculated from power input, flow rate and heat capacity data corrected for losses.
b) Corrected for heat losses.
c) After 62-hr weekend shutdown.
d) During period of surging operation.
e) T.C. No. refers to order of printout on 24-pt recorder. Location is measured from start of heated section.
f) T and B indicate junction on Top or Bottom of horizontal test section.
f) New filter installed after 52 hr.

Table XXIII. PRODUCT ANALYSES

Run Number (Time, hr)	Feed	32	46	101 (98)	113 (98)[a]	56	81 (4)	81 (9)	81 (20)	58	75	52	48	68	73
Exchanger Tube															
Material		Hast. C	Hast. C			Hast. C				Hast. C	Hast. C	Hast. C	Hast. C	Hast. C	Hast. C
O.D., in. (cm)		1/8 (0.32)	1/8 (0.32)			1/8 (0.32)				1/8 (0.32)	3/16 (0.48)	1/8 (0.32)	1/8 (0.32)	1/8 (0.32)	3/16 (0.48)
Nominal Operating Cond:															
Heat Flux, Btu/sec-in^2 (MW/m^2)		4 (6.54)	1 (1.63)			.2 (.327)				.2 (.327)		.2 (.327)	.2 (.327)	.02 (.033)	
Outlet Fuel Temp., °F (°C)		1000 (538)	1000 (558)			1000 (538)				1000 (538)		800 (427)	500 (260)	1000 (538)	
Inlet Pressure, psia (MN/m^2)		1000 (6.90)	1000 (6.90)			1000 (6.90)				500 (3.45)		1000 (6.90)	1000 (6.90)	1000 (6.90)	
Gaseous Product Analysis, %m															
H$_2$		19.7		22.3	22.5	8.9	8.7		14.4		16.3				
CH$_4$		57.3		52.7	52.2	37.4	37.2		50.0		49.0				
C$_2$H$_4$		6.4		10.6	11.6	14.8	14.8		13.0		16.8				
C$_2$H$_6$		8.8		8.0	8.0	17.0	16.0		12.0		10.0				
C$_3$H$_6$		3.0		3.3	3.1	11.2	11.6		5.1		4.4				
C$_3$H$_8$		2.8		1.9	1.7	6.2	6.8		3.6		2.1				
C$_4$H$_8$		.8		.6	.6	2.7	3.3		1.0		.9				
C$_4$H$_{10}$		.8		.4	.2	1.0	1.0		.5		.2				
>C$_4$		.3		.1	0	.7	.6		.3		.2				
Average Mol. Wt.		17.6		16.8	16.6	25.4	25.8		20.3		19.4				
% of Feed to Gas		(.02)[b]	-	.04[c]	.05[c]	1.3	1.4	(.24)[d]	.13	(<.01)[d]	.14	(.2-.02)[d]	(<.01)[d]	(.10)[d]	(.37)[d]
Liquid Product Analysis, %w															
C$_3$		.03				.05	.1					.02		.03	
C$_4$		.08				.35	.3					.1		.09	.1
C$_5$		.3	.05			.5	.2					.1		.15	.5
C$_6$		.3	.04			.5	.4					.1		.15	.3
C$_7$		.2	.06			.4	.6					.2		.2	.3
C$_8$	.1	.4	.2			.7	1.2	.3		.4		.3	.2	.6	.4
C$_9$	4.3	4.6	4.7			4.7	4.9	4.6		4.2		4.4	4.0	4.3	4.4
C$_{10}$	13.3	13.7	13.6			13.4	12.7	13.3		13.4		13.5	13.0	13.5	13.5
C$_{11}$	14.4	14.5	14.0			14.5	13.4	14.0		14.9		14.9	14.2	14.8	13.7
C$_{12}$	19.5	19.0	19.4			19.7	19.7	20.3		20.0		19.7	19.3	19.9	20.0
C$_{13}$	18.8	18.0	18.4			18.1	17.9	18.9		18.6		18.3	18.3	17.9	18.1
C$_{14}$	14.2	14.0	14.5			15.4	13.7	14.4		15.0		14.4	14.5	15.0	14.4
C$_{15}$	10.6	9.8	10.4			9.8	10.6	11.1		10.4		10.1	10.3	10.5	9.7
C$_{16}$	3.3	3.3	3.1			2.7	2.3	2.4		2.5		2.9	5.5	2.4	2.8
C$_{17}$	.8	1.5	.9			.7	.9	.6		.5		.7	.5	.5	.8
C$_{18}$	.4	.3	.5			.2	.3			.1		.3	.1	.1	.3
C$_{19}$	.2	.1	.1			.1	.4					.1	.05		.1
>C$_{19}$	.1		.05				.2								
Color[e]	(1)	(1)	(1)	(1)	(3)[f]	(6)	(6)	(4)	(3)	(1)	(3)	(4)	(1)	(2)	(5)
Gum, mg/100 ml[g]	0	—		4	3	18				0		6			

a) Run 113 was the only test made with air-saturated fuel.
b) Based on gas rate measured during other tests at same operating conditions.
c) Gas make reached a low of < .005% during first 10-hour cycle of these 100-hour tests.
d) Gas analysis not made. Gas make calculated using Mol. wt. = 20.
e) Arbitrary color code: (1) water-white, (2) slight yellow tint, (3) very light yellow, (4) light yellow, (5) yellow, and (6) amber.
f) Product had slight tint at start of test. Changed gradually to very light yellow.
g) Analyzed by ASTM Designation D381-61T.

SYMBOLS

A   observed backscatter count rate for pure deposit

B   observed backscatter count rate for clean tube

c_p specific heat at constant pressure

d   tube diameter

Gr'   modified Grashof number $\left[\dfrac{gd^3\rho\Delta\rho}{\mu^2}\right]$

g   gravitational acceleration

h   heat transfer coefficient

I   observed backscatter count rate for deposit on tube

k   thermal conductivity

Nu   Nusselt number $\left[\dfrac{hd}{k}\right]$

Pr   Prandtl number $\left[\dfrac{\mu c_p}{k}\right]$

q   heat flux

Re   Reynolds number $\left[\dfrac{du\rho}{\mu}\right]$

T   temperature

u   linear velocity

X   deposit surface density (weight of deposit per unit surface area of tube)

Z_1 average atomic number of deposit

Z_2 average atomic number of tube

μ viscosity

ρ density

Subscripts

B   bulk fluid conditions

P   Poiseuille flow

W   wall conditions

S-14115

REFERENCES

1. Watt, J. J., Evans, A., Jr., and Hibbard, R. R., "Fouling Characteristics of ASTM Jet A Fuel When Heated to 700°F in a Simulated Heat Exchanger Tube," NASA TN D-4958, Dec., 1968.

2. Schnurr, N. M., "Heat Transfer to Carbon Dioxide in the Immediate Vicinity of the Critical Point," J. Heat Transfer, Trans. ASME, Ser. C, 91 (1), 16-20 (Feb., 1969).

3. Shiralkar, B. S., and Griffith, P., "Deterioration in Heat Transfer to Fluids at Supercritical Pressure and High Heat Fluxes," J. Heat Transfer, Trans. ASME, Ser. C, 91 (1), 27-36 (Feb., 1969).

4. Smith, J. D., "The Effect of Metals and Alloys on the Thermal Stability of Avtur 50," Aircraft Engineering, 19-27 (April, 1967).

5. Droegemuller, E. A., Paper presented at Sixth World Petroleum Congress, Frankfurt: Main, June, 1963.

6. Snitserov, Yu V., "The Effect of Additives on the Formation of Deposits in Fuel T-1 at High Temperatures," Khim i Tekhnol Topliv i Masel, 11, 55-59 (1961).

7. Nixon, A. C., Ch. 17 in "Autoxidation and Antioxidants," vol. II, Lunberg, ed., Interscience Publishers, 1962, p. 755.

No. Cop.

1. NASA-Lewis Research Center 8
   Report Control Office   MS 5-5
   21000 Brookpark Road
   Cleveland, Ohio 44135   1

2. NASA-Lewis Research Center 8
   Technology Utilization Office   MS 3-19
   21000 Brookpark Road
   Cleveland, Ohio 44135   1

3. NASA-Lewis Research Center 8
   Library MS 60-3
   21000 Brookpark Road
   Cleveland, Ohio 44135   2

4. NASA-Lewis Research Center 8
   Fluid System Components Division MS 5-3
   21000 Brookpark Road
   Cleveland, Ohio 44135   1

5. NASA-Lewis Research Center 8
   J. Howard Childs MS 60-4
   21000 Brookpark Road
   Cleveland, Ohio 44135   1

6. NASA-Lewis Research Center 8
   Leonard W. Schopen MS 77-3
   21000 Brookpark Road
   Cleveland, Ohio 44135   1

7. NASA-Lewis Research Center 8
   E. L. Warren MS 60-4
   21000 Brookpark Road
   Cleveland, Ohio 44135   15

8. NASA-Lewis Research Center 8
   J. B. Esgar MS 60-4
   21000 Brookpark Road
   Cleveland, Ohio 44135   1

9. NASA-Lewis Research Center 8
   F. S. Stepka MS 60-6
   21000 Brookpark Road
   Cleveland, Ohio 44135   1

10. NASA-Lewis Research Center 8
    R. R. Hibbard MS 3-5
    21000 Brookpark Road
    Cleveland, Ohio 44135   1

	No. Cop.
11. NASA-Lewis Research Center 8 H.H. Ellerbrock MS 60-4 21000 Brookpark Road Cleveland, Ohio 44135	1
12. NASA-Lewis Research Center 8 Dr. B. Lubarsky MS 3-3 21000 Brookpark Road Cleveland, Ohio 44135	1
13. NASA Scientific and Technical Info. Facility 8 NASA Representative RQT-2448 P.O. Box 33 College Park, Maryland 20740	6
14. NASA Headquarters 8 N.F. Rekos (RLC) 600 Independence Avenue, S.W. Washington, D.C. 20546	1
15. Mr. J. Richens AFAPL (APTC) 8 Wright-Patterson AFB, Ohio 45433	1
16. Mr. John H. Miller (APRT) 8 Wright-Patterson AFB, Ohio 45433	1
17. Air Force Office of Scientific Research 8 Propulsion Research Division USAF Washington, D.C. 20025	1
18. Department of the Navy 8 Robert Brown, RAPP14 Bureau of Naval Weapons Washington, D.C. 20025	1
19. Department of the Navy 8 G.L. Graves Bureau of Ships Washington, D.C. 20360	1
20. NASA-Langley Research Center 8 Mark R. Nichols Langley Station Technical Library Hampton, Virginia 23365	1
21. NASA-Langley Research Center 8 John V. Becker Langley Station Technical Library Hampton, Virginia 23365	1

	No. Cop.
22. United Aircraft Corporation 8 R.A. Schmidtke Pratt and Whitney Aircraft Division Florida Research and Development Center P.O. Box 2691 West Palm Beach, Florida 33402	1
23. United Aircraft Corporation 8 R.P. Huggins Pratt and Whitney Aircraft Division Florida Research and Development Center P.O. Box 2691 West Palm Beach, Florida 33402	1
24. United Aircraft Library 8 G. Andreini UAC Research Bldg. 400 Main Street East Hartford,Connecticut 06108	2
25. United Aircraft Library 8 John Goncar UAC Research Bldg. 400 Main Street East Hartford,Connecticut 06108	2
26. Northern Research and Engineering Corp. 8 K. Ginwala 219 Vassar Street Cambridge, Massachusetts 02139	1
27. General Electric Company 8 Dr. C.W. Smith - Library Bldg. 2-40M Flight Propulsion Division 930-1000 Western Avenue West Lynn, Massachusetts 01905	1
28. Curtiss-Wright Corporation 8 S. Lombardo Wright Aeronautical Division Wood-Ridge, New Jersey 07075	1
29. AiResearch Manufacturing Co. 5 Robert O. Bullock The Garrett Corporation, Arizona Division 402 South 36th Street Phoenix, Arizona 85934	1

30. AiResearch Manufacturing Co. 4   1
    Mr. R.D. Mueller
    The Garrett Corporation
    9851 Sepulveda Blvd.
    Los Angeles, California 90009

31. AVCO Corporation 8   1
    C.W. Bolton
    Lycoming Division
    550 South Main Street
    Stratford, Connecticut 06497

32. AVCO Corporation 8   1
    Charles Kuintzle
    Lycoming Division
    550 South Main Street
    Stratford, Connecticut 06497

33. Continental Aviation and Engineering Corp. 8   1
    Eli H. Benstein
    12700 Kercheval Avenue
    Detroit, Michigan 48215

34. Continental Aviation and Engineering Corp. 8   1
    Howard C. Welch
    12700 Kercheval Avenue
    Detroit, Michigan 48215

35. International Harvester Co., Solar 4   1
    P.A. Pitt
    2200 Pacific Highway
    San Diego, California 92112

36. International Harvester Co., Solar 4   1
    Mrs. L. Walper
    2200 Pacific Highway
    San Diego, California 92112

37. Goodyear Atomic Corporation 8   1
    Department No. 423 for: C.O. Longebrake
    Box 268
    Piketon, Ohio 45661

38. Commander, Naval Air Systems Command 8   1
    AIR-330
    Washington, D.C. 20360

39. The Boeing Company 5   1
    G.J. Schott, MS 80-66
    Commercial Airplane Division
    P.O. Box 3707
    Seattle, Washington 98124

40. The Boeing Company 5   1
     R.D. Kunkle, MS 73-19
     Commercial Airplane Division
     P.O. Box 3707
     Seattle, Washington 98124

41. The Boeing Company 8   1
     Warren K. Thorson
     Missile and Information Systems Division
     224 N. Wilkinson Street
     Dayton, Ohio 45402

42. Air Force Materials Laboratory 8   1
     MAAM, Mr. Hughes
     Wright-Patterson Air Force Base, Ohio 45433

43. Air Force Materials Laboratory 8   1
     MAMP, Mr. Hendricks
     Wright-Patterson Air Force Base, Ohio 45433

44. Douglas Aircraft Company 4   1
     Technical Info. Center, CL-250 for: J.E. Merriman
     3855 Lakewood Blvd.
     Long Beach, California 90801

45. Douglas Aircraft Company 4   1
     W.B. King
     3855 Lakewood Blvd.
     Long Beach, California 90801

46. General Motors Corporation 8   1
     J.N. Barney
     Allison Division
     P.O. Box 24013
     Indianapolis, Indiana 46206

47. General Motors Corporation 8   1
     G.E. Holbrook
     Allison Division
     P.O. Box 24013
     Indianapolis, Indiana 46206

48. General Motors Corporation 8   1
     Library
     Allison Division
     P.O. Box 24013
     Indianapolis, Indiana 46206

49. General Motors Corporation 8   1
     H.E. Helms
     Allison Division
     P.O. Box 24013
     Indianapolis, Indiana 46206

No. Cop.

50. Engineering Library 8
    Elizabeth Barrett, Librarian
    TRW Inc.
    23555 Euclid Avenue
    Cleveland, Ohio 44117   1

51. Engineering Library 8
    J. Edward Taylor, Director Product
    Development Jet and Ordnance Div.
    TRW Inc.
    23555 Euclid Ave.
    Cleveland, Ohio 44117   1

52. Westinghouse Electric Corporation 8
    S.M. De Corso
    Small Steam and Gas Turbine Engineering B-4
    Lester Branch
    P.O. Box 9175
    Philadelphia, Pennsylvania 19113   1

53. Westinghouse Electric Corporation 8
    J.J. Watt
    Small Steam and Gas Turbine Engineering B-4
    Lester Branch
    P.O. Box 9175
    Philadelphia, Pennsylvania 19113   1

54. McDonnell Aircraft Company 7
    R.E. Mattes
    Dept. 353, Building 33, Level 6
    St. Louis, Missouri 63166   1

55. McDonnell Aircraft Company 7
    J.M. Sinnett
    Dept. 353, Building 33, Level 6
    St. Louis, Missouri 63166   1

56. U.S. Air Force 8
    Mr. Alan E. Zengel, AFPL
    Research and Technology Division
    Aero Propulsion Laboratory
    Wright-Patterson AFB, Ohio 45433   1

57. U.S. Air Force 8
    Mr. J. Norris
    Research and Technology Division
    Aero Propulsion Laboratory
    Wright-Patterson AFB, Ohio 45433   1

No. Cop.

58. U.S. Air Force 8   1
     Capt. W. Noll
     Research and Technology Division
     Aero Propulsion Laboratory
     Wright-Patterson AFB, Ohio   45433

59. U.S. Naval Air Engineering Center 8   1
     Mr. J.E. Picktelberger
     Aeronautical Engine Laboratory
     Philadelphia, Pa.   19112

60. Federal Aviation Agency 8   1
     Mr. M.A. Lott, Fa-140
     Washington, D.C.   20553

61. North American Aviation, Inc. 8   1
     Mr. Royce Bradley NALA
     Wright-Patterson AFB
     Bldg. 42a, Area B
     Dayton, Ohio   45433

62. United Air Lines 1   1
     Mr. Paul Campbell
     Performance and Development Section
     San Francisco International Airport
     San Francisco, California   94128

63. E.I. DuPont DeNemours and Co. 8   1
     Mr. W.E. Bettoney
     Petroleum Laboratory
     Wilmington, Delaware   19898

64. Pratt and Whitney Aircraft Division 8   1
     Mr. George Jonke
     United Aircraft Corporation
     East Hartford,Connecticut   06110

65. Texaco, Inc. 8   1
     Mr. K.H. Strauss
     P.O. Box 509
     Beacon, New York   12508

66. Union Oil Company 4   1
     Mr. E.L. Wiseman
     P.O. Box 76
     Brea, California   92621

67. Aerospace Corporation 4   1
     W.J. Bennison
     Library, Technical Documents Group
     P.O. Box 95085
     Los Angeles, California   90045

	No. Cop.
68. American Oil Company 8 R.M. Brown P.O. Box 431 Whiting, Indiana 46394	1
69. Ashland Oil and Refining Company 8 A.M. Leas Technical Service Department Research and Engineering Building Ashland, Kentucky 41101	1
70. Atlantic Refining Company 8 F.C. Burk Product Development and Technical Service 260 S. Broad Street Philadelphia, Pa. 19101	1
71. The Boeing Company 6 C. Dufur Airplane Division - Wichita Branch 7100 Materials Technology Unit - PLT. 1 Wichita, Kansas 67201	1
72. The Boeing Company 5 G. Hays Airplane Division P.O. Box 74-40 Renton, Washington 98055	1
73. Chevron Research 1 J.A. Bert P.O. Box 1627 Richmond, California 94802	1
74. General Electric Company 8 M.W. Shayeson, AETD (E-51) Flight Propulsion Divison Cincinnati, Ohio 45315	1
75. General Motors Corporation 8 F.E. Salb, Dept. 7893 Plant No. 8 Allison Division P.O. Box 814 Indianapolis, Indiana 46206	1
76. Lockheed-California Company 4 Propulsion Dept./E.F. Versaw Advanced Systems Research Dept. 72-25, Bldg. 63-4, Plant A 1 P.O. Box 551 Burbank, California 91503	1

		No. Cop.
		1

77. North American Aviation, Inc.   4
    K.M. Holden, DFT 382
    Los Angeles Division
    Research and Development
    International Airport
    Los Angeles, California   90900

78. Phillips Petroleum Company   7   1
    R.M. Schirmer
    Research and Development Division
    Phillips Research Center
    Building C-7
    Bartlesville, Oklahoma   74004

79. Chandler Evans Control Systems Div.   8   1
    Mr. Erich Beckstein
    Colt Industries
    Charter Oak Blvd.
    West Hartford, Conn.   06110

80. Socony Mobil Oil Company, Inc.   8   1
    D.P. Osterhout, Jr.
    Research Department
    Paulsboro Laboratory
    Billingsport Road
    Paulsboro, N.J.   08066

81. University of Dayton Research Institute   8   1
    John Webb
    Dayton, Ohio   45409

82. Systems Engineering Group (RDT)   8
    SEKNB
    Wright-Patterson AFB, Ohio   45433

83. North American Aviation, Inc.   4   1
    Mr. Hal Goodman, D/056-108, Bldg. 2
    Los Angeles Division
    International Airport
    Los Angeles, California   90009

84. Dr. J. Nixon, Dr. W. Taylor   8   1
    Government Research Laboratory
    Esso Research and Engineering Co.
    Linden, New Jersey   07036

85. Monsanto Research Corporation   8   1
    Dr. William Scribner
    Station B - Box 8
    Dayton, Ohio   45407

	No. Cop.

86. Grumman Aircraft Engineering Corporation 8   1
    Mr. Chuck Spencer
    333 West First Street
    Dayton, Ohio 45402

87. Headquarters USAF 8   1
    AFRDDG (Mr. A. Eaffy)
    Washington, D.C. 20330

88. U.S. Naval Research Laboratory 8   1
    Bruce David Boss
    Code 6180, Fuels Branch
    Washington, D.C. 20390

89. Garrett Corp. 4   1
    Airesearch Mfg. Div.
    Library
    Yvonne Millar
    2525 West 190th Street
    Torrance, California 90509